Particle Incorporation into Bacterial Cellulose in a Rotating Disk Bioreactor

by

Dale E. Weber

A Thesis Submitted to the Graduate

Faculty of Rensselaer Polytechnic Institute

in Partial Fulfillment of the

Requirements for the degree of

MASTERS OF SCIENCE

Major Subject: Chemical Engineering

Approved by the
Project Advisors:

_____

B. Wayne Bequette, Thesis Adviser

_____

Joel L. Plawsky, Thesis Adviser

_____

Henry R. Bungay, Thesis Adviser

Rensselaer Polytechnic Institute
Troy, New York

February 2010
(For Graduation May 2010)

Table of Contents

List of Tables

List of Figures

Abstract

Bacterial cellulose produced by *Gluconacetobacter xylinus* (formerly *Acetobacter xylinum*) in a rotating disk bioreactor (RDB) is preferentially found on the rotating disk, not in the bulk media, and thickens in the axial direction. It has been found that 25-250μm particles suspended in the growth media are incorporated into the cellulose matrix. Biocomposite materials of particles in a bacterial cellulose (BC) matrix have applications in medical wound dressings, tissue engineering scaffolds, and paper batteries. Here we improve on the RDB design, successfully reducing the growth of stray BC in the reactor chamber that is unaffiliated with the disk, achieve near-perfect particle mixing, and adopt direct biocomposite characterization techniques: gravimetric analysis and photomicroscopy. These techniques support each other with gravimetric analysis is a coarse high throughput method used primarily is experimental design. Photomicroscopy is a more precise measurement method, but is much more time intensive and is used to assess incorporated particle concentrations in BC products. Particle incorporation in the improved apparatus is verified with both characterization techniques. A three-step mechanism of particle incorporation is presented with theoretical foundation and experimental support. The dominant forces sequentially acting on the particles describe the three steps of the mechanism: hydrodynamics and diffusion across a boundary layer; particle-surface non-covalent interactions; and mechanical entrapment by the cellulose fibers. The proposed mechanism predicts negatively charged particles will be spatially incorporated at a rate proportional to the tangential velocities on the disk face and positively charged particles will be incorporated uniformly of the disk surface at a rate proportional to the rotational rate. Experimental results for all particles show a discontinuity in the radial distribution of incorporated mass profiles in the BC products. The mass incorporated at the outer edge of the disk is much greater than anywhere in the disk interior. Repeated visualization of tracer particles at various speeds and disk-to-chamber aspect ratios reveal that the surface bound boundary layer breakdown at disk withdrawal from the liquid phase generates eddies at the disk edge that draw particles into an aggregate cloud greatly enhancing uptake. Numerical analysis and integration of an empirical correlation of thickness of the entrained fluid film attached to the disk surface in the air-phase is proposed to refine the analytical result from infinite plate withdrawal

theory. The empirical correlation promises to capture the influence of gravity on the fluid film and be a more realistic starting point for evaluating the mass profiles of experimental BC products. Finally a set of experiments and a detailed photomicroscopy procedure is presented to visually confirm the rotational rate or tangential velocity dependence on particle uptake.

1. Introduction and Historical Review

The goal of this research is to experimentally determine the hydrodynamics of the rotating disk bioreactor (RDB). Knowledge from this study will be used to develop a model for the incorporation of solids into a growing cellulose pellicle. A review the existing literature is provided to get some understanding of the bacterial species, fluid mechanics, and cellulose surface chemistry. These three areas characterize an operating RDB and the fundamental physical principles of particle uptake.

The biological needs of the organism will define the operating parameters of the system. This species, *Gluconacetobacter xylinus*, produces cellulose from certain feedstocks under a limited range of conditions and it is only within these constraints, ergo in a system producing cellulose, can particles have a growing matrix into which they can incorporate. Fluid mechanics in the RDB describe how particles move about the liquid space, i.e., in the reactor chamber and on the cellulose surface. Particles at the cellulose surface deposit on the cellulose in accordance with their surface chemistry, specifically the non-covalent interactions between the particle and the cellulose fiber. A review of the existing knowledge of these concepts allows for meaningful analysis of the experimental results collected in this research.

1.1 Gluconacetobacter xylinus

The bacterium, *Gluconacetobacter xylinus* (formerly *Acetobacter xylinum)*, has been identified as a non-competitive contaminant in vinegar fermentation (AJ Brown, 1886). It is observed to be a 2 μm long rod shaped bacterium that produces cellulose at the medium surface when grown in flasks containing 50% red wine – 50% water. When grown in flasks of "yeast-water," the cellulose appears at the bottom of the flask.

Most bacterial species that produce extracellular polysaccharides (EPS) are speculated to do so for energy storage as a stress response mechanism. However, an absence of cellulases in the cell-free extracts supports an alternative role that is played by cellulose in these systems (Gromet et al., 1957). Instead, it is believed that the function of bacterial cellulose is to float the viable cells to the air, to protect cells from UV radiation from the sun, and to contain a microenvironment that is inhospitable to competition.

Bacterial cellulose is only found extracellularly. This fact, along with the kinetics of synthesis, suggests that a catalyst for production lies on the outer surface of the cell (Hestrin and Schramm, 1954b). Cell-free extracts of *G. xylinus* do not produce cellulose from glucose (Gromet et al., 1957), which further indicts a membrane bound complex requiring proper orientation and preparation of precursors to create cellulose chains. Several researches have visualized cellulose chains emerging from pores on the cell membrane using freeze-etching and electron microscopy (Brown et al., 1976, Zaar, 1979). The pores are regularly aligned on the longitudinal axis of the cell with an average spacing of 3.8 pores per 100 nm. This corresponds to 0.5 % of the cell wall area contributing to cellulose production. The rate of ribbon elongation was directly measured as 2 μm/min.

There have been many studies on the mechanism of cellulose synthesis. Experiments with radioactive [1-^{14}C]glucose suggests that carbon moves *in vivo* through the following sequence: glucose → glucose 6-phosphate → glucose 1-phosphate → UDP-glucose → cellulose (Swissa et al., 1980). The UDP-glucose is added to the cellulose chain and extruded across the cell wall via transmembrane cellulose synthase complexes. The cellulose synthase is activated by cyclic diguanylic acid (c-di-GMP), which can be deactivated by membrane bound phosphodiesterases. Calcium ion concentration in the bacterial cell regulates the synthase activation/deactivation with the presence of calcium inhibiting c-di-CMP decomposition (Ross et al., 1986, Ross et al., 1987).

The look and structure of bacterial cellulose varies widely depending upon reactor conditions. Pellicles only form at the surface with static conditions. If the surface tension is broken, the pellicle sinks and a new one begins to appear in a day or two. In spite of being chemically identical to plant cellulose, bacterial cellulose pellicles have a much higher Young's modulus. The speculated reasons for this increase in strength are a due to the higher degree of polymerization, the hierarchy of entanglement, and fibril branching resulting from cell division (Iguchi et al., 2000). Agitated cultures, on the other hand, produce a large number of small, reticulated cellulose spheres. The elimination of transport limitations increases cellulose yield, but the reticulated nature of the cellulose limits industrial applications (Hwang et al., 1999, Zuo et al., 2006). The properties of the cellulose product are also adjustable by growing cells in media containing cellulose

fibers. For example, cellulose produced in media containing carboxymethylcellulose has less fiber entanglement and a higher water holding capacity than regular samples (Haigler, 1982).

Important factors for maximizing yield in static culture are pH, temperature, surface area and wall–cellulose interaction. The optimal pH for cellulose production varies between authors, but is always between 4 and 7, and while most research is performed at pH 5 or 6, cellulose production at pH 4-4.5 can give better results because contaminants will not survive. Environmental pH affects membrane structure and permeability and, therefore, substrate uptake and cellulose extrusion (Embuscado et al., 1994). The optimal growth temperature is reported to be 25-30°C (Jonas and Farah, 1997). Static growth will cover the entire surface available in the reactor vessel; so large interfacial area-to-volume ratios are preferred. The vessel wall shape and roughness also play a role in cellulose yield. Smooth chamber walls that taper outwards in the liquid, see Figure 2.1, just at the interface (Hornung et al., 2006b). In other words, growth in a vessel like an Erlenmeyer flask will produce more cellulose that a straight walled beaker.

Glucose is not the only the substrate that can be used as a carbon source for *G. xylinus* metabolism and cellulose production; mannitol (Oikawa et al., 1995a), fructose (Toyosaki et al., 1995), sucrose (Embuscado et al., 1994), arabitol (Oikawa et al., 1995b), and glycerol (Masaoka et al., 1993) are among the polysaccharides that have been proven to be carbon sources for the organism. Feeding cellobiose, the strict monomer of cellulose (a dimer of β-1,4 bonded glucose molecules) produces cellulose with very low yields relative to a glucose-fed control. Several methylated glucose derivatives did not produce coherent cellulose pellicles (Geyer et al., 1994). A broader survey of the utility of glucose derivatives finds that amorphous, non-pellicular cellulose is synthesized as long as C-6 remains a quaternary carbon (Schmauder et al., 1992).

When glucose is used as a carbon source, a number of (keto)gluconates, generally grouped as gluconic acid, are produced. The final pH of experiments run in batch culture with glucose as a substrate, along and mixed with other carbon sources, is always around 3 (Embuscado et al., 1994). As an alternative carbon destination, acid production competes with cellulose for glucose and reduces the yield of an already low-yield process. The culture does not lose viability at pH 3, but usually cellulose production stops. In

pure batch, static culture acid production problems have been mitigated by mutagenesis and clever chemistry. Ionizing ultraviolet radiation induces random mutations in bacteria, some of which are non-acid producing strains that overproduce cellulose compared to the wild type. These mutants are enriched from the population by plating on agar with $NaBr/NaBrO_3$ added. Mutants that produce acid are killed by elemental bromine produced when the acid reacts with the modified agar; non-acid producers survive (De Wulf et al., 1996). Adding acetic acid to the growth media also helps regulate pH. Consumption of acetic acid (pKa = 4.75) will raise the pH to counter the decrease that results from gluconic acid production (Vandamme et al., 1998). The bacteria use acetic acid for metabolic carbon needs, but not cellulose production, therefore including it in the growth media increases cellulose yield from glucose because more glucose carbon goes towards cellulose production while metabolic needs are met by the acetic acid.

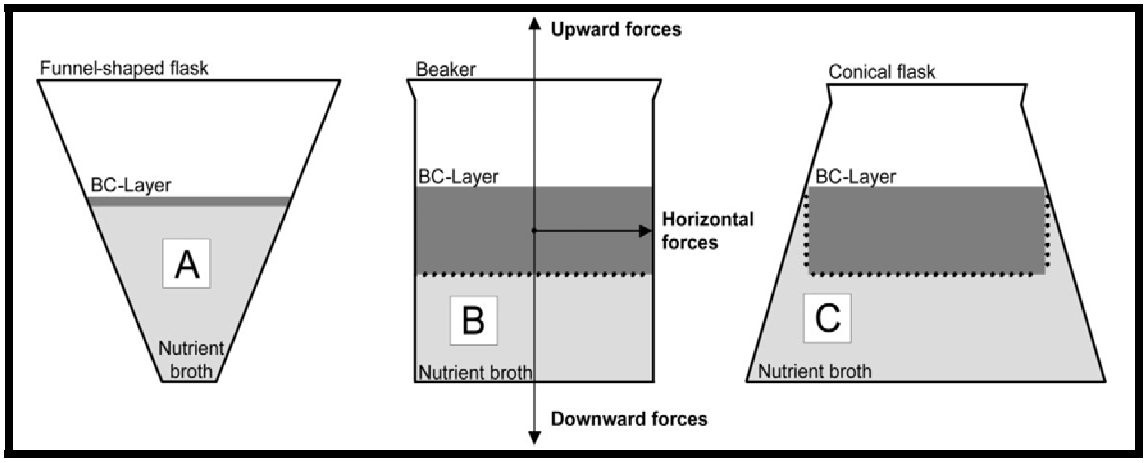

Figure 1.1 Effect of beaker geometry on cellulose production (Hornung et al., 2006b)

1.2 Fluid Mechanics

Serafica (1997) adapts the RDB from the rotating biological contactor (RBC) of the environmental engineering field. RBCs essentially consist of a set of disks, partially submerged in wastewater and partially exposed to air, mounted on a horizontal shaft being rotated by a motor or compressed air (Patwardhan, 2003). Fluid entrained by the disk aerates the liquid media (Bintanja et al., 1975) and at rotational speeds greater than 10RPM, active oxygen transport by the rotating disk dominates passive diffusion at the

surface (DiPalma et al., 2003). Some researchers analyze RBC systems assuming that the liquid film adhering to the disk in the air phase is stripped off and mixes completely with the bulk liquid as the disk reenters the liquid phase (Yamane and Yoshida, 1972; Bintanja et al., 1975). More recent experimental results emphasize the importance of the liquid boundary layer that forms on the disk as it rotates through the liquid phase and suggest this layer is significant to mixing because it must be shed when the disk emerges into the air (Suga and Boongorsrang, 1984) as illustrated in Figure 2.2

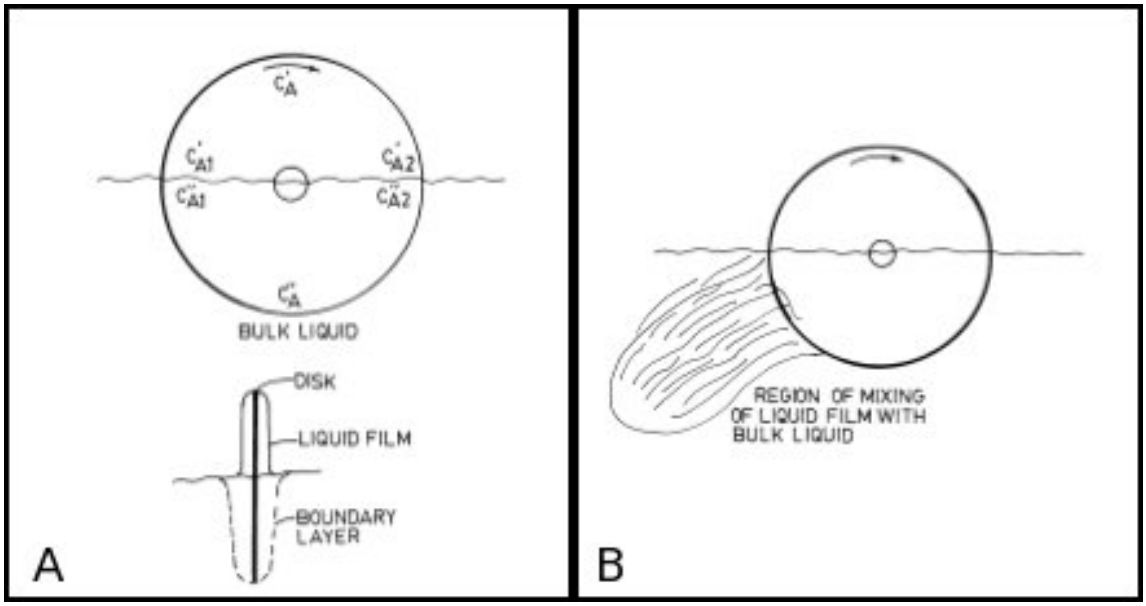

Figure 1.2 Hydrodynamics of RBCs & RDBs: A. Schematic representation of film and boundary layer formation on disk surface, B. Stripping of the liquid film and its subsequent mixing within the liquid (Patwardhan, 2003)

Estimation of the thickness of the entrained liquid film follows flat plate withdrawal theory pioneered by Jeffreys (1930). There are four forces that influence the development of the liquid film on the disk: viscous (μu/h); gravitational (ρgh); capillary (σ/h); and inertial (ρu^2) (Groenveld, 1970c). Important dimensionless groups that characterize the importance of these forces are the film Reynolds number, $\mathrm{Re}_f = \frac{\rho u h}{\mu}$, and the Capillary number, $\mathrm{Ca} = \frac{\mu u}{\sigma}$. Simplifications to the Navier-Stokes equations exist for each physically meaningful combination of forces, and for each, an appropriate solution

is derived. The Navier-Stokes equations for incompressible Newtonian fluids are presented in Equations (2.1) and (2.2).

$$\nabla \cdot \mathbf{v} = 0 \tag{1.1}$$

$$\rho\left(\frac{\partial \mathbf{v}}{\partial t} + \mathbf{v} \cdot \nabla \mathbf{v}\right) = \rho \mathbf{g} - \nabla P + \mu \nabla^2 \mathbf{v} \tag{1.2}$$

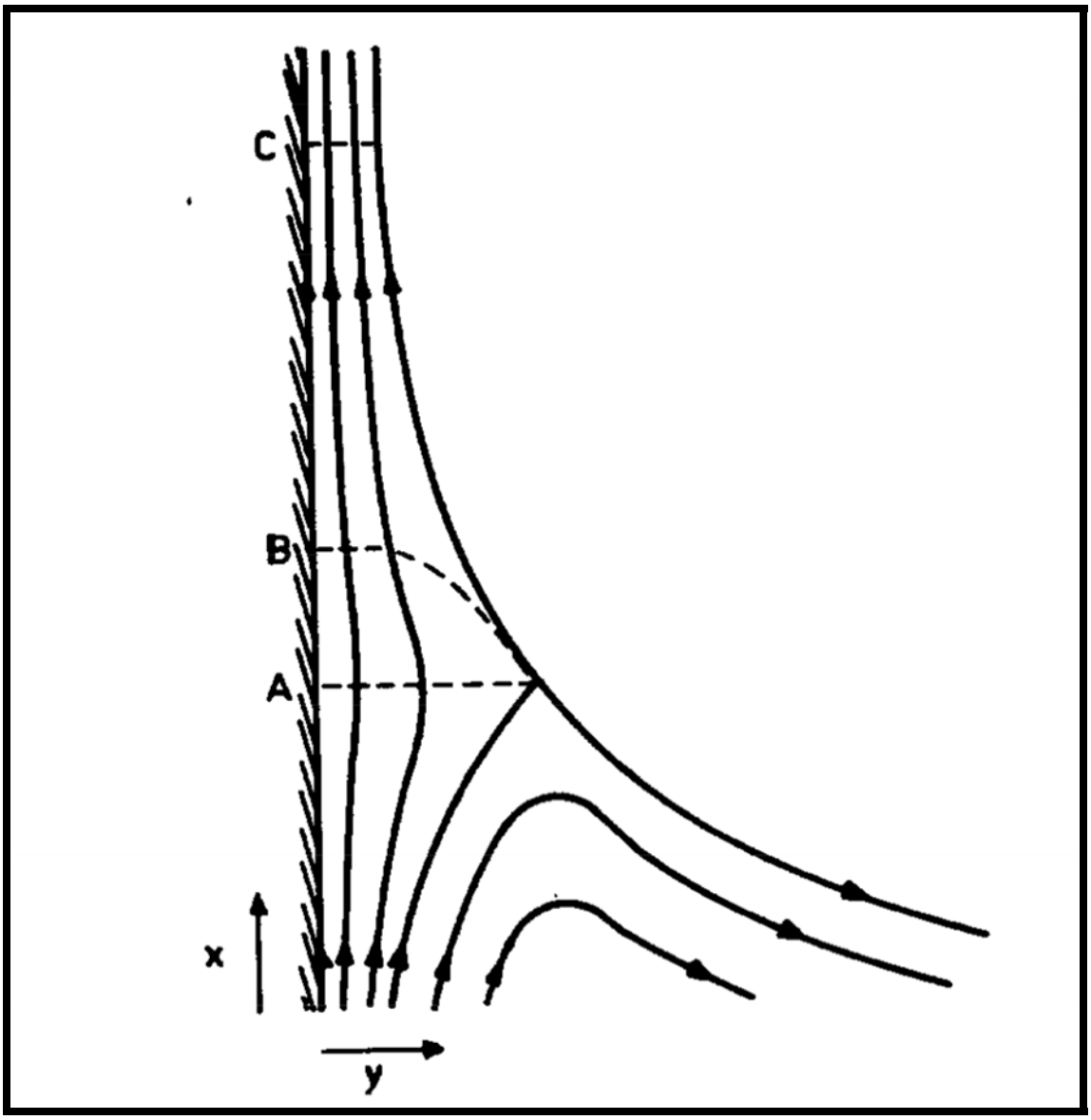

Figure 1.3 Streamlines in the meniscus formed by a plate being pulled from a fluid in the +x direction (Groenveld, 1970a)

The starting point for all the derivations of the thickness of the fluid film is that the action of moving the plate out of the fluid creates streamlines in the meniscus like those

shown in Figure 2.3. There are two characteristics of this assumption: at an intermediate height, there is a stagnation point on the fluid-air interface, and, far from the surface, there is plug flow. There is a four step method to deriving the entrained film thickness: 1) simplify Equations (2.1) and (2.2) based on assumptions about the contributing forces; 2) solve for the fluid flux per unit length through the cross section at the stagnation point (e.g., plane A in Figure 2.3); 3) set this flux equal to the flux through a cross section in the plug flow region (e.g., plane C Figure 2.3); and 4) solve for film thickness. An early treatment of this problem makes use of the lubrication approximation (i.e., the thickness dimension is much smaller than the plate length, h/L << 1, and small inertial forces) and assumes gravity is negligible compared to surface tension (Landau and Levich, 1942). In this regime, capillary forces dominate. The simplified Navier-Stokes equation is as follows:

$$\mu \frac{\partial^2 u}{\partial y^2} - \rho g + \sigma \frac{d^3 h}{dx^3} = 0 \qquad \textbf{(1.3)}$$

where the boundary conditions are: no slip at the wall; no tangential forces on the interface; no capillary pressure at the transition to the flat film (bulk liquid-meniscus boundary); and finite negative pressure at the transition to the stationary meniscus (meniscus-liquid film boundary) (Groenveld, 1970b).

The resulting fluid thickness profile is:

$$h_0 = 0.944 \frac{(\mu u_0)^{2/3}}{\sigma^{1/6} (\rho g)^{1/2}} \qquad \textbf{(1.4)}$$

where h_0 is the ultimate film thickness, u_0 is the plate velocity, and σ is the surface tension (White and Tallmadge, 1965). The assumption that capillary forces dominate gravitational forces can be shown to be valid as long as $Ca < 10^{-3}$ (Groenveld, 1970b). It is common to express the entrained film thickness as a dimensionless variable, T_0, defined as follows:

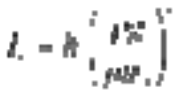

The dimensionless Landau-Levich result is:

$$T_0 = 0.944\ \mathrm{Ca}^{1/6} \tag{1.5}$$

The film thickness result in Equations (2.4) and (2.5) are not valid in situations where the influence of viscous forces dominates the influence of capillary forces. To find a solution in this regime, small Re and large Ca, singular perturbation linearization is applied to Equation (2.3). The resulting approximate solution contains the film thickness implicitly as seen in Equation (2.6) (White and Tallmadge, 1965):

$$\frac{T_0}{\left(1-T_0^2\right)^{2/3}} = 0.944\mathrm{Ca}^{1/6} \tag{1.6}$$

There is a trade-off in Equation (2.6) between the broader range of applicable Ca and solution accuracy. Starting at the Navier-Stokes equations and neglecting the inertial terms (i.e., left hand side of Equation (2.2)) will reach a more precise solution to the film profile thickness at higher Ca. The boundary conditions for this situation are: no slip at the wall; no tangential forces at the interface; and constant pressure at the interface. The resulting thickness, absent capillary forces, is (Groenveld, 1970a):

$$h_0 = 0.66\left(\frac{\mu u_0}{\rho g}\right)^{1/2} \text{ or } \mathrm{T_0} = 0.66 \tag{1.7}$$

The final regime to understand is the situation when inertial forces are significant, such as during fast withdrawal of a low-viscosity fluid. The simplification of the Navier-Stokes equation is preceded by a two-step scaling analysis. 1. The Fourier number, $\mathrm{Fo} = \frac{\mu t}{\rho h_0^2}$, as a ratio of the penetration depth of momentum to the distance momentum must transfer is order 1 because through the meniscus, momentum transfer decelerates the fluid from u_0 to zero below the stagnation point and from 0 back to u_0 above it. 2. By defining a dimensionless length $n = l/h_0$, where l is the vertical distance above the bulk surface required to change the velocity profiles, the following rearrangement of Fo shows Re is proportional to n:

$$\mathrm{Fo} = \frac{\mu t}{\rho h_0^2} = \frac{\mu\left(l/u_0\right)}{\rho h_0^2} = \frac{\mu\left(n h_0\right)}{\rho u_0 h_0^2} = \frac{n}{\frac{\rho u_0 h_0}{\mu}} = \frac{n}{\mathrm{Re}} \approx 1$$

The significance of this relationship is that for high Re withdrawal, n will be high and l can be modest considering how very small h_0 is. In other words, plug flow is assumed

throughout the meniscus and the corresponding simplification to the Navier-Stokes equations is shown in Equation (2.8):

$$\mu \frac{\partial^2 u}{\partial y^2} = \rho g \tag{1.8}$$

The boundary conditions and the condition that determines the location of the stagnation point are: no slip at the wall; no tangential forces at the interface; and zero velocity at the interface. The terminal thickness that results in this situation is (Groenveld, 1970c):

$$h_0 = 0.52\left(\frac{\mu u_0}{\rho g}\right)^{1/2} \text{ or } T_0 = 0.52 \tag{1.9}$$

The operating conditions and fluid properties define three regions where a different force dominates the film forming behavior as a plate is pulled from a bulk liquid. Two dimensionless groups, Re and Ca, are used to describe the strength of these forces. The regimes and dimensionless thickness solutions are listed in Table 2.1 and displayed graphically in Figure 2.4.

Table 1.1 Withdrawal theory regimes of applicability (Groenveld, 1970c)

Regime	Film Thickness	Influencing Force
Re « 1, Ca « 1	$T_0 = 0.944\ Ca^{1/6}$	Capillary
Re « 1, Ca » 1	$T_0 = 0.66$	Viscous
Re » 1	$T_0 = 0.52$	Inertial

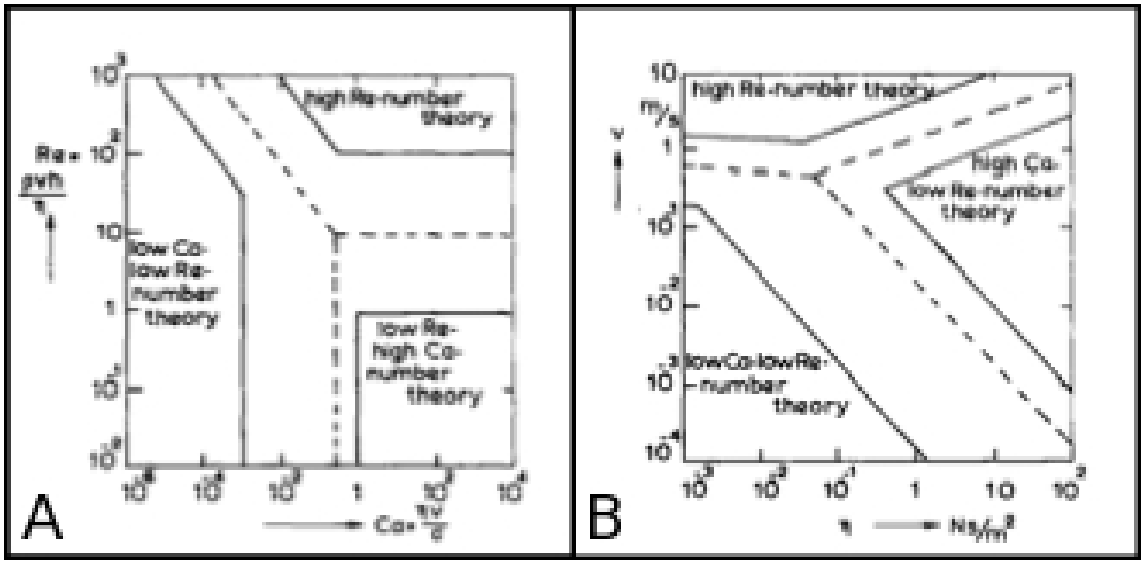

Figure 1.4 Regions of applicability of the three withdrawal theories: A) Plotted as Ca vs Re; B) Plotted as μ vs u_0 for ρ = 1000kg/m^3 and σ = 0.7N/m (Groenveld, 1970c)

1.3 Electrostatic Properties of Cellulose

The atomic composition and arrangement of cellulose make it a very chemically active species. The cellulose monomer, cellobiose (shown in Figure 2.5) is characterized as having a fixed dipole oriented towards the C1 carbon (i.e., the carbon involved in two ether bonds) and numerous hydroxyl groups that are available for hydrogen bonding.

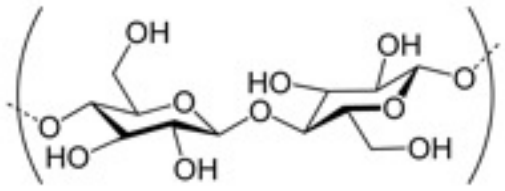

Figure 1.5 Cellobiose (cellulose monomer)

The hydroxyl groups around the glucose rings lie in the equatorial conformation, and form planar hydrogen bonding networks, as illustrated in Figure 2.6. The C-H bonds, oriented axially, create hydrophobic regions above and below the plane of the ring as shown in Figure 2.7. In the homogenous surroundings of a cellulose network, this multiplicity of bonding sites provide the great mechanical strength for which cellulosic

materials are known. At the matrix surface, a particle of most any compositions is expected to experience an attraction to the cellulose.

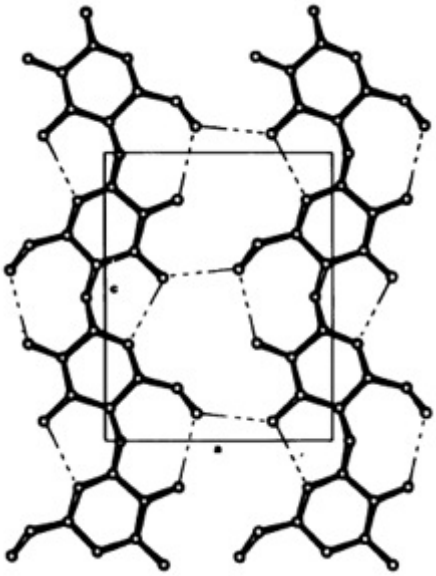

Figure 1.6 Inter- and intra molecular hydrogen bonding between cellulose chains (Ross et al., 1991)

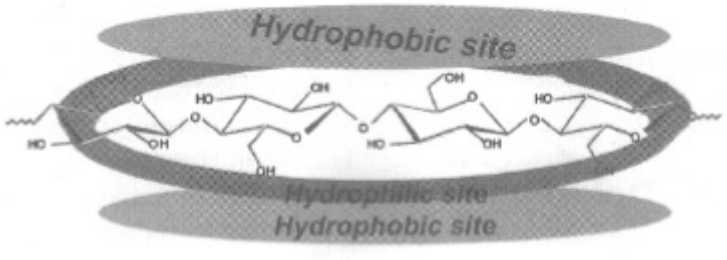

Figure 1.7 Hydrophilic and hydrophobic regions surround cellulose chains (Kondo, 2005)

Bastidas et al. (2005), functionalized AFM tips with either –OH, -CH_3, or –COOH groups and measured the pull-off force from cellulose fibers and regenerated cellulose films over a range of pH. In the relevant pH range of *G. xylinus* growth (4-7), they observe similar forces between the cellulose surface and the –OH and –CH_3 tips. Figure 10 shows their adhesion force results for the –OH tip and a synthetic –OH functionalized model surface. Their results for interactions between modified tips and cellulose fibers are shown in Figure 2.8 and Figure 2.9.

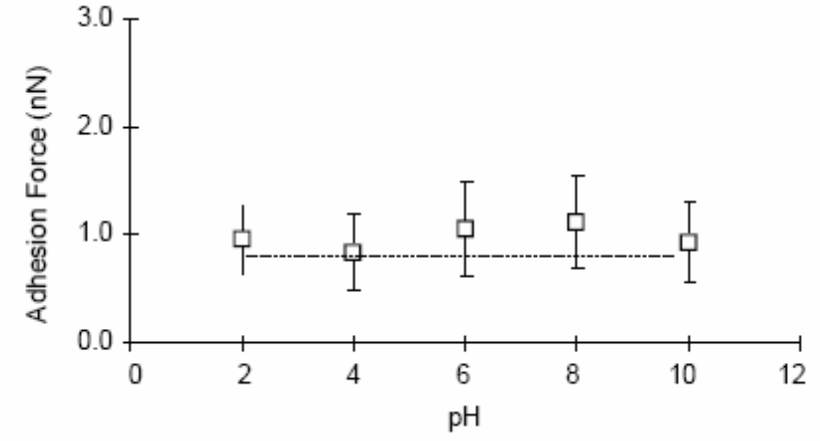

Figure 1.8 Interactions between -OH AFM tip and -OH model surface

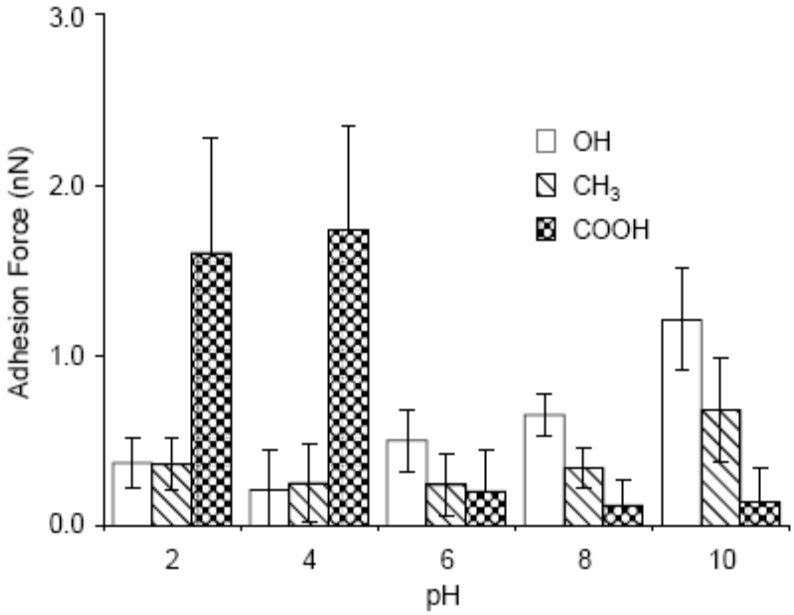

Figure 1.9 Interactions between modified AFM tips and cellulose fibers

2. Materials and Methods

The experiments in this research are performed to understand three things: how the fluid motion affects bacterial cellulose (BC) growth on the rotating disk, how the fluid motion affects particle location and transport throughout the liquid phase; and how the Van der Waals interactions between the particles and BC surface affect incorporation.

2.1 Gluconacetobacter xylinus

Two strains of *G. xylinus* are explored in this study: ATCC 23769 and 23770. The former is maintained in complex and minimal media, whereas, the latter in complex media only. All static cultures are subcultured at 10 to 14 day intervals in 100mL media in Erlenmeyer flasks. These are maintained in an incubator at 30°C. Samples of all three lines are periodically placed in long term storage vis-à-vis 50% glycerol (Sigma G6279)-50% inoculum stored at -80°C.

2.2 Growth Media

The two tables below (Table 3.1 and Table 3.2) list the composition of one liter of the respective media. The pH of the media is adjusted to 4.2 ± 0.5 prior to autoclaving.

Table 2.1 Components of minimal and complex media

Compound	Complex media (Mormino 2002) (g)	Minimal Media (Forng 1989) (g)	Supplier	Catalog #
Ammonium Sulfate	5	-	Sigma	A5123
Ammonium Chloride	-	1	Acros	199975000
Disodium Phosphate	2.7	2.7	Fluka	71642
Magnesium Sulfate	1	0.25*	Sigma	M-1880
Potassium Chloride	-	0.1	Fisher	S77375-1
Yeast Extract	0.5	-	Sigma	Y-0375
Bactopeptone	0.5	-	BD	211677
Citric Acid	1.2	1.15	Sigma	251275
Glucose *	50	1	Sigma	G8270
Trace Elements (mL)**	2	-	-	-
Cycloheximide (mL)**	10	-	Fluka	01810
Nicotinamide (mg)**	-	7.5	Fluka	72340
* Autoclaved separately				
** Filter Sterilized				

Table 2.2 Trace Elements

Component	Amount (mg)	Supplier	Catalog #
EDTA Tetrasodium Salt	570	Sigma	03695
$FeSO_4 + 7\ H_2O$	200	Sigma	215422
$ZnSO_4 + 7\ H_2O$	10	Sigma	Z4750
$MnSO_4 + H_2O$	26	Sigma	63141
H_3BO_3	30	Sigma	B2645
$CoCl_2 + 6\ H_2O$	20	Sigma	31277
$NiCl_2 + 6\ H_2O$	3.2	Sigma	13613
$(NH_4)6Mo_7O_{14} + 4\ H_2O$	2.4	Sigma	431346
DI Water (mL)	1000	-	-

2.3 Rotating Disk Bioreactor

2.3.1 Configurations

The rotating disk bioreactors (RDBs) in this study are based on the reactors of Serafica (1997) and Mormino (2002): 12cm perforated plastic disks are mounted to a 6.4mm shaft and rotate in a 15.3cm I.D. cylindrical chamber. There are four reactor designs in this research: the conventional design inherited from the previous work, the simple, hinged RDB (SH-RDB); the single-chamber hinged, ported RDB (SCHP-RDB); the dual-chamber hinged, ported RDB (DCHP-RDB); and the single-chamber glass RDB (SCG-RDB). The evolution of RDB design arrives from the necessity of increasing experimental complexity. The features and purpose of each RDB is elucidated in the following sections. The chambers are all 10.8cm in length, thus a 1 L reservoir volume. A range of rotational speeds is studied using the following synchronous AC gear motors from McMaster-Carr: 9, 12, 16, and 24 RPM. A programmable stepper motor is used, as well.

2.3.1.1 Simple Hinged Rotating Disk Bioreactor

The original implementation of the RDB is a horizontal cylinder with a hinged lid, divided into chambers in which disks can rotate on an axial shaft driven by a motor. Serafica (1997) and Mormino (2002) introduce and characterize this reactors type, labeled here the simple, hinged rotating disk bioreactor (SH-RDB). The SH-RDB is suited for unmeasured batch operation, but can be extended to open-loop, fed-batch operation by accessing the chamber contents by opening the lid. Mixing in the SH-RDB is poor for most particles studied because fluid agitation primarily occurs by the rotation of the disk through the liquid phase. Additional mixing is achieved with a stir plate, but stir-bar size is limited to 1.3cm due to the curvature of the cylindrical reactor wall. A CAD drawing of a two chamber SH-RDB is shown in Figure 3.1.

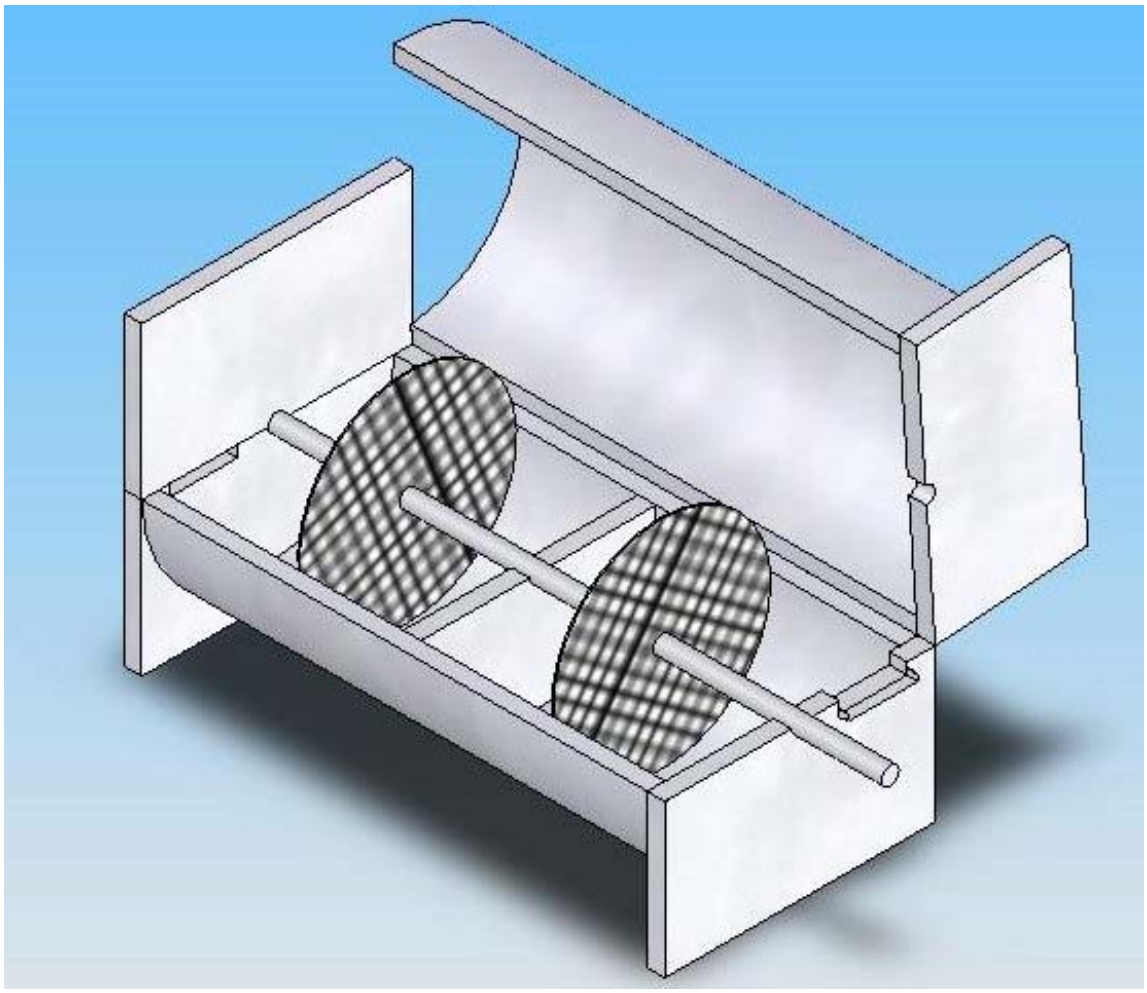

Figure 2.1 Simple Hinged RDB with two chambers

2.3.1.2 Single-chamber Hinged, Ported Rotating Disk Bioreactor

A reactor design improvement suggested by Mormino (2002) is the addition of a pump-around fluid recirculation system to improve mixing of particles in the liquid phase. The first reactor of this type has one chamber, ports for recirculation, and is designated as a test unit for subsequent design variations. This reactor is labeled the single-chamber hinged, ported RDB (SCHP-RDB) and is shown in Figure 3.2. Not shown are the copper nipples on the inside of the return ports for the mounting of tubing and nozzles to manipulate the path and speed of the return stream. The SCHP-RDB is used to test return stream configurations to maximize bulk liquid agitation. In addition to improving fluid agitation, the ports provide the capacity for continuous operation. The SCHP-RDB also tests measurement device integration directly to the reactor, devices such as a pH probe, a thermocouple, and an IR-LED BC thickness sensor.

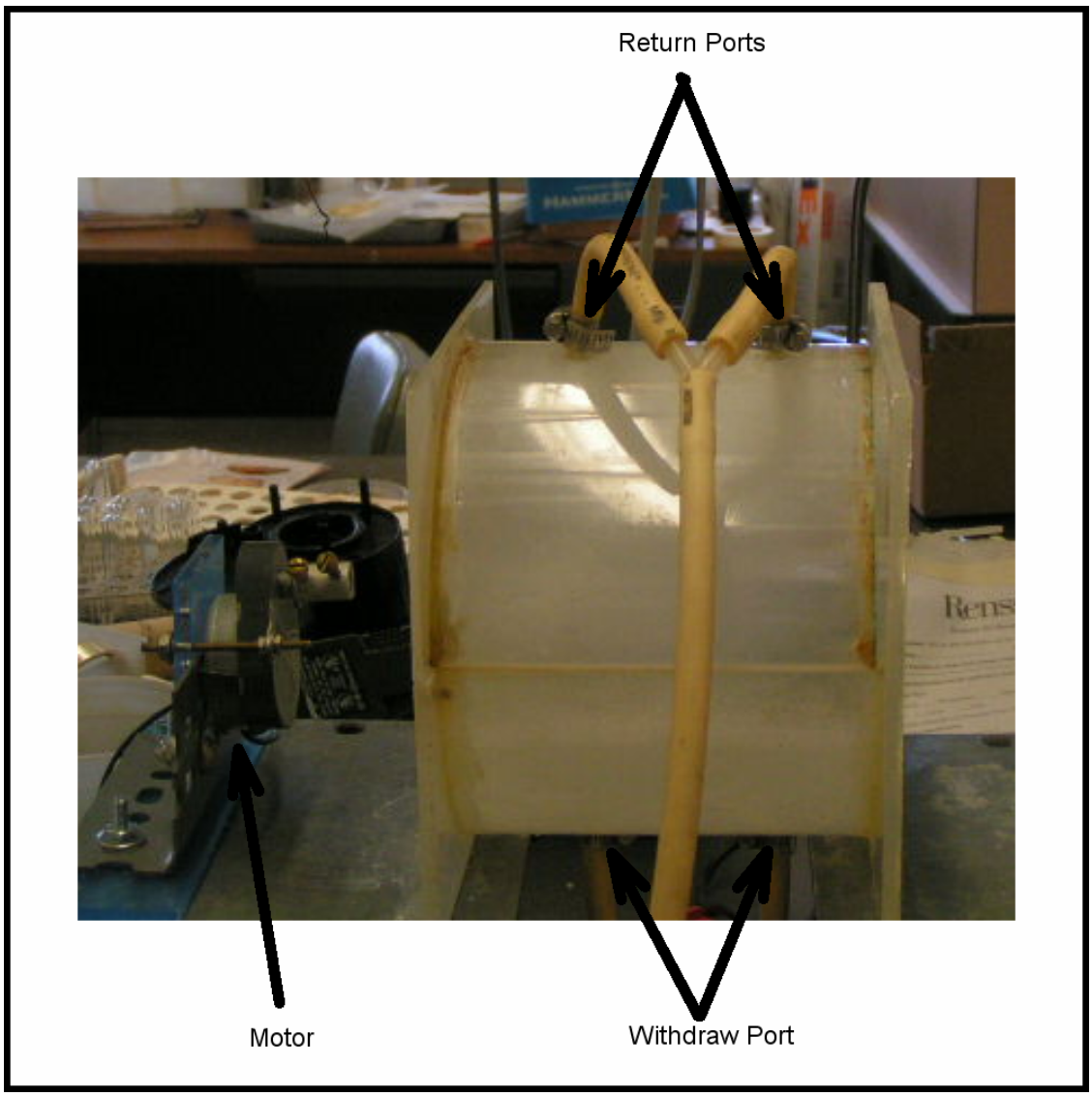

Figure 2.2 Single-chamber Hinged, Ported RDB

2.3.1.3 Dual-chamber Hinged, Ported Rotating Disk Bioreactor

The pump around configuration that provides the best mixing returns the fluid to the chamber through a constricting nozzle along the cylindrical reactor bottom. An experimental version of this design is shown in Figure 3.3, which also shows the internal piping and nozzle orientations featured in this study: "counter" and "parallel" directed jets, and is labeled the dual-chamber hinged, ported RDB (DCHP-RDB). The second chamber is a control that is run in parallel to the test chamber with a single experimental variable left in a default state. For example, by initializing both the test and control chambers identically, but not agitating the control the effect of agitation on particle

distribution in the BC product is isolated. The DCHP-RDB is typically operated in batch or fed-batch mode with periodic measurements and control adjustments enabled by opening the reactor lid.

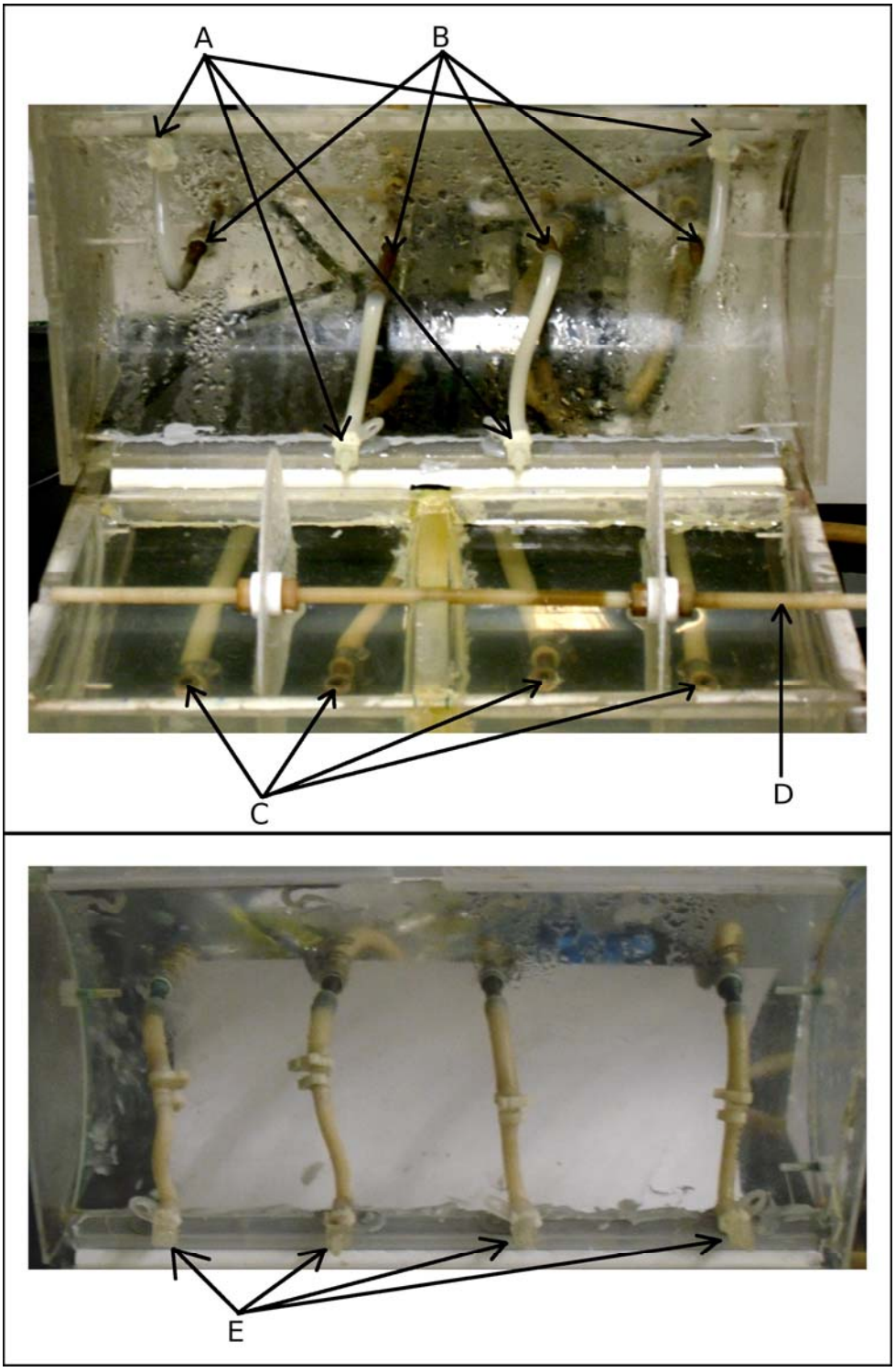

Figure 2.3 Dual-chamber Hinged, Ported Rotating Disk Bioreactor (A. Jet nozzles in "counter" orientation; B. Inlet port brass nipples; C. Withdrawal ports; D. Rotating shaft with disks; E. Jet nozzles in "parallel" orientation)

2.3.1.4 Single-chamber Glass Rotating Disk Bioreactor

An RDB specifically designed for closed-loop operation is the single-chamber glass RDB (SCG-RDB). The reactor chamber is not accessible during operation, but instead a measurement chamber is located in the recirculation path where a thermocouple, pH, and/or other probes access the media. Instead of having a hinged top, the SCG-RDB has a removable end that is bolted to the cylindrical chamber over an o-ring. Both the fixed and free end plates have ports. This reactor was specifically designed and fabricated for measurement and control studies. Matching plates mounted with alternating rare-earth magnets are used to drive the disk rotation through the glass wall. A CAD drawing of the SCG-RDB is shown in Figure 3.4.

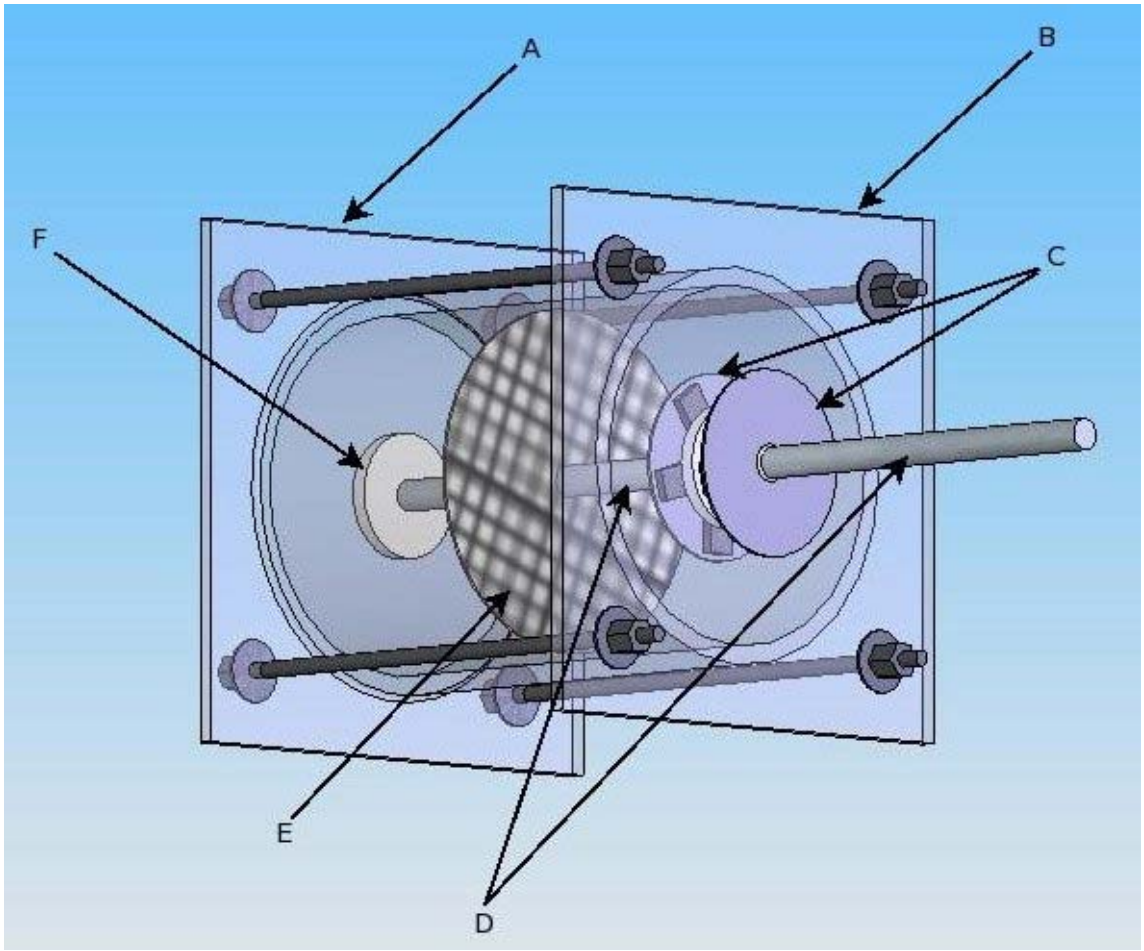

Figure 2.4 Single-chamber Glass Rotating Disk Bioreactor (A. Fixed End Plate; B. Free End Plate; C. Inner and Outer Stainless Steel Disks with Alternating Magnets; D. Inner and Outer Shafts; E. Plastic Disk; F. Glass Bearing)

2.3.2 Sterilization

The SH-RDB is sterilized by leaving it overnight in a germicidal UV chamber with the disk and shaft in place. A bleach solution, 0.75%, is used to sterilize the SCHP-RDB and the DCHP-RDB along with the recirculation tubing. The solution is made by adding 2mL of 15% bleach (Sigma 425044) to 1L of water in the chamber. After thirty minutes of bleach exposure, the chamber and tubing are rinsed multiple times with autoclaved water. The rinse water needs to be cooled to below 50ºC to avoid warping of the plastic reactor vessel. The SCG-RDB is sterilized by circulating water at 70°C for 30 minutes. These methods are designed to also sterilize the tubing and other apparatus that complement each setup.

2.3.3 Closed-Loop RDB

As previously noted, the single-chamber glass RDB is specifically designed for closed-loop studies. The piping and instrumentation diagram (P&ID) for the closed-loop apparatus is shown in Figure 3.5. The terms in the P&ID are explained in Table 3.3.

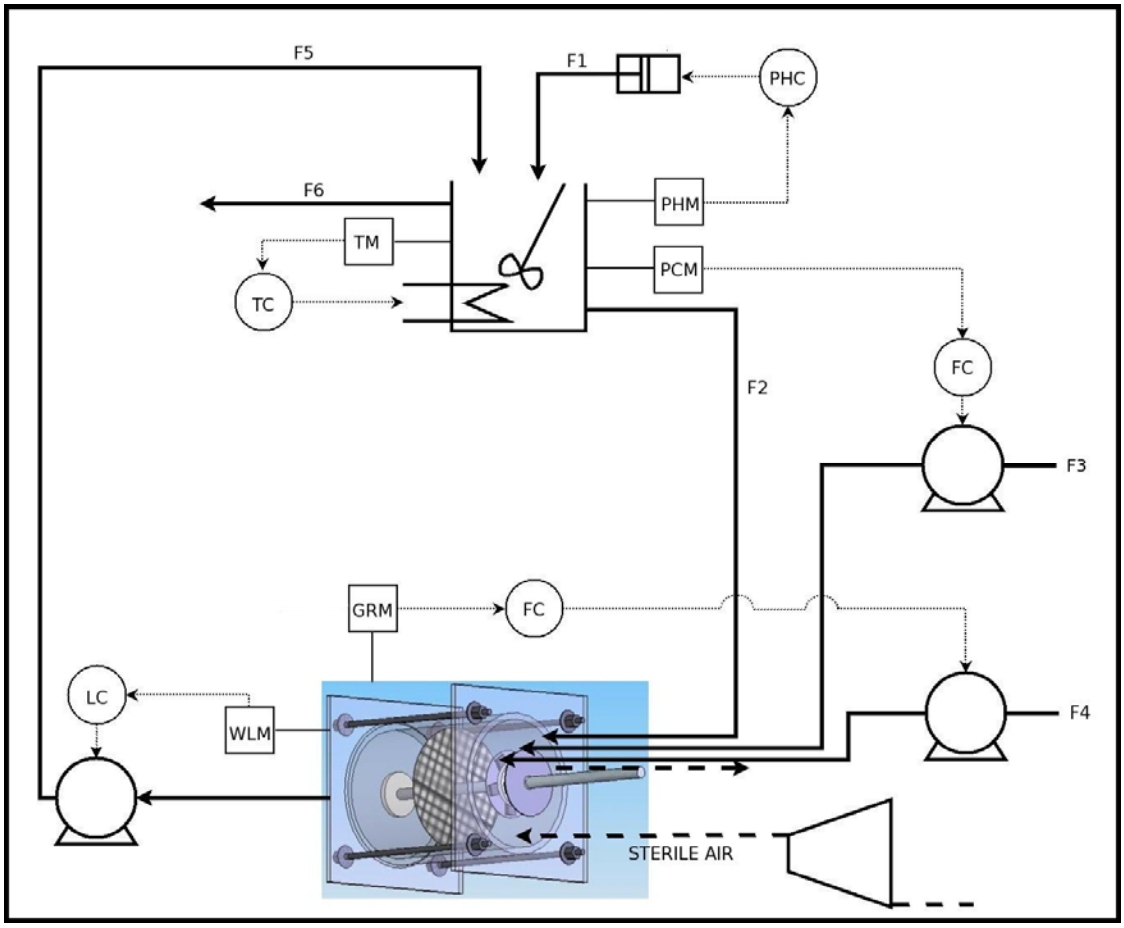

Figure 2.5 P&ID for closed-loop RDB

Table 2.3 P&ID terms for Closed-loop RDB

Term	**Meaning**	**Term**	**Meaning**
TM	Temperature Measurement	F1	Caustic Feed
TC	Temperature Controller	F2	Mixer Return
PHM	PH Measurement	F3	Particle Feed
PHC	PH Controller	F4	Media Feed
PCM	Particle Concentration Measurement	F5	Recirculation
FC	Flow Controller	F6	Waste Effluent
GRM	Growth Rate Measurement		
WLM	Webcam Level Measurement		
LC	Level Controller		

2.4 Particles

An array of particles is studied by size, surface chemistry, and medium pH to address a suitable range of phenomena involved in the particle uptake problem. The particles studied are listed in Table 1.4.

Table 1.4 Particle size and surface characteristics

Particle	Functional Group	Size (μm)	pKa/pI	Charge @ pH 5	Charge @ pH 7
Activated Carbon	$-CH_3$	< 150	1.5-6.0	+/0	-
Acetylated CPG	$-COCH_3$	150	N/A	-	-
Amine CPG	$-NH_2$	150	8.5	+	+
Basic Alumina	Al_2O_3	43-234	7.0-9.0	+	-
Jeweler's Rouge	SnO	N/A	4.0-4.5	+/0	-
Q Sepharose FF	$-N^+(CH_3)_3$	45-165	N/A	+	+
SP Sepharose FF	$-SO_3^-$	45-165	N/A	-	-
Silica Gel (643)	-OH	35-60	1.7-3.5	-	-
Silica Gel (646)	-OH	250-500	1.7-3.5	-	-
Silica Gel -CVL	$-C_6H_3N^+(CH_3)_3$	N/A	N/A	+	+

2.4.1 Silica Gel Preparation

The primary silica gel particle of study is Davisil grade 643 (Sigma 23610), because of its size distribution relative to the incorporated range reported by Serafica (1997). Two other grades are also studied to compare the effect of particle size and pore size (see Table 3.5). In aqueous media silica gel particles swell and shift the size distribution slightly higher than reported by the manufacturer.

Table 2.5 Silica Gel

Davisil Grade	Size Range (μm)	Pore Size (Å)	Sigma Catalog #
643	35-70	100	23610
633	35-70	60	236772
646	250-500	150	236845

There are two techniques used for staining silica gel with the goal of easing and enhancing visualization of the composite product. The first attaches chromate to the silica by the following three-step process (Rislove, 1988):

1. Combine 0.5g $K_2Cr_2O_7$ + 10mL 3M H_2SO_4 + 10mL DI H_2O + heat to dissolve crystals.

2. Mix 1mL chromate solution per 600m^2 silica gel surface area.

3. Heat mixture and stir to dryness. Allow to cool in a sealed container.

The silica gel is stained orange and undergoes an orange-to-green color change when exposed to ethanol.

A second, more stable, stain, binds crystal violet lactone (CVL; Sigma 332488) to silica gel in two steps (Turner, 1962 and Wolcott, 1988):

1. Prepare a 2 % (w/v) solution of CVL in chloroform.

2. Mix in excess CVL solution with silica gel and let dry in the fume hood

A 50μm silica hydrophobic aerogel is also used. The aerogel can be made hydrophilic with heat treatment at 300ºC for three hours to decompose the hydrophobic surface groups.

2.4.2 Controlled Pore Glass Preparation

To investigate the role of chemistry on particle adsorption, 420μm controlled pore glass (CPG, Biosearch Technologies BG5-2000) is used as a solid support for surface modification. The vendor supplies both native and aminopropyl beads. The following procedure adds an acetyl functionalization to the amine:

1. Mix aminopropyl CPG in a solution of 3% (w/v) pyridine in acetic anhydride at room temperature for 18hrs.

2. Wash beads six times with acetone. Let air-dry.

2.5 Cellulose Growth Rate

The production of bacterial cellulose (BC) is measured both in terms of changing sample thickness and also on a mass basis.

2.5.1 Thickness Determination

There are three methods of measuring BC thickness: image analysis; "blob tracking"; and physical probing. The imaging method is based on comparing the BC gel with a reference object captured in the image's field of view, such as the ruler in Figure 3.6; this method is further explained in Section 3.7. The blob tracking method uses a USB webcam interfaced to LabView using the NI Vision Builder for Automated Inspection package as its image analysis software to follow a laser pointer spot on the growing BC surface. As seen in Figure 3.7, as the BC gel grows, the spot, projected at an angle θ to the surface normal, will appear to move upwards from the perspective of the webcam looking directly at the BC gel.

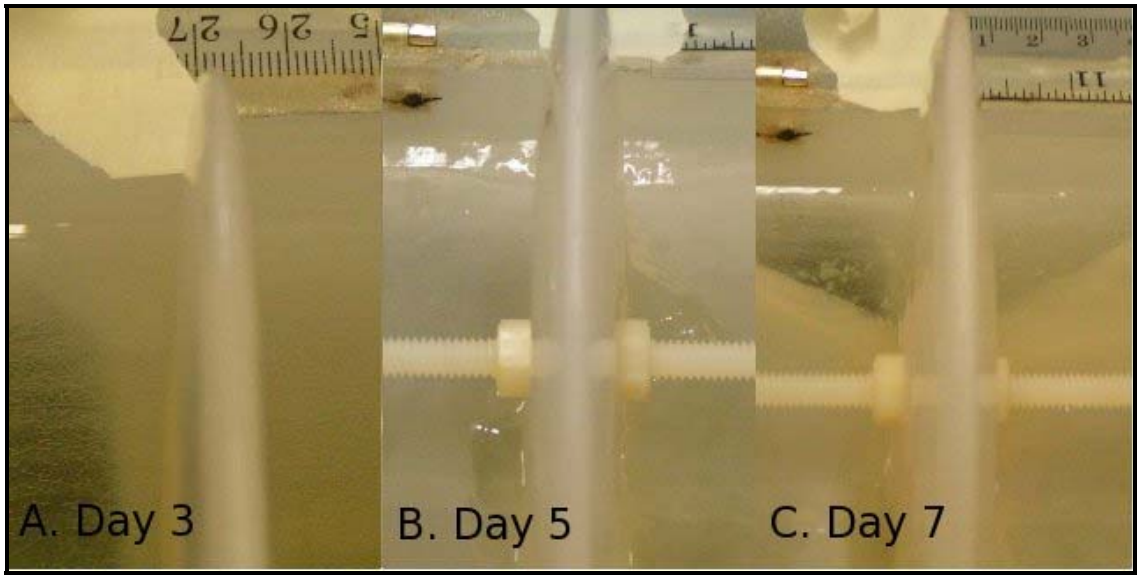

Figure 2.6 An image sequence of RDB BC to be measured by image analysis software

The blob tracker is calibrated by tracking a white disk made of cardstock moving in known increments before the experimental trial begins. It is important to keep the position of the light source, webcam, and reactor vessel fixed once it has been calibrated. The LabView algorithm stores the calibration data (Δt_c and Δy_c) and calculates BC thickness (Δt_{BC}) from the measured spot movement (Δy_{meas}) according to the proportional relationship in Equation (3.1).

$$\Delta t_{BC} = \frac{\Delta t_c}{\Delta y_c} \Delta y_{meas} \tag{2.1}$$

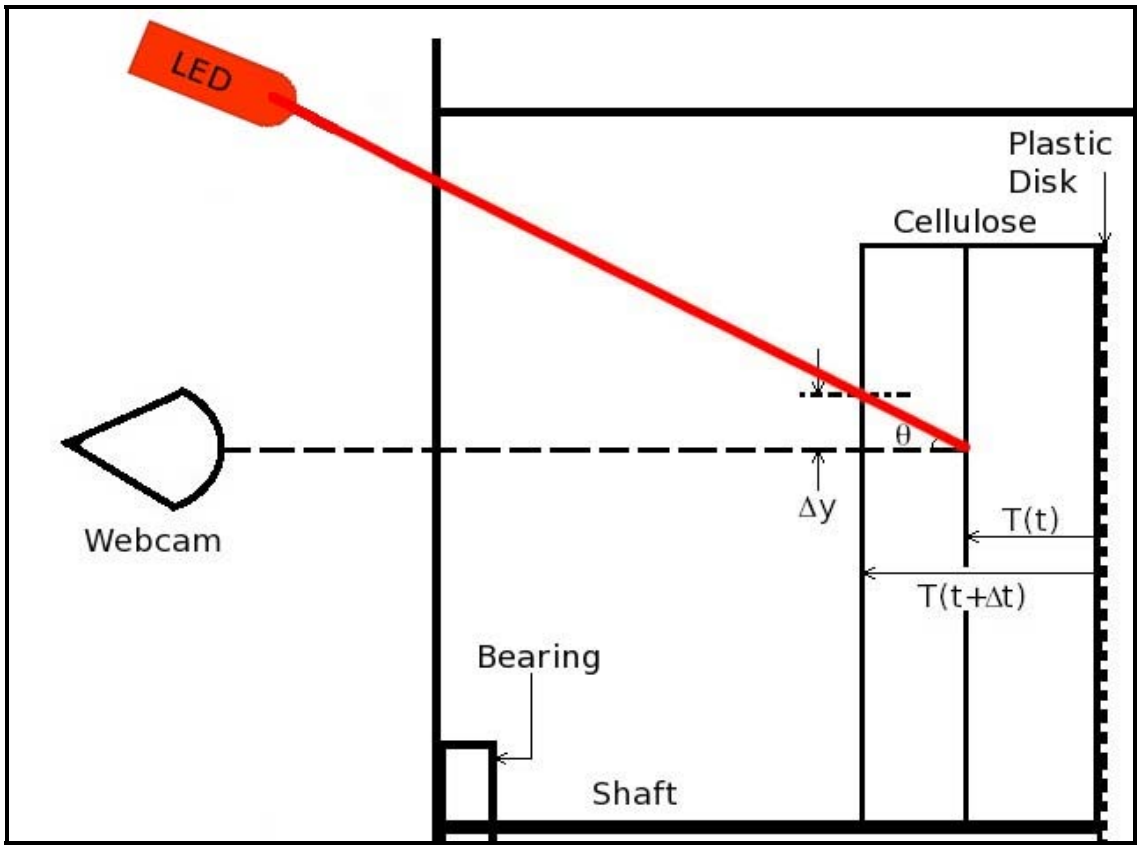

Figure 2.7 Schematic diagram of the "blob tracking" BC thickness measurement technique

The probing method of BC thickness measurement uses the device in Figure 3.8A, which mounts to the reactor chamber divider; therefore it is only applicable to SH-RDB, SCHP-RDB, and DCHP-RDB. An advantage to direct probing over image analysis or blob tracking is that the BC thickness profile along the radius can be measured. To obtain absolute thickness data, the baseline distance to the plastic disk must be measured before beginning the experiment. The actual quantification of the measurement is performed with a caliper measuring the distance between the darkened lip at the back of the probe and the anterior nut on the jig.

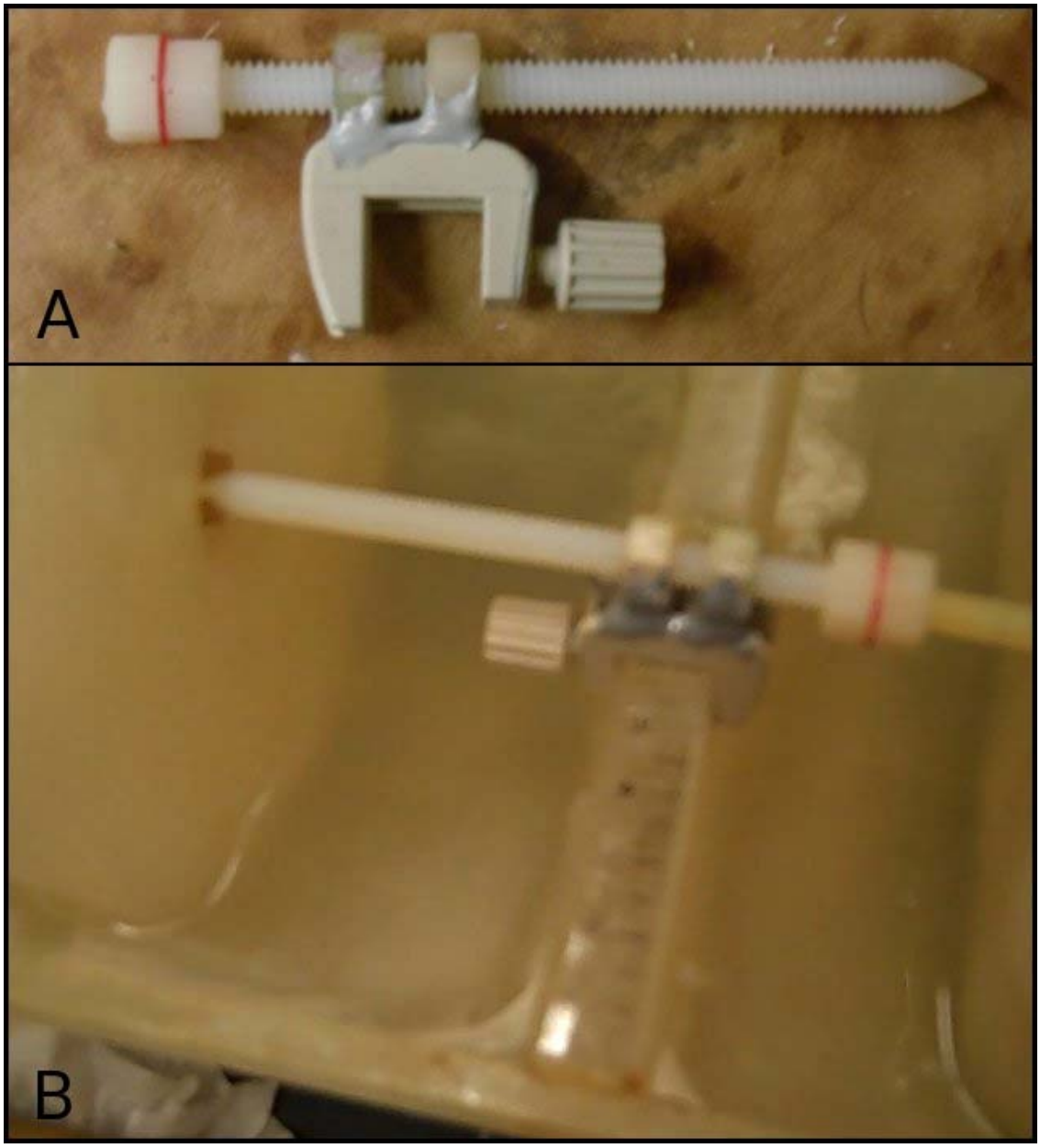

Figure 2.8 A. Device for measuring local BC thickness; B. Device in-use, mounted on ruled reactor chamber divider

2.5.2 Mass Determination

The mass-based growth rate of the BC gel is determined by drying and ashing cork bore samples of the BC at regular intervals. A size 14 cork borer, sharpened regularly, is used to collect at least two BC samples at each time point. To account for non-uniformity of the extracted cellulose samples, they are digitally photographed prior to ashing and the mass data is normalized by sample area.

2.6 Particle Distribution

2.6.1 Segmented Ashing

After harvesting, the gels are dried on wax paper and the dimensions of the gels are measured with a vernier caliper. A template of concentric annuli is created in MATLAB (Mathworks, Inc). A typical gel template is divided into ten annular segments, either based on constant spacing or constant annular area. The template is traced onto the dried cellulose (see Figure 3.9), which is then cut into annuli. Each annulus is digitally photographed for *post hoc* area measurement, placed into a crucible, dried and ashed. The mass of particles incorporated into the trial annulus is calculated by subtracting away the mass of the control annulus of the same radial position.

Figure 2.9 Dried gel with traced annuli. Also drawn are locations of cork bore samples that were taken from this gel

2.6.2 In Situ Visualization

A technique for direct visualization of particles in BC is to place the harvested gel on top of a pellicle growing in a sufficiently large static reactor, for example an eight quart steel pot. After allowing the active bacteria in the host pellicle to grow through the experimental gel's cellulose matrix, the entire fused product is draped over the open end of a glass cylinder. This hybrid cellulose pellicle that dries without a backing is then re-wet, thereby, as in Figure 3.10, making the cellulose translucent and making stained particles easy to see.

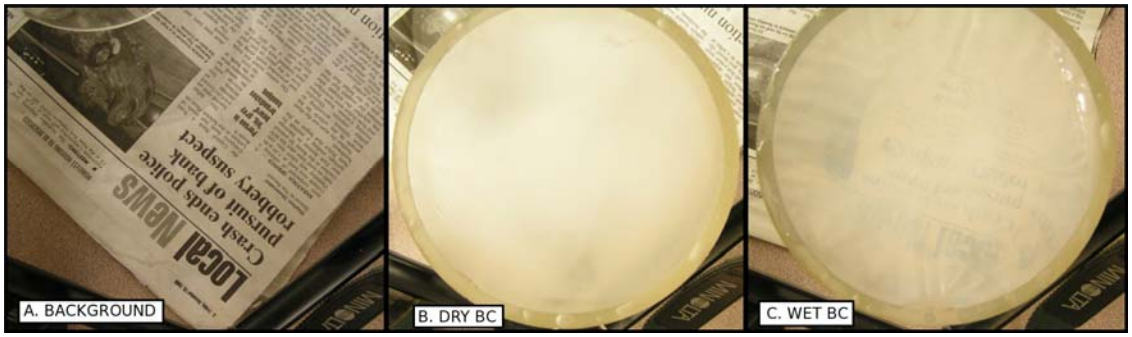

Figure 2.10 Translucence of wet BC. A: Background image. B: Dry, opaque BC. C: Wet, translucent BC.

2.6.3 Photomicroscopy

Another direct method for the determination of particle size and location distributions within a bacterial cellulose product is microscopy. Normally, two slides are prepared from each RDB BC gel: a bird's eye view and a cross section in the tangential direction. Preparation of the latter is outlined in the schematic diagram, Figure 3.11. Two scalpels fixed together are used to cut thin slices from the harvested RDB BC. Particle identification is performed using phase contrast microscopy with a 20x objective. This magnification shows 0.24mm^2. To cover larger regions, sequences of photomicrographs are taken covering an area and the stitched together with Hugin panorama software. To choose the field from which to collect data, the slide is placed on the microscope stage so the radial coordinate of the sample is aligned with the direction of the lateral stage adjustment. Then the z position is found where the longest radial sequence can be observed without interruption by sample folding or other discontinuities.

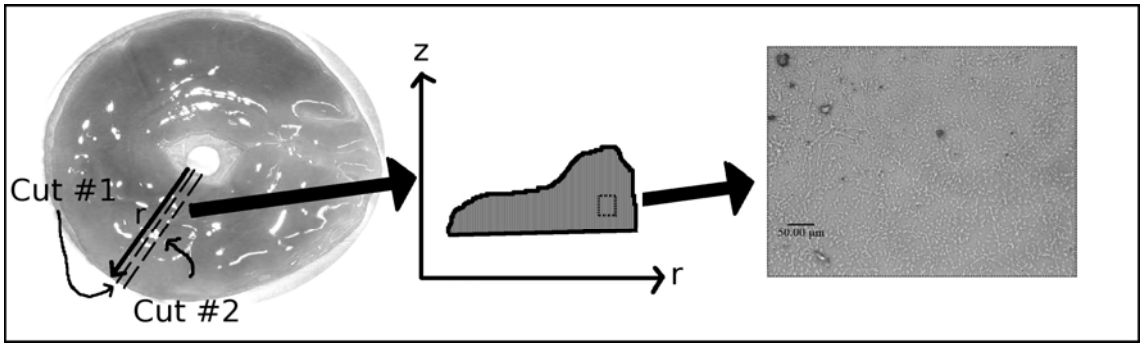

Figure 2.11 Schematic representation of BC sectioning and visualizing procedure

2.7 Image Capture and Analysis

Images are captured digitally in the laboratory by three devices: a digital still camera, (Minolta Dimage Z-1); a camcorder (Quasar VM-D52) connected to a TV tuner card in the PC; and USB webcam. For real-time acquisition from the camcorder, the Virtual Dub (www.virtualdub.org, Date Last Accessed: 01/10/2006) software package is used. MATLAB is used for time lapsed acquisitions by taking still images at a regular interval and converting them to an AVI file. Other sources of digital images are the camera on the microscope (NIKON) and a flatbed scanner (HP). The microscopy images are captured with SPOT Imaging Software (Diagnostic Instruments, Inc.).

Particle sizing and counting analysis is done with ImageJ (rsb.info.nih.gov/ij/, Date Last Accessed: 01/26/2009). The image scale is set using a ruler placed in the image or known scale bars. The software converts physical units from the reference instrument to the image's native pixel units. Then image is converted to grayscale and a gray threshold is set to distinguish objects of interest from the background. ImageJ includes algorithms to size objects, count objects, and report the spacial distribution of objects. In addition to particles, these same tools are used to size wet and dry BC gels, too.

2.8 Ashing

Samples are oven (Thermolyne F6028CM) dried at 100°C for three hours, weighed, and then ashed at 700°C for three more hours.

2.9 Oxygen Limitation

Several methods are employed to study oxygen variation in both the air and liquid regions in flasks and the RDB. In flask cultures the following methods are used to create a reduced oxygen environment: sublimating dry ice in the growth media, after transfer, but prior to inoculation; adding a layer of sterile mineral oil on top of the growth media; bubbling nitrogen gas through the media throughout growth; and adding a layer of molten wax on top of inoculated growth media. Molten wax is also used to create a low-oxygen environment in the RDB by pouring it on the surface of a full reactor chamber. A temporary barrier made of card stock is used to hold the wax off of the disk until it solidifies.

2.10 Adsorption Isotherms

Two methods have been designed to study the van der Waals interactions between particles and cellulose. The first exposes only the outer cellulose face to a homogenized particle suspension and the second submerges a small cellulose segment into the agitated slurry. Studies are performed at pH 5 and 7 in citric acid-monosodium phosphate buffer. Particles are pre-soaked in buffer before all experiments. Equilibrium adsorption trials are run for at least 36 hours. The range of particle concentrations investigated is 0-6g/L.

2.10.1 Stirred Beakers

As shown in Figure 3.12, 60mm plastic petri dish lids are affixed to 1mL plastic pipettes to create a boom device such that cellulose samples are sown over the outer face and exposed to a particle suspension in a stirred 200mL glass beaker. A ring stand holds up the boom and the cellulose sample is raised and lowered to the particle suspension by a laboratory jack.

When RDB BC is used for the cellulose sample, a control piece of the gel is sectioned off to be photographed, dried, and ashed for baseline compositional values. The experimental piece is also photographed to subtract the baseline from the whole piece, but the experimental contact area is always assumed to be 190mm^2.

2.10.2 Falcon Tubes

The submerged sample isotherm experiments use cellulose extracted from harvested RDB gels with a size 12 cork borer. Five samples are run simultaneously along with a sixth in buffer as a blank. The slurry filled tubes are rotated in the vertical plane at 50 RPM.

Figure 2.12 Adsorption isotherm boom device

2.11 Specialized batch reactors

Cultures of *G. xylinus* are grown in covered 10 x 10 x 4cm plastic boxes for the purpose of studying BC as a substrate for microfluidic devices. The boxes and lids are sterilized in a UV chamber overnight and inoculated with 150mL media with 1% glucose. After a pellicle starts to grow in the box, the fluid channel pattern is laid down on the BC surface using a non-porous material (e.g. thread or tubing). Within a week, the growing cellulose encapsulates the channel pattern material, which is extracted to leave channels in the BC.

A transparent storage box (U.S. Plastic 65016), with six - 15.6 x 4.3 x 3.8cm compartments is used to grow cultures for the study of electroactive paper materials. The eleven conductive meshes examined are listed in Table 1.6 along with their biocompatibility. The plastic box is sterilized by soaking in 0.75% bleach solution and the meshes by autoclaving in water. It is important to maintain the transparency of the plastic, so the box is not placed under UV. Placing the mesh in the media at inoculation and looking for the presence of a cellulose pellicle in a few days tests the biocompatibility of a mesh. Placing a mesh sample on top of a growing pellicle and observing if cellulose production continues unabated, growing through the mesh, tests the incorporation potential of the fabric.

Table 1.6 Conductive Meshes (Less EMF Inc.)

#	Fabric Name	Conductive Material	Resistivity (ohms/square)	Biocompatible
1	Nylon Rip Stop	Ni/Ag	<0.1	N
2	Seethru Conductive Fabric	Ag >99%	<5.0	N
3	NaturaShield	Conductive Interior	10^9	N
4	Flectron Conductive Fabric	Cu	<0.1	Y
5	Stretch Conductive Fabric	Ag	13	N
6	Ex-Static Conductive Fabric	BASF Resistat	10^5	N/A
7	Zelt Conductive Fabric	Cu/Sn	<0.09	Y
8	SHIELDIT	Ni/Cu/conductive Acrylic	<0.1	Y
9	Flectron – N Conductive Fabric	Cu/Ni	<0.1	Y
10	VeilShield	Blackened Cu	0.1	Y
11	High Performance Silver Mesh Fabric	Ag	<0.5	N

3. Results and Discussion

The broadest goal of this research is to understand the mechanism of incorporation of suspended particles into a thickening bacterial cellulose (BC) gel growing on a rotating disk in a cylindrical bioreactor. In other words, on what does the particle location in the harvested gel depend? One previous study determines the range of particle sizes (e.g. alumina, silica gel, talc) that can be incorporated into growing BC as 25 - 250μm (Serafica, 1997) and another finds that fiber incorporation (e.g. shredded paper and Sigmacell 20) varies inversely with disk rotational speed (Mormino, 2002). While fiber uptake is thought to be mechanistically different than particle uptake (Serafica et al., 2002), the fiber result informs the main testable hypothesis about the particle uptake, specifically that particle incorporation is a function of tangential velocity, not simply disk rotational speed. An experimental plan to test this claim must be divided into three high-level tasks: replication of the previous work; development of an uptake model; and testing of the model. Prior investigations into bacterial cellulose (BC) production in a rotating disk bioreactor (RDB) are few and those that study particle incorporation are fewer still. The apparatus and experimental methods used in those studies are in their infancy and require rigorous critique because it is from their finding that a central tenet is passed down: that particles are, in fact, incorporated into the BC gel. An analysis of the previous work, its methods, and its findings comprises the first section of this chapter, *§4.1* Procedural Studies. The shortcomings of the previous work are identified, the manners in which these shortcomings jeopardize their findings are illustrated and improved procedures are introduced.

An unexpected finding in this audit is that the experimental design in the previous work is ill equipped to reach the conclusions that they did. Specifically, the authors measure particle disappearance from suspension, i.e., a combination of particle uptake and particle settling, rather than appearance in the BC gel. The consequence of this misstep is that the very existence of particle incorporation is called into question. Therefore, before an uptake model is proposed, particle uptake as a phenomenon must be independently verified with the refined apparatus and methods. Direct experimental evidence of particle uptake is presented in the second section of this chapter, §4.2 Verification Studies.

With confidence that particles are incorporated into the growing BC gel, the mechanics as to how are investigated for the first time in this study. To vigorously test the hypothesis, the incorporation mechanism must account for the experimental variables of disk rotational speed and particle charge. A three-step model of incorporation is proposed: 1. Suspended particles diffuse across a boundary layer at the rotating disk surface as it passes through the liquid phase; 2. Non-covalent interactions between the particles and cellulose matrix hold the particles at the cellulose surface; and 3. The active bacteria on the cellulose surface continue thickening the gel around the particles and encapsulate it within the matrix. In the section, §4.3 Mechanistic Studies, theoretical and experimental motivation for each step is provided.

The final section of this chapter, §4.4 Validation Studies, will discuss the experiments that have been performed to validate the proposed model. For the hypothesis to be shown true, two experimental observations are required: the distribution of particles in each experiment is radially non-uniform and, in experiments at different rotational speeds, the particle concentrations need to be similar at positions of similar tangential velocity. However, the first observation is a discontinuity in the radial distribution of particles profile that does not agree with theory and needs to be explained. The profile discontinuity is found to be an unavoidable consequence of the RDB geometry and experiments are provided to support this argument. The radial profile inside the discontinuity, i.e., at smaller radial positions, does agree with the theories inherent in the model. This data is presented and the corresponding physical principles are restated for clarity.

3.1 Procedural Studies

Early in this research, it became clear that there were improvements to be made to the design of the Rotating Disk Bioreactor (RDB) and the experimental measurement techniques. There are three paradoxical design flaws in the protocols put forth by previous investigators that jeopardize the validity of their findings: the lack of abatement of unbound cellulose growth in the reactor chamber; inadequate mixing for particle suspension; and ambiguous particle measurement techniques. Unbound cellulose refers to bacterial cellulose (BC) that is produced in the RDB, but is not attached to the disk and essentially turns the liquid phase semi-solid, eliminating particle mobility. Failure to

keep particles suspended is detrimental to understanding chemical engineering transport problems because there is no knowledge of the gradient driving material flux. The ambiguity in the particle measurement is that the rate of particle incorporation into the BC is inferred from the rate of disappearance from the bulk. What is actually being reported in these studies is the combined rate of particle settling in the reactor chamber and uptake into the growing BC gel. The details of these flaws are discussed, along with design corrections, and direct experimental evidence that the redesigns improve investigative protocol.

3.1.1 Unbound RDB Cellulose

A complication to producing microbial cellulose-based composite materials in the RDB is unbound cellulose production, i.e. cellulose growing in the reactor chamber that is not attached to the plastic disk. This cellulose can be attached to inner seams of the reactor, but can also be freely suspended. The propagation of unbound cellulose is typically very swift, with all the liquid growth media becoming gelled and viscous within a few days of first appearance. The rate of unbound cellulose production is illustrated in Figure 4.1: within four days the unbound phase transforms from a uniformly clear liquid (A) to a gelatinous phase of ultra-hydrated cellulose with a tough, white pellicle at the surface and only a narrow patch of liquid at the surface at the moving disk face (B), to the unbound growth being so plentiful that it is pulled from the reactor wall by the rotation of the disk (C).

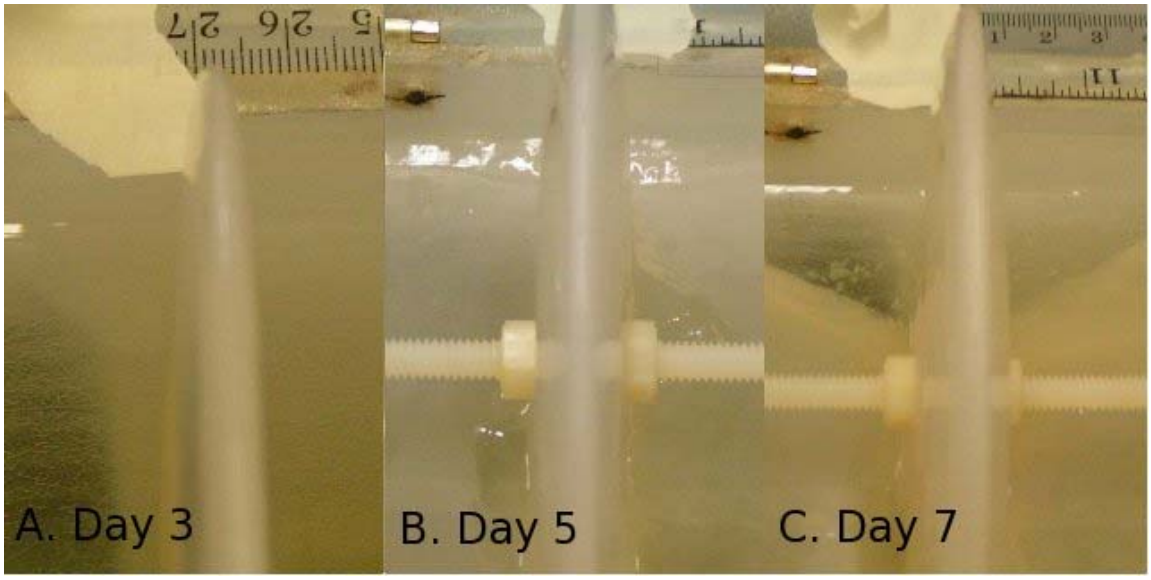

Figure 3.1 Evolution of unbound cellulose growth at 9RPM

Cellulose produced off the disk is problematic for several reasons: surface-bound cellulose is a barrier to oxygen transport into the bulk; it increases the viscosity of the bulk phase and inhibits particle transport; and microbial growth and cellulose production off the disk wastes metabolic resources. Additionally cellulose that is not attached to the rotating disk can clog reactor plumbing and foul sensors. The only mention by a previous researcher studying particle dynamics in the RDB of extraneous cellulose production is pH probe fouling (Mormino, 2002). Investigators studying *Gluconacetobacter xylinus* in an RDB-like reactor, but with cylinders as the solid media and no particles involved, report unbound cellulose being an erratic disturbance to their experiments, as well (Seema Dean, personal communication, November 6, 2007). These investigators do not propose an origin to this phenomenon and deal with it by opening the reactor chamber to remove the cellulose manually. This is an inefficient remedy that requires frequently opening the reactor and exposing the chamber to contaminants; a more robust solution to this dilemma is sought and reached as discussed in subsequent paragraphs.

The theory is that unbound cellulose forms as a stress response to a lowered oxygen environment in the RDB chamber away from the disk. Indeed Vershuren et al. (2000) measures a rapid decrease of available oxygen in the growth media of static cultures of *G. xylinus*. The oxygen profiles from their experiments are presented in

Figure 4.2. In the RDB chamber, aeration primarily occurs by the disk's motion at rotational speeds above 10RPM (DiPalma et al., 2003); therefore it assumed, but not yet experimentally verified, that the oxygen concentration far from the disk becomes drastically lower that what it is near it as a trial proceeds.

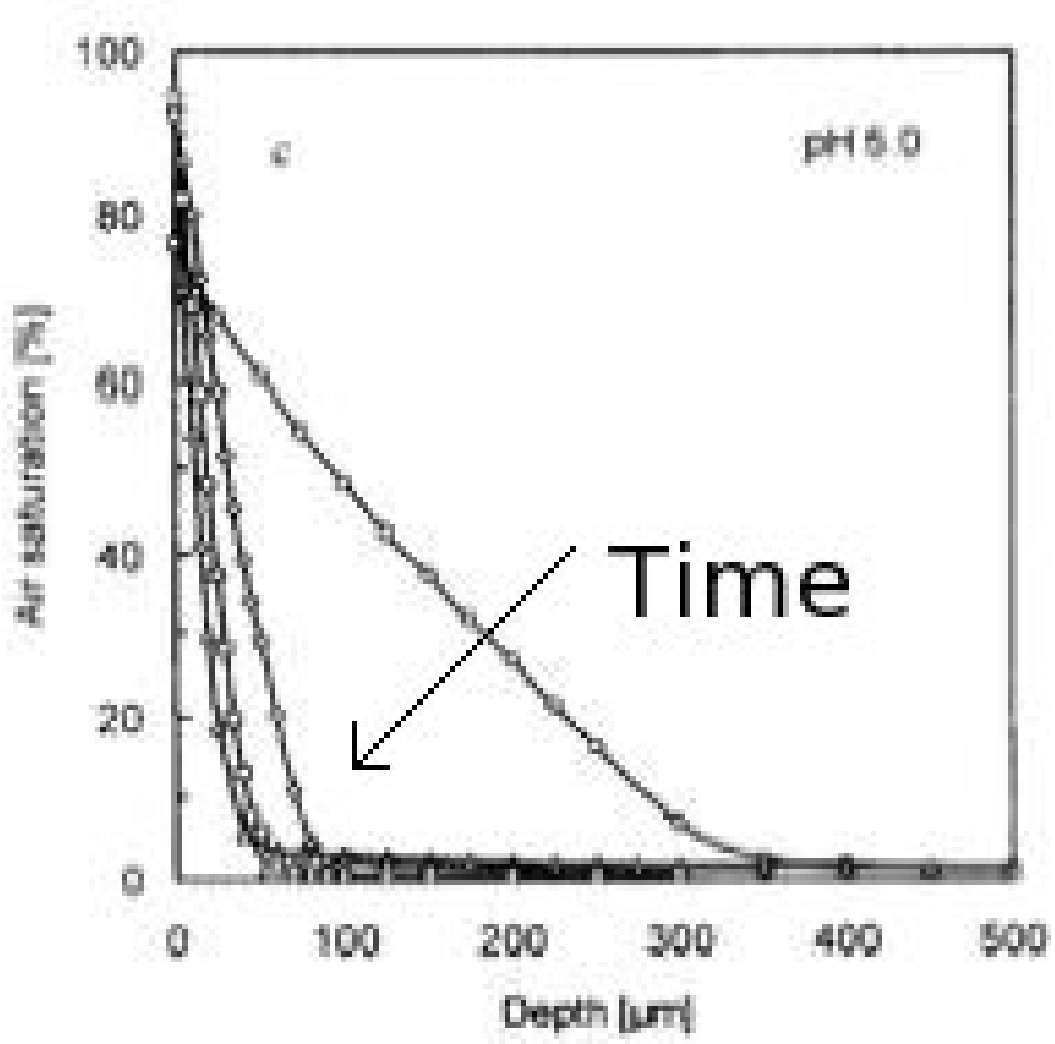

Figure 3.2 Oxygen profiles in the growth media from Vershuren et al. (2000) at day 1 (○), 3 (△), 7 (◊), and 15 (□).

Of the two studies that address the dependence of cellulose formation on available oxygen in static culture (Hestrin and Schramm, 1954; Watanabe and Yamanaka, 1995), Watanabe also discusses the morphological dependence of the cellulose gel on oxygen content. They find that the density of cellulose chains decreases with lower oxygen concentration in the air phase. They use SEM to verify that the cellulose fibril width remains constant and, instead, it is the distance between chain branches that is responsible for the differences in cellulose density. Fibril branching occurs during *G. xylinus* cell division (Yamanaka et al., 1989), so a change in branching frequency indicates an alteration of the cell life cycle, such as nutrient starvation. Watanabe studies cellulose production in a 12L static vessel at oxygen tensions in the headspace down to 5%. As seen in Figure 4.3, the most drastic increases in pellicle thickness are observed between 10%-15% oxygen tension; the cell density does not vary appreciably, and the pellicle thickness at 5% is roughly the same as it is at atmospheric oxygen tension.

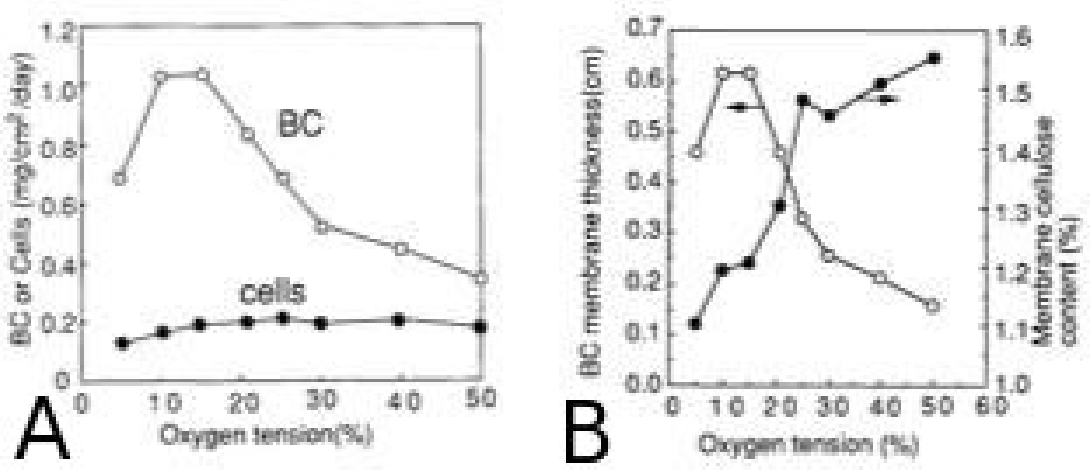

Figure 3.3 Results from Watanabe and Yamanaka (1995)

The consistency of the unbound cellulose is very gelatinous without the toughness of typical pellicular BC (except at the air liquid interface). The results of DiPalma et al., (2003), Vershuren et al., (2000), Yamanaka et al., (1989), and Watanabe and Yamanaka (1995) are sufficiently consistent with the observed unbound cellulose production rates, locations, and morphology to prompt the investigation of a solution by manipulation of oxygen flux to the RDB growth media. It is predicted from Figure 4.3A that a dramatic decrease in available oxygen will halt BC production by inhibiting cell function. This prediction has been experimentally verified using paraffin wax as an oxygen barrier,

seen from the top in Figure 4.4. The wax layer, however, creates significant drawbacks such as prohibiting pump-around recirculation and fixing the maximum thickness of the BC to the width of the spacing between the wax blocks.

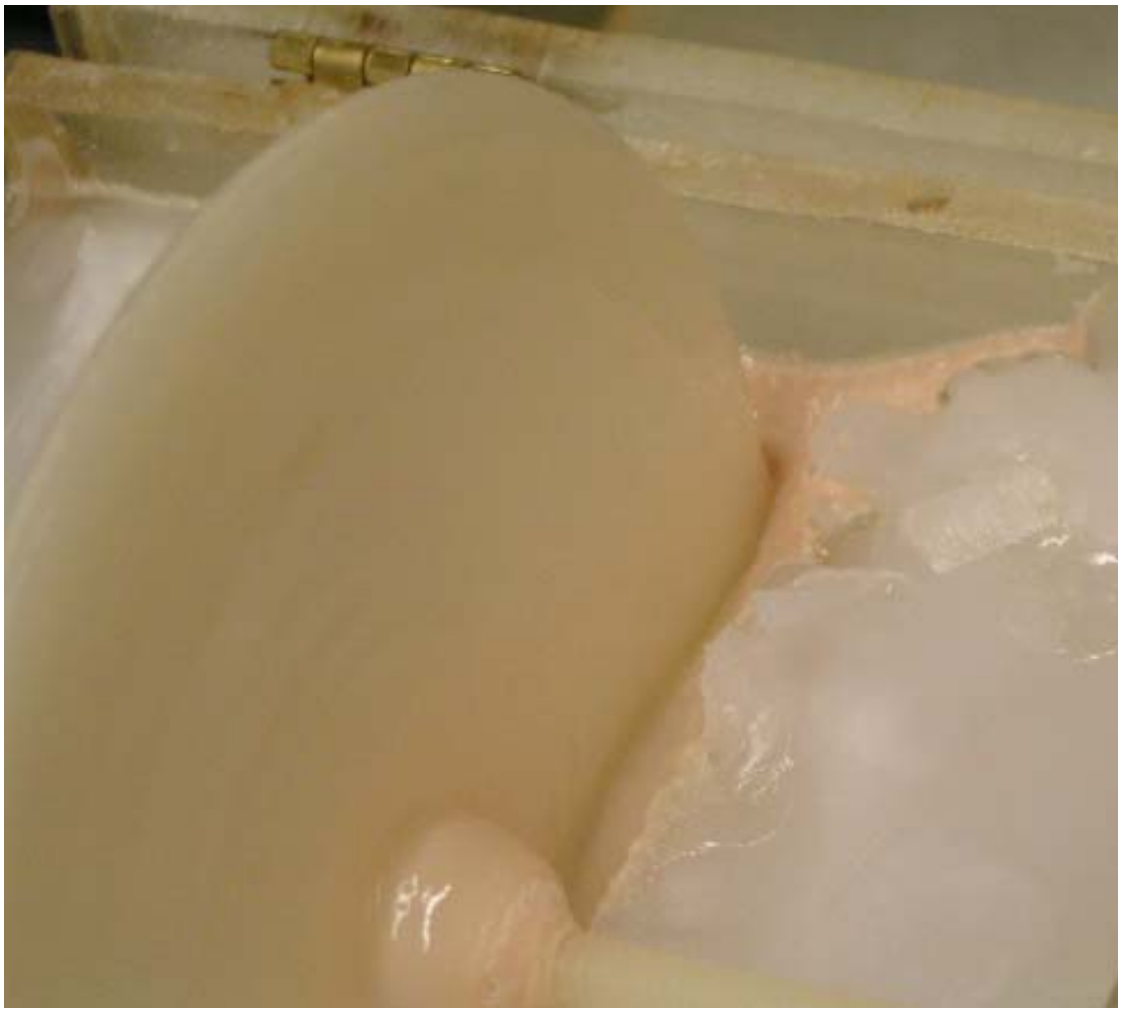

Figure 3.4 BC gel grown in wax-covered chamber at 9 RPM

A more robust solution to the unbound cellulose problem is to increase the frequency of bacteria suspended in the media contacting the rotating disk. This is done with vigorous mixing through an improved recirculation system. Bacterial dispersion by agitation also prevents extruded cellulose chains from combining into fibers in the bulk liquid. The development of the improved recirculation system is discussed in the following section.

3.1.2 Particle Suspension

When the mixing of heavier-than-water particles is poor, all the other procedural difficulties related to the particles in the liquid phase are accentuated. Suspended particle measurement, either by grab sample or flow cell, clearly will be inaccurate if particles settle. This is the case however with the quantitative uptake data presented by the previous researchers. The liquid agitation design put forth by the previous researchers is a pump-around system that discharges the recirculating fluid at the apex of the RDB's cylindrical top, so that it falls onto the surface of the media (Mormino, 2002). As part of this study, several agitation designs are compared using Davisil 643 silica gel as a model particle (bulk density 350kg/m^3).

The comparison of different agitation methods is illustrated in Figure 4.5, where the agitation methods being compared are: "Stir Bars," two stir 0.5-inch stir bars; "Tubes," a pump around system where the fluid returns through two ports with copper tubing penetrating 0.5 inches through the reactor lid and falls onto the media surface (replicates Mormino (2002)); and "Jets," a pump around system where the two return ports are piped to nozzles on the reactor wall at the liquid surface that direct the high velocity return stream along the reactor bottom (a novel design). To assess the quality of mixing, an optimal mixing profile in a 1L liquid chamber has a slope of unity. Only the "Jets" profile approaches this limit.

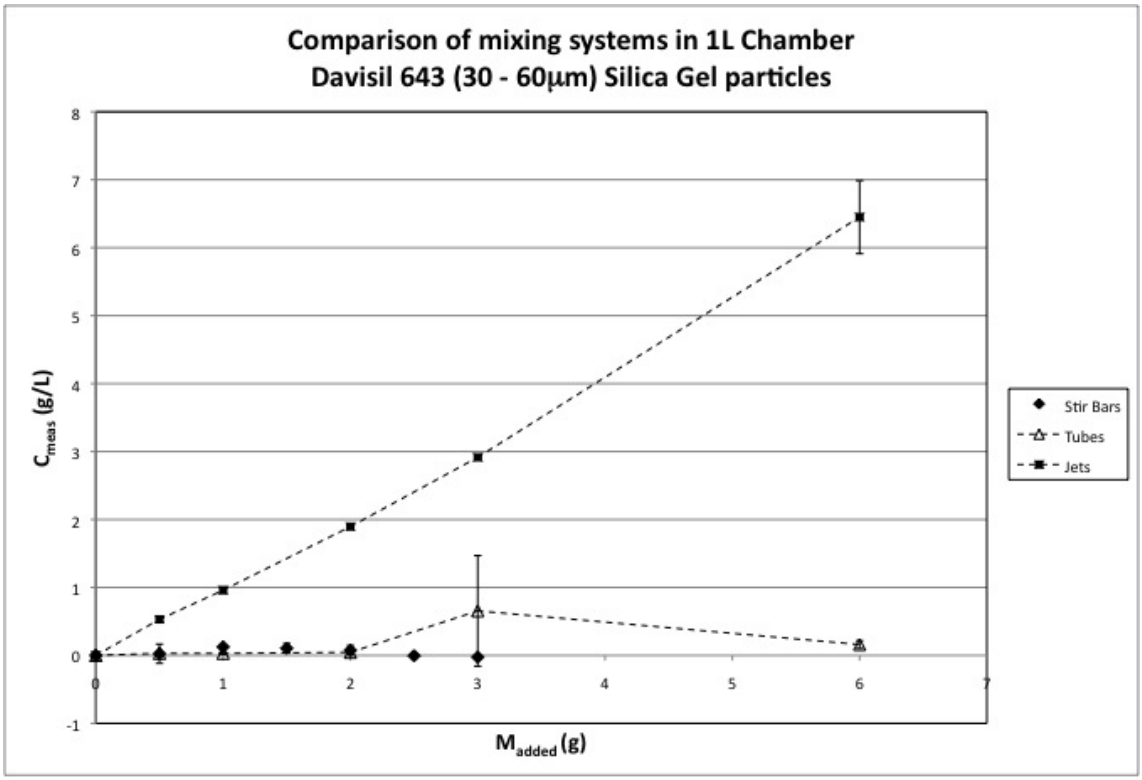

Figure 3.5 Comparison of mixing systems in 1L Chamber using Davisil 643 silica gel particles

Clearly, the agitation system proposed in the previous research, a pump around system with return discharge at the lid apex does a poor job at maintaining particles in suspension and, even at low concentrations, provides negligible agitation.

The consequences of this error are grave. Mormino (2002) presents suspended particle concentration change data as uptake rate into the BC, but this cannot be the case in a poorly mixed system where the measurement is greatly influenced by particle settling to the reactor bottom. As Figure 4.5 indicates, of all the particle agitation methods studied in this or other investigations, recirculation with jets is the only arrangement that allows for accurate determination of the relationship between suspended particle concentration and the uptake of particles into the BC matrix. No other method is able to maintain a suspended particle concentration higher than 1g/L.

Using of a more effective mixing setup in the RDB is not without drawbacks, however. A reactor chamber with too much external motion and shear stresses demonstrates a hindered ability to produce bacterial cellulose. More specifically, the observation thus far is that *Gluconacetobacter xylinus* will not attach to the rotating plastic disk if the

agitation occurs in the period between inoculation and initial matrix formation. Once an initial cellulose film is formed on the rotating disk, however, the thickening of the BC is not significantly impacted by enhanced fluid circulation. The organism is able to withstand much higher shear forces from within the cellulose matrix.

3.1.3 Particle Measurement

Previous studies of particle adsorption or incorporation into BC do not examine the concentration of particles successfully incorporated into the BC. The only true measurement has been suspended particle concentration change, which as elucidated previously, provides only questionable data due to poor reactor mixing. The improved recirculation design created in this work, "Jets," does restore confidence to bulk grab-sample suspended particle concentration measurement. Even so, the hypothesis under scrutiny in this work requires positional incorporation data that cannot be provided by grab-samples. Some studies offer micrographs as proof-of-concept support of incorporation (Mormino, 2002), but these images have not been used to describe the particle distribution within the cellulose matrix or understand the mechanism of uptake. It is necessary to design experiments and analytical procedures to characterize pure BC and particle/BC composites. This study introduces complementary coarse- and fine-grained methods of BC product inspection with the capacity to extract spatial and temporal distribution of particles. The coarse-grained technique is gravimetric analysis using pyrolysis to separate inorganic particles from the organic cellulose matrix (samples with organic particles are only dried and compared with particle free samples). The fine-grained method is photomicroscopy and image analysis. With these tools, experiments are designed to isolate the contributory routes to incorporation and study them individually.

3.1.3.1 Gravimetric analysis

An efficient method for large-scale (> 10mm) particle distribution determination is developed in this research. The four-step procedure is: 1. Harvest the BC and dry it on wax paper; 2. Section the harvested BC into radial annuli; 3. Liberate the particles from the cellulose matrix; and 4. Determine the mass of the particles contained in the annuli.

The measured variable is the area-normalized mass in each annular segment. Area measurement is performed on a digital image of each segment with image analysis software. Normalized mass used because the dried BC gel is brittle and flakes of BC get lost in the cutting process. A typical digital image of a sectioned RDB BC annulus is presented in Figure 4.6.

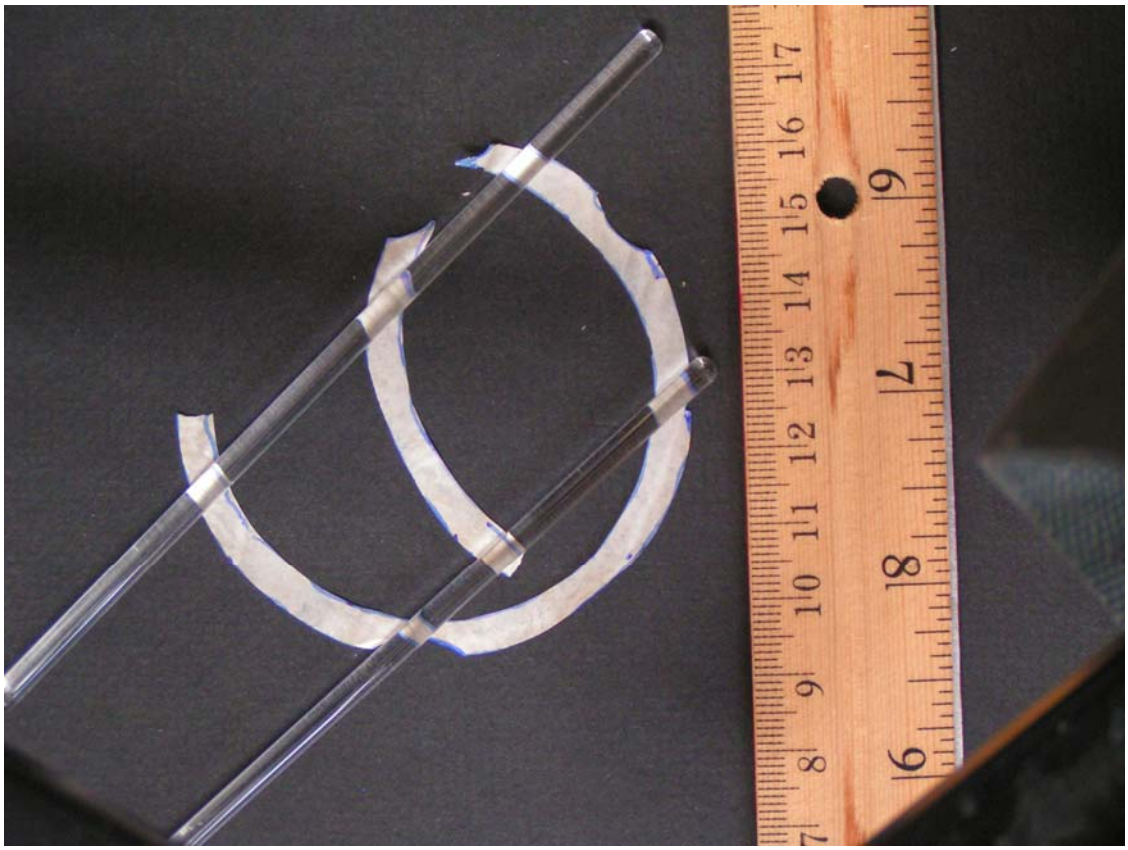

Figure 3.6 RDB BC annulus

Pyrolysis is used to liberate inorganic particles from the cellulose matrix because it is more economical and less time consuming than other methods considered. The process is generalized for organic particle studies by inserting a drying step before ashing. However, organic particle studies also require a particle-free trial run identically in parallel with the experimental trial so that a comparison of the dried weights provides the particle incorporation data. A disadvantage of this method is the requirement for a ceramic crucible, which often weighs considerably more than the sample of interest. The trade-off for a quicker measurement is a loss of precision.

Other methods of particle liberation were investigated, but were prohibitive due to cost and effectiveness. They will be discussed here, however, because the findings of this exploration may prove useful to future investigators. There are three additional theoretically feasible ways to separate particles from the cellulose product: 1. acid hydrolysis; 2. enzymatic hydrolysis; and 3. selective solubilization.

Dried, particle laden BC segments soaked in concentrated (6M) sulfuric acid for several days, even at elevated temperature, do not appreciably decompose. Likewise, extended treatments of similar samples with cellulase from *Trichoderma reesei*, show poor efficacy. Other researchers also find that cellulose from *G. xylinus* is much more difficult to hydrolyze than cellulose from plant sources. The cited reasons for this difference in reactivity is the steric inhibition by the tighter fiber weave in the bacterial cellulose matrix and the alternating polarity of the BC chains, whereas the chains in plant cellulose are typically oriented in parallel (Samejima et al., 1997). The extent of hydrolysis is dependent on the origin of the cellulase as shown in Figure 4.7, where EG II is similar to the cellulase used in this research. These results indicate that enzymatic hydrolysis is a more practical solution towards the RDB particle extraction problem with a different enzyme or combination of enzymes (Samejima et al., 1997).

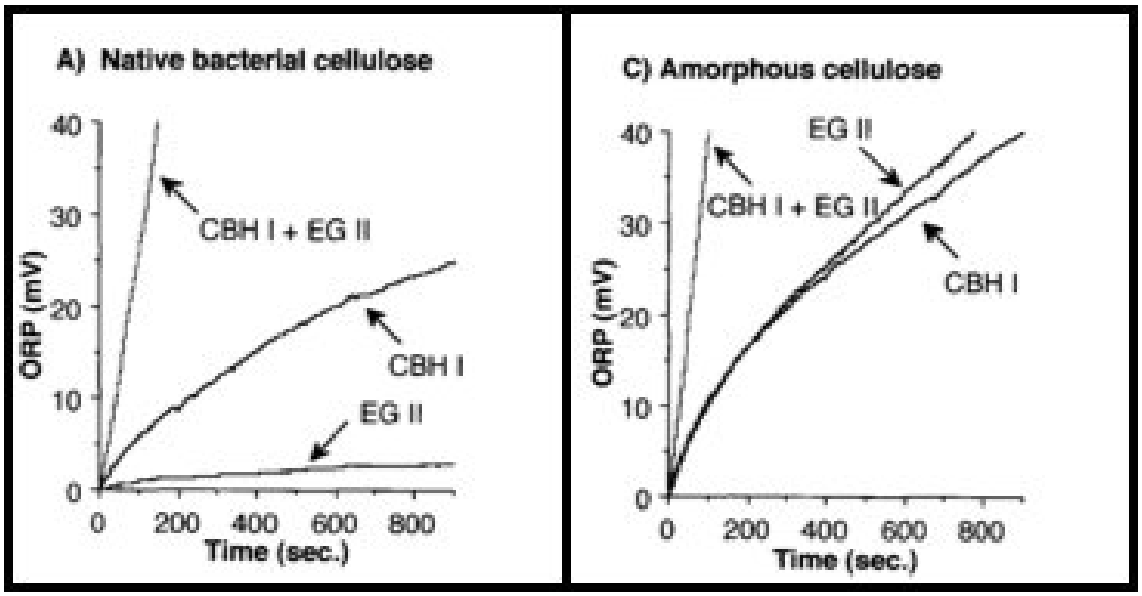

Figure 3.7 Cellulase efficacy for hydrolyzing BC and amorphous cellulose (Samejima et al., 1997) (CBH I: cellobiohydrolase I; EG II: endoglucanase II; ORP: oxidation-reduction potential)

An alternative to hydrolyzing the BC to liberate embedded particles is to solubilize BC in a solvent that leaves particles unaffected so they can be separated by filtration. Using room temperature ionic liquids (RTILs) is an effective, modern solvent to dissolve plant cellulose for alternative energy applications (Pushparaj et al., 2007). Two RTIL formulations, however, do not dissolve significant amounts of RDB BC, namely 1-butyl, 3-methylimidazolium chloride (T. J. Park, personal communication, November 2, 2007) and 1-ethyl, 3-methylimidazolium acetate (T. Doherty, personal communication, August 31, 2009). This difference in activity of plant and bacterial cellulose is hypothesized to be because of steric limitations in the BC matrix. With plant cellulose, RTILs have a great effect when the materials are ground to a fine powder before exposure to the solvent. Mechanical grinding of RDB BC introduces too much variation for it to be included in the analytical procedure.

3.1.3.2 Microscopy

The most intuitive method to analyze the BC product of an RDB trial is direct observation through microscopy. However, preparing thin cross-sections of hydrated BC is difficult and time consuming. In this study, microscopy is useful when more details are sought than gravimetric analysis can provide. Some of these measurements include particle number distribution, overall particle size distribution, particle size distribution variation with position, and even particle shape distribution. A well-prepared sample can also provide temporal uptake information from the cross-section, but requires additional growth rate measurements to extract time details from the thickness location of the microscopy field, i.e. applying distance = rate x time.

The difficulties of preparing samples for microscopy is due to the toughness inherent to the fiber weave combined with a total lack of structural rigidity. The method that provides the most consistent BC cross-sections is to affix a pair of surgical scalpels together with tape, pin the BC to the table, and cut along a radius with a single stroke. In the development of this technique, many other fixation methods were attempted with unsatisfactory results, including: soaking in Formalin; encasing in paraffin; stiffening with gelatin; and freezing. Multiple cutting implements were investigated, as well. The

ineffective ones were: a traditional and frozen microtome; a razor blade; a surgical scalpel run along a straightedge; a guillotine and rotary paper cutter; and a hot wire.

A typical photomicrograph of particles embedded in BC at 20x is shown in Figure 4.8A. At this magnification, the field of the image is 0.56mm x 0.42mm. This research is the first to use image analysis software on micrographs of BC to determine the position and size of incorporated particles, an example of which is shown in the plot in Figure 4.8B. This type of quantification capacity can be scaled up to larger regions of the BC cross section by taking sequential micrographs panning over the slide and stitching them together in software. A sample of a ten-image sequence is shown in Figure 4.9 with an alternative representation of the particle distribution data.

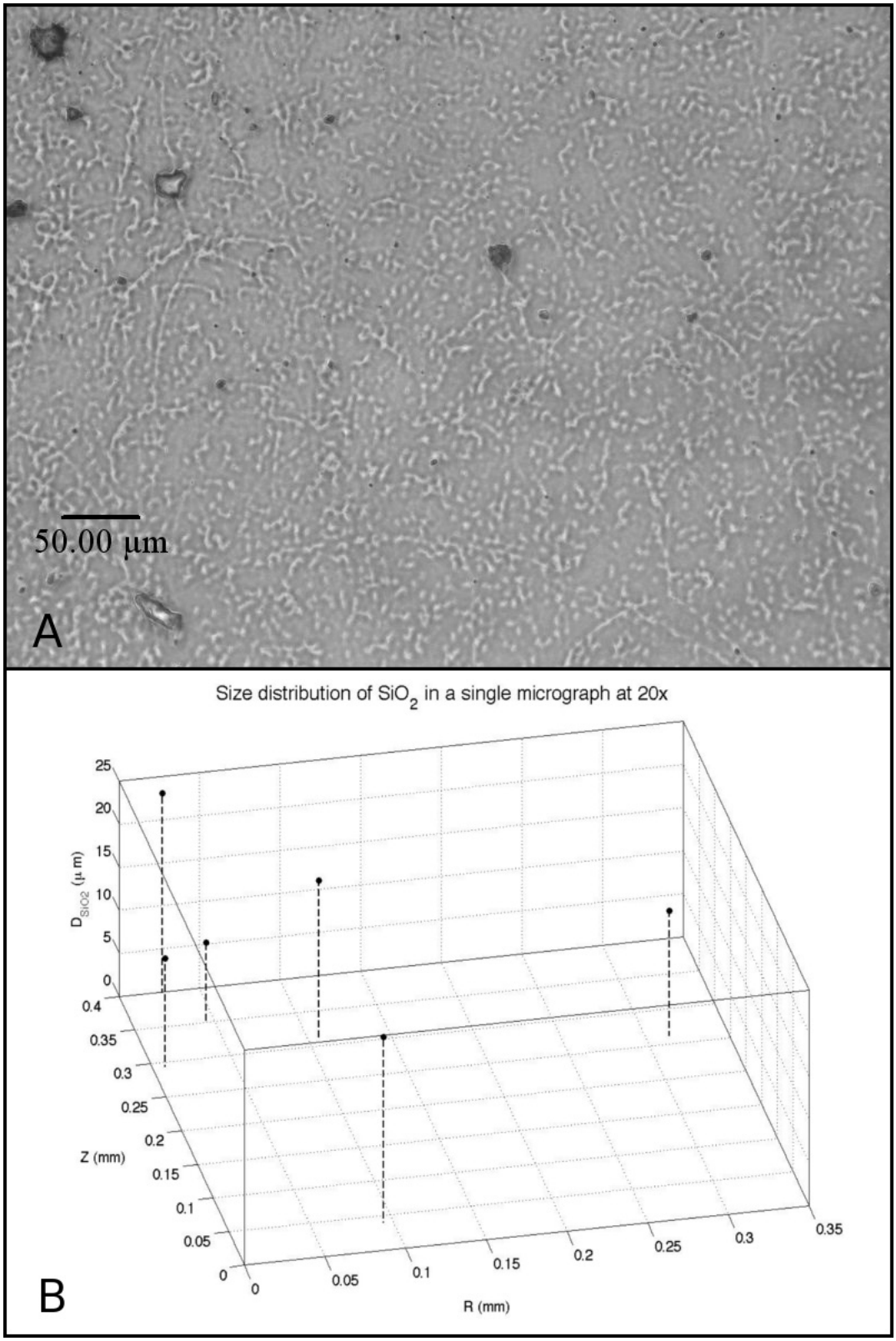

Figure 3.8 A sample image and analysis of particles incorporated in bacterial cellulose. A. CVL-silica gel at 20x. B. Location and size analysis of the image

The pairing of microscopy with image analysis as an incorporation tool has more weaknesses than strengths. While it is desirable to directly verify particle uptake, the microscopy and imaging tools used in this study (i.e., NIKON, SPOT, ImageJ) are only useful for local measurement. The ten-image sequence in Figure 4.9 covers less than 10% of sample in the radial direction. The stitching and particle counting software is not developed enough for complete automation, due to the narrow contrast margin between the particles and background. Therefore, microscopy is a powerful tool for specialized uses, but is not fitting as a standard particle distribution analysis. Nevertheless, analysis of discrete locations along a radial trajectory provides insight into particle incorporation. A proposed refinement to the photomicroscopy quantification method is to examine how particle density in regularly spaced zones varies with radial position along with the size distribution of particles found in those zones.

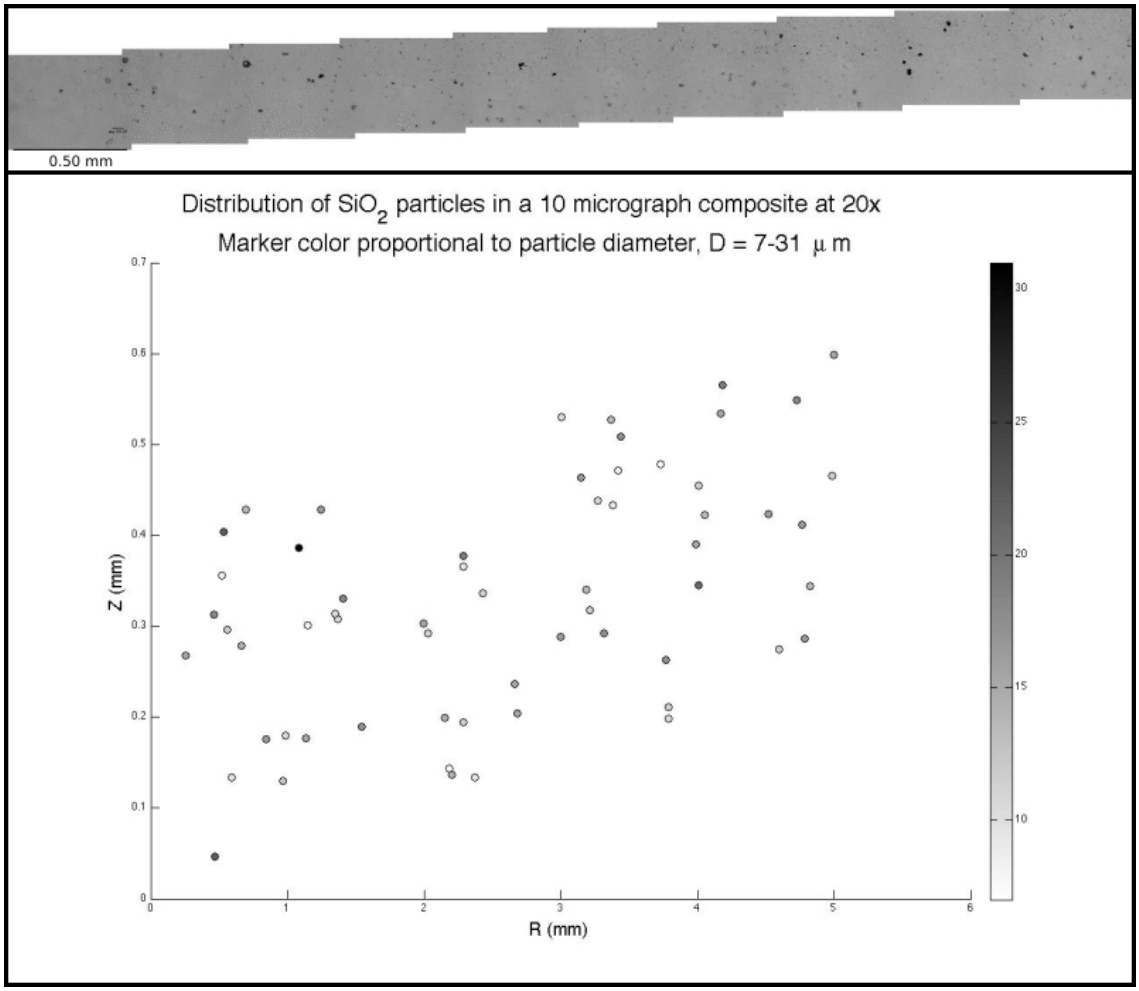

Figure 3.9 Particle size and distribution analysis of composite micrographs

3.2 Verification Studies

The incorporation rate data presented by previous researchers is unreliable. There is no quantitative analysis on the finished particle/BC composite. Also, measuring rate of change of suspended particle concentration to infer rate of uptake requires there be no alternative destination for particles leaving suspension other than into the growing BC. An examination of the previous RDB mixing design shows this assumption to be ludicrous, essentially questioning the entire premise of the study. Are particles actually incorporated into growing BC?

Presented here are a few brief examples of experimental results, collected using the improved apparatus and methods that show, in fact, that particle uptake occurs.

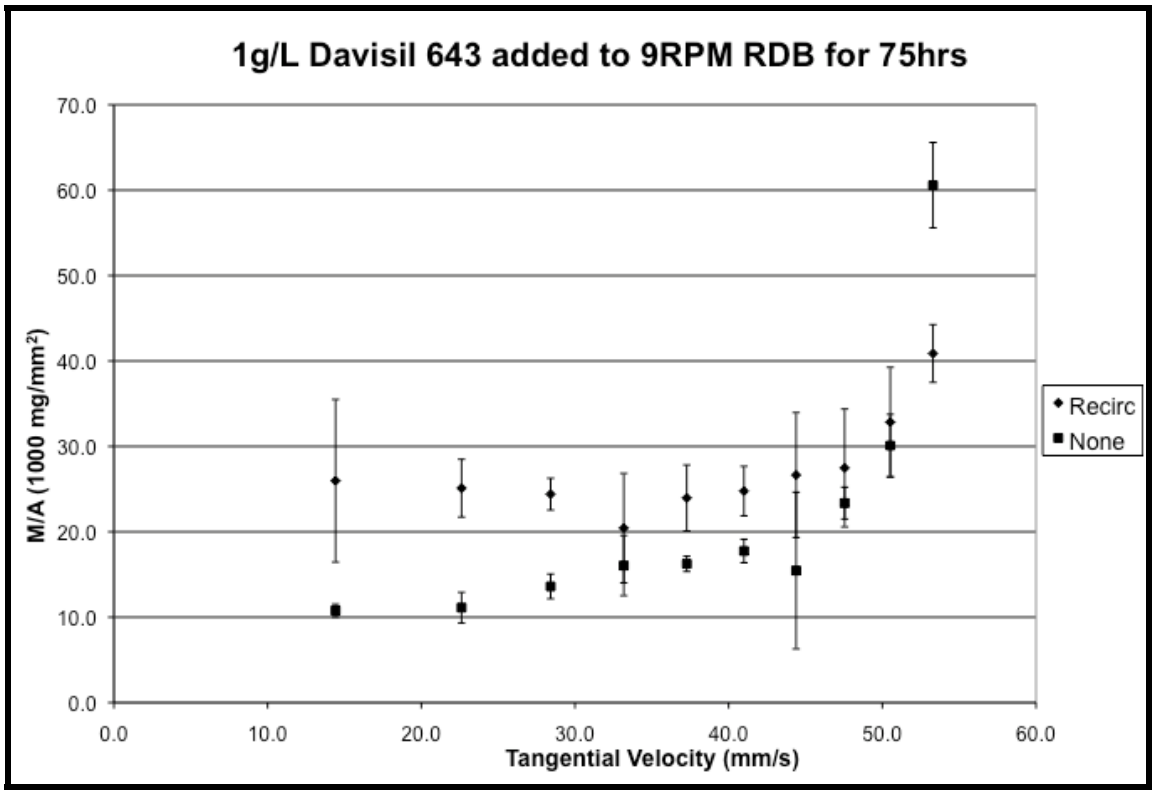

Figure 3.10 Effect of adding particles to RDB

Figure 4.10 is an example of the results of gravimetric analysis, wherein it is straightforward to verify that particles have been incorporated. Two identical chambers are incubated for 130hrs and then 1g of Davisil 643 silica gel is added to a recirculating RDB chamber, "Recirc." The particles are exposed to the growing BC for 75hrs before harvesting. The other chamber, "None," is grown at identically, except that no particles are added. This experiment, run at 9RPM, clearly shows that particles are incorporated into the growing BC as indicated by the greater masses measured in the exposed chamber. The extreme disparity of the measured mass values at outer disk edge is common to all samples analyzed. The explanation for this phenomenon is detailed in a later section, §4.4 Validation Studies. In brief, visualizing the surface flow patterns with tracer particles at different rotational speeds and disk-to-chamber aspect ratios shows accumulation of particles at the disk's outer withdrawing edge to be an unavoidable side effect of the RDB.

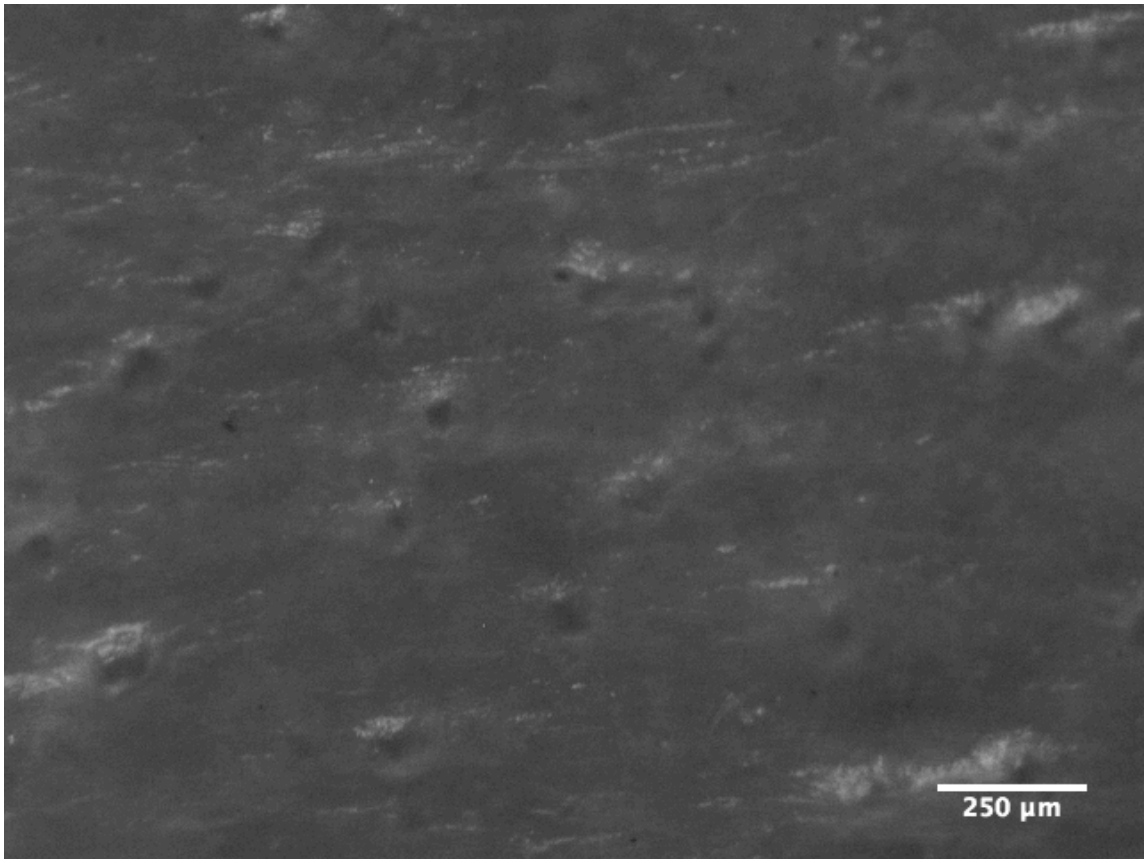

Figure 3.11 Particle/BC composite micrograph - 9RPM, 3g CVL-Silica Gel

The alternative composite analytical tool is the photomicrograph and an example is shown in Figure 4.11. In this sample, an initial BC gel was allowed to form for 120hrs at 9RPM and then exposed to crystal violet lactone-coated silica gel for 48hrs. This example demonstrates the advantages and disadvantages of microscopy as an analytical method. The large black spots are particles and simple counting can assess their number. However, the layers of BC that encapsulate the particles hide their size. An "apparent" size distribution can be calculated, but even this is non-trivial because of the narrow range of grays in the image and the heterogeneity in the shade of the cellulose background.

3.3 Mechanistic Studies

The objective of this study is to identify the critical steps of the particle incorporation process in the rotating disk bioreactor (RDB) system and build a mechanistic model from the chemical engineering phenomena that underlie each step. There are three steps

to particle incorporation: 1. transport of particles from the bulk liquid to the bacterial cellulose (BC) surface; 2. attachment of particles to the BC matrix; and 3. encapsulation of the particle by the surface movement in the direction normal to the disk face. In the first step, the velocity field of the liquid phase dictates the particle motion. Shear between the moving disk and viscous fluid create a hydrodynamic boundary layer along the submerged disk face. Within this boundary layer, a diffusion boundary defined according to the particle size characterizes the particle concentration gradient that drives Fickian diffusion towards the BC surface. A secondary hydrodynamic driving force at small length scales is the flow field within the entrained fluid film on the BC surface rotating through the air phase. In the second step of the incorporation process, at particle-BC distances on the order of the Debeye length, electrostatic forces dictate particle motion. The strength of these interactions is based on the particle charge, surface charge, and media properties. The third step of the incorporation process is dictated by the rate of cellulose production by the bacteria, which in turn is affected by experimental conditions. A series of experiments, designed to isolate and study each step, are presented and discussed to appreciate the significance of these phenomena.

There are challenges to understanding experimental observations within the frameworks from which these theoretical treatments originate arising from the unique conditions of the RDB. Many important properties like velocity and growth rate vary with position on rotating disk surface. The air-liquid interface that is crossed twice per rotation undermines hydrodynamic theory as the boundary layer is stripped from the disk during withdrawal generating intense localized turbulence. The warping of the fluid field at the disk edge cannot be neglected either.

What is assumed about the system, however, is that the agitation system does not interfere with boundary layer formation. It is also assumed that the particles remain dispersed in the bulk region and do not interact with suspended cell bodies, stray cellulose fibers, or media components. Finally it is assumed that the liquid holdup in the BC matrix remains constant as the disk rotates through the air phase so there is no forced convection driving a particle away from the disk surface.

3.3.1 Hydrodynamic Phenomena

Rotation of the disk in the RDB generates three distinct zones of fluid behavior: the fluid that adheres to the rotating disk as it withdraws from the liquid phase; the fluid inside the boundary layer that forms as the disk passes through the liquid phase; and the bulk liquid in the chamber outside of the hydrodynamic boundary layer. Fluid is exchanged amongst the zones by turbulence generated from the disk bringing fluid across the air-liquid interface at the withdrawal and submergence edges. The turbulent convection of liquid and Fickian diffusion drive three long-range transport phenomena in the particle incorporation problem: attachment/detachment of bacterial communities to the rotating disk; access of dissolved gas and nutrients to the attached bacterial communities; and transport of particles to the cellulose biofilm.

The mechanics of bacterial attachment and detachment from the rotating plastic disk and the development of the BC film are outside the scope of this report, with the exception of the observation that external agitation retards colony attachment. Cellulose forms on disks rotating between 9 and 20RPM when there is no external mixing. When the bulk liquid is thoroughly agitated early in the experiment, i.e. after inoculation, but before a BC gel forms, the bacteria do not colonize the rotating disk or form a BC film. However, disks with stable BC films continue to grow at speeds up to 50RPM.

The transport processes that both sustain the bacteria and introduce particles to the surface happen inside the hydrodynamic boundary layer in the liquid phase and inside the fluid film in the air phase. Specifically, liquid phase transport of mass occurs across a diffusion boundary layer that is inside the hydrodynamic boundary layer, the thicknesses of which are related by the Schmidt number, Sc, defined in Equation(4.1). Before transport experiments can be analyzed, these fluid characteristics need to be calculated. As discussed by Groenveld (1970c), prior to calculating the theoretical fluid film profile over the disk, the dominant forces acting on the gas-liquid interface must be computed. The dimensionless groups that contain this information are the Capillary number, Ca, and the film Reynolds number, Re, which are defined in Equations (4.2) and (4.3).

$$Sc = \frac{\nu}{D} \tag{3.1}$$

$$Ca = \frac{\mu v_{\theta,0}}{\sigma} = \frac{2\pi r \mu \omega}{\sigma} \tag{3.2}$$

$$Re = \frac{\rho v_{\theta,0} \cdot h}{\mu} = \frac{2\pi r \rho \omega h}{\mu} \tag{3.3}$$

The Schmidt number is a ratio of momentum diffusivity to mass diffusivity, where ν is the kinematic viscosity, μ/ρ, and D is the diffusivity. The Capillary number is a ratio of viscous to capillary forces and the Reynolds number is a ratio of inertial to viscous forces where μ is the fluid viscosity, $v_{\theta,0}$ is the tangential velocity of the disk, σ is the surface tension of the fluid, ρ is the fluid density, and h is the entrained fluid film thickness. It is apparent that, unlike the pulling plate analogs of these groups, in the rotating disk system their value varies with location. To see which fluid forces are at work, it is convenient to only solve at the extremes of the typically operating conditions. On a plastic disk with an inner diameter of 10mm and an outer diameter of 60mm most frequently used at 9, 12, or 16 RPM the highest velocity encountered is when the outer edge of the disk is rotating at 16RPM, which is 100.5mm/s, and the slowest is when the inner edge is rotating at 9RPM, which is 9.42mm/s. For water at room temperature, μ is 0.10019P, σ is 73.05dyne/cm, and ρ is 1g/cm^3. The operating range of Ca is 1-14x10^{-4}, below the heuristic limit of 1x10^{-3} defining the capillary-force dominant regime, and therefore Equation (2.4) is the appropriate equation to calculate the film thickness (Groenveld, 1970b).

$$h = 1.34 \left(\frac{12\mu\omega r^2}{\sigma}\right)^{2/3} \tag{3.4}$$

The film thickness profile over the typical operating velocity range, along with the film Re, is shown in Figure 4.12. The maximum value of Re, 3.4, and the thickness varies from 7-34μm.

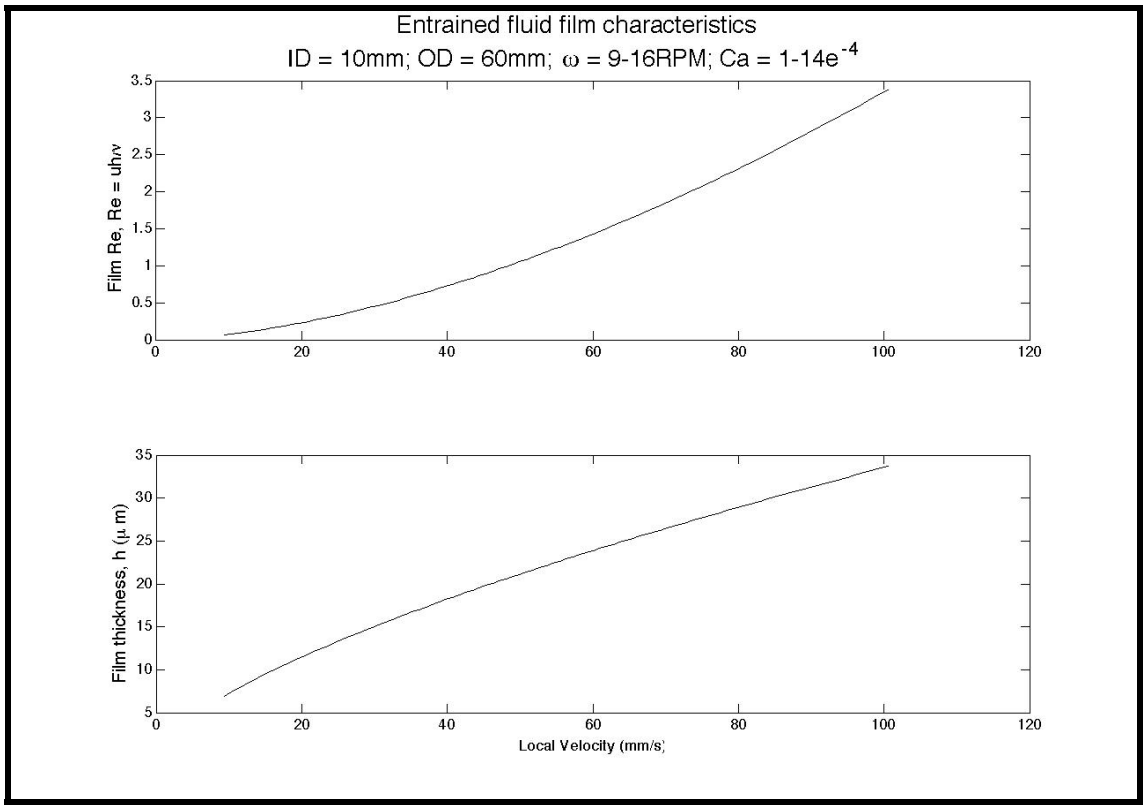

Figure 3.12 Reynolds number and air-phase fluid film thickness

The boundary layer that develops as the disk moves through the liquid phase is also modeled by theory originating from flows involving flat plates. The Blasius solution to flow over laminar boundary layers over a flat plate is expressed in Equation (4.5) with the corresponding local Reynolds number, where x is distance from the leading edge of the plate, is defined in (4.6) (Welty et al., 1984).

$$\delta_x = 5\sqrt{\frac{\nu x}{u}} = 5\sqrt{\frac{x}{Re_x}} \tag{3.5}$$

$$Re_x = \frac{u x}{\nu} \tag{3.6}$$

Equations (4.5) and (4.6) can be transformed into rotational coordinates, resulting in Equations (4.7) and (4.8), respectively. The angular coordinate, θ, is expressed in radians. The geometric dependence of the adhered-liquid profiles in the two environments are quite different. The withdrawal film is strictly dependant on local velocity and so has no variation over the course of the rotation. Alternatively, the hydrodynamic boundary layer is strictly a function of the time of contact between the fluid and the solid

wall, $x/v_{\theta,0}$, so for a disk in rigid rotation, there will be no radial variation of the thickness. This dependency does not allow the boundary layer thickness profile to collapse onto a single curve, but rather the boundary layer thickness is a characteristic of the rotational speed. The ultimate boundary layer thicknesses at disk withdrawal are shown in Figure 4.13.

$$\delta_x = 5\sqrt{\frac{\nu x}{v_{\theta,0}}} \tag{3.7}$$

$$Re_x = \frac{\rho v_{\theta,0} x}{\mu} \tag{3.8}$$

Also plotted in Figure 4.13 are momentum boundary layer thicknesses calculated using Equation (4.9) (Riley and Carbonell, 1993a). To estimate a diffusivity, the Stokes-Einstein equation, (4.10), is applied.

$$\frac{\delta}{\delta_x} = 1.5\left(\frac{\nu}{D}\right)^{1/3} \tag{3.9}$$

$$D = \frac{kT}{6\pi\mu a} \tag{3.10}$$

In Equation (4.10), k is the Boltmann constant, T is the absolute temperature (taken to be 298K), and a is the particle radius (taken as 50μm in Figure 4.13)

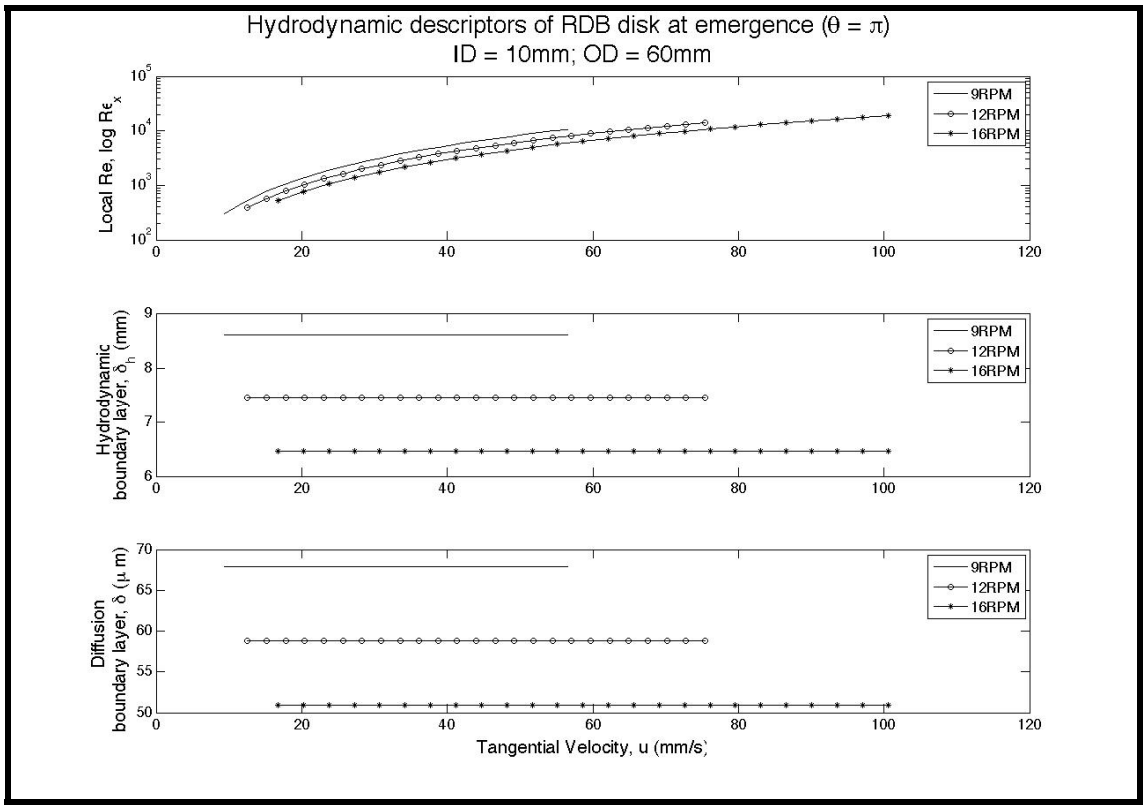

Figure 3.13 Rex and boundary layer thicknesses for submerged phase

After characterizing the hydrodynamic state of the RDB during non-agitated operation, experimental observations can be analyzed in proper context. The distribution of inorganic mass in RDB BCs grown without particles or agitation at 9 and 20RPM is shown in Figure 4.14. Both gels have similarly shaped profiles; mass is uniformly distributed on the inner portion of the disk and radially distributed at the outer portion of the disk. Grouping the data from the inner regions, as an *ad hoc* visual aid, reveals the mass density in the uniform region increases with increasing rotational speed. This is insightful because momentum boundary layer thickness is inversely proportional to rotational speed, meaning the gradient , where $C_{i,BC}$ is the concentration of inorganic matter at the BC surface and $C_{i,\delta}$ is the concentration in the bulk liquid, is steeper at higher rotational speeds, which results in higher mass flux.

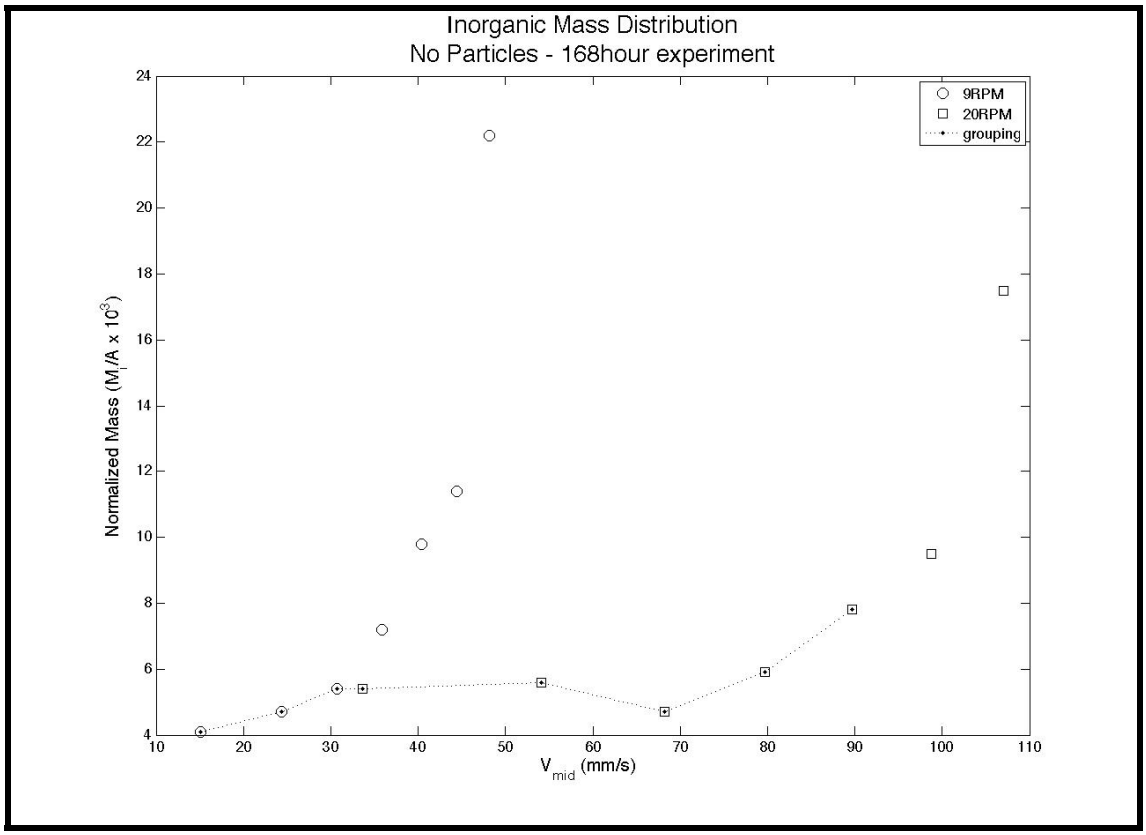

Figure 3.14 Distribution of Inorganic Mass in RDB BC operated at 9 and 20RPM

It appears that transport to the BC from the bulk liquid is dominated by the hydrodynamics of the liquid phase at the inner region of the rotating disk. Alternatively, the outer region's profile indicates transport via the withdrawing fluid film is more significant as the shape of the tail half of each distribution curve is similar to the fluid film thickness profile, i.e. [illegible] (surface tension-dominated film) for 9RPM and [illegible] for 20RPM (inertial-dominated film). The transition from boundary layer transport regime to fluid film transport regime occurs in the same radial position, r =38.1mm, at both speeds. The only common hydrodynamic parameter at that position is the entrained film thickness, 75μm. The common radius suggests a geometric cause for the shape similarity, such as an interaction with chamber wall or disk edge, but the local velocity at 20RPM is twice that at 9RPM, which would contradict that hypothesis. The common entrained film thickness suggests a hydrodynamic cause to the shape similarity, such as gravity collapsing the film region beyond a thickness threshold causing the near surface inorganic mass to

adsorb as the liquid drained. This question requires **more** experimental trials for a definitive answer.

3.3.2 Surface Phenomena

In order to gain more insight into the electrostatic interactions between the actual components of the RDB system, i.e. particles, bacterial cellulose, and growth media, experiments are designed to expose BC to particle slurries in citric acid-phosphate buffer. The buffer pH, particle composition, and slurry concentration are the parameters under investigation, but preliminary experiments are first run to elucidate the timescales of adsorption equilibrium. For the initial investigations, BC is stitched to the adsorption apparatus diagramed in Figure 4.15 and lowered into the slurry just far enough for liquid coverage of the entire face.

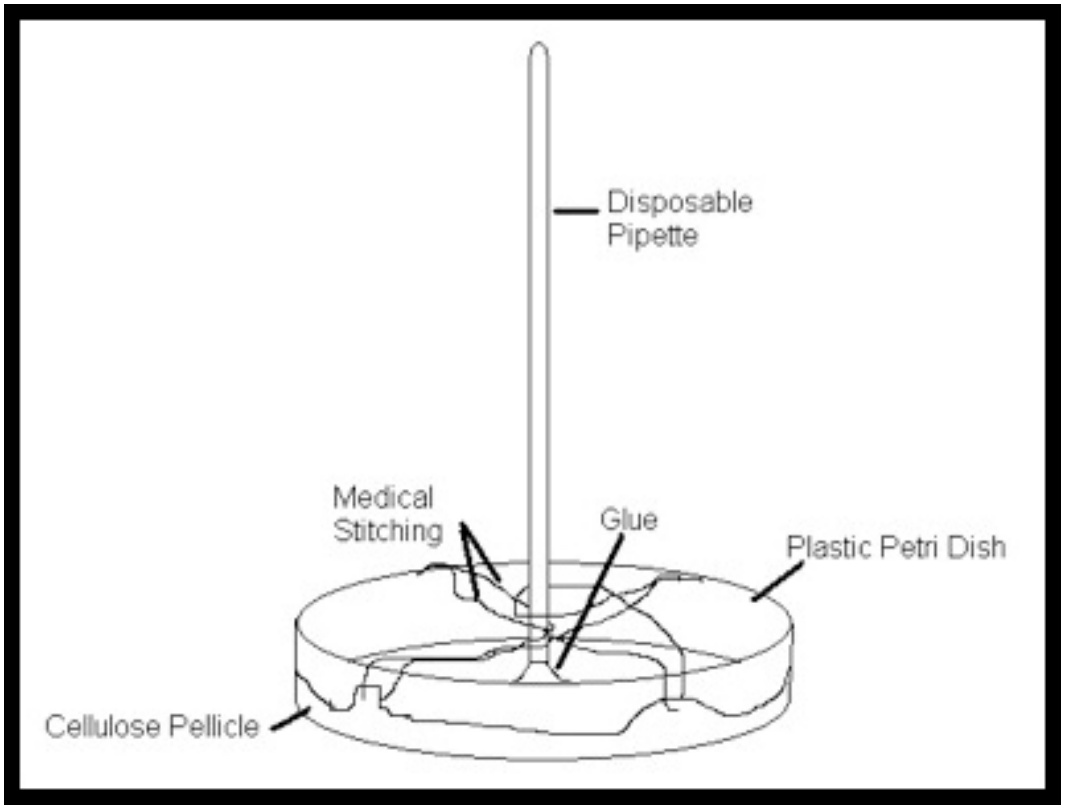

Figure 3.15 Cellulose-particle adsorption apparatus

In 200mL of media and exposed to a 29cm^2 cellulose surface, a 1g/L slurry of Davisil 643 particles equilibrates in about 10 hours at pH 7, as seen in Figure 4.16, and about 22

hours at pH 5. In order to select a practical time scale for the experimental protocol, the initial adsorption rate of silica gel near its pKa, 3.5, is investigated. A 1g/L particle slurry adsorbs to BC at pH 4 88% slower than at pH 5 and 91% slower than at pH 7, as seen in Figure 4.17. Therefore to be conservative, experimental trials last at least 36 hours.

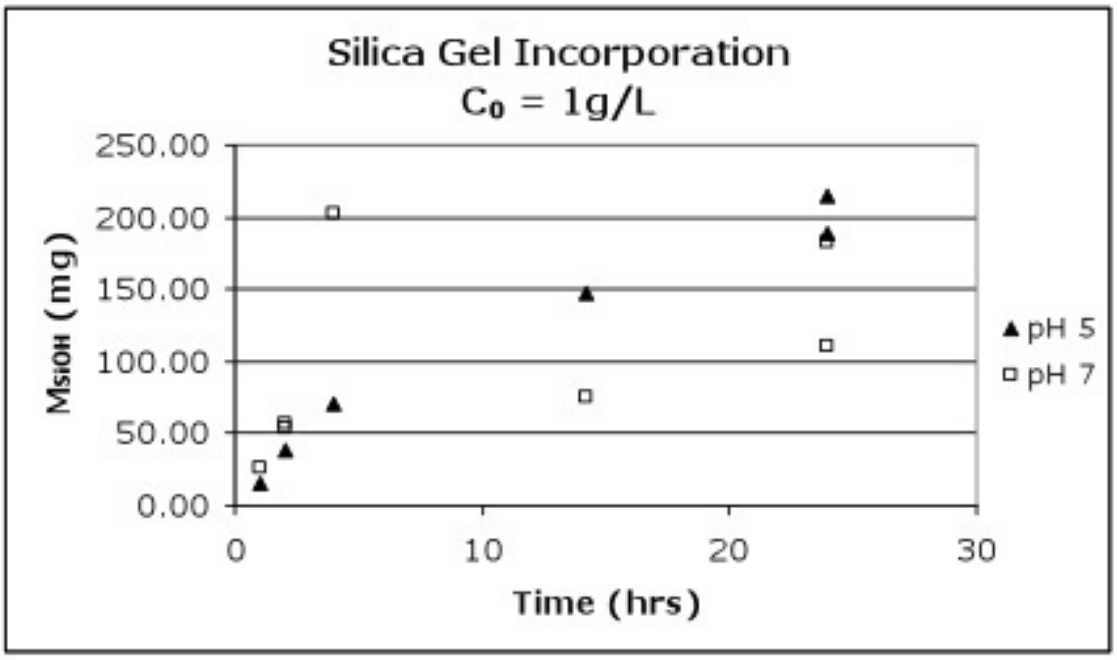

Figure 3.16 Adsorption kinetics of Davisil 643

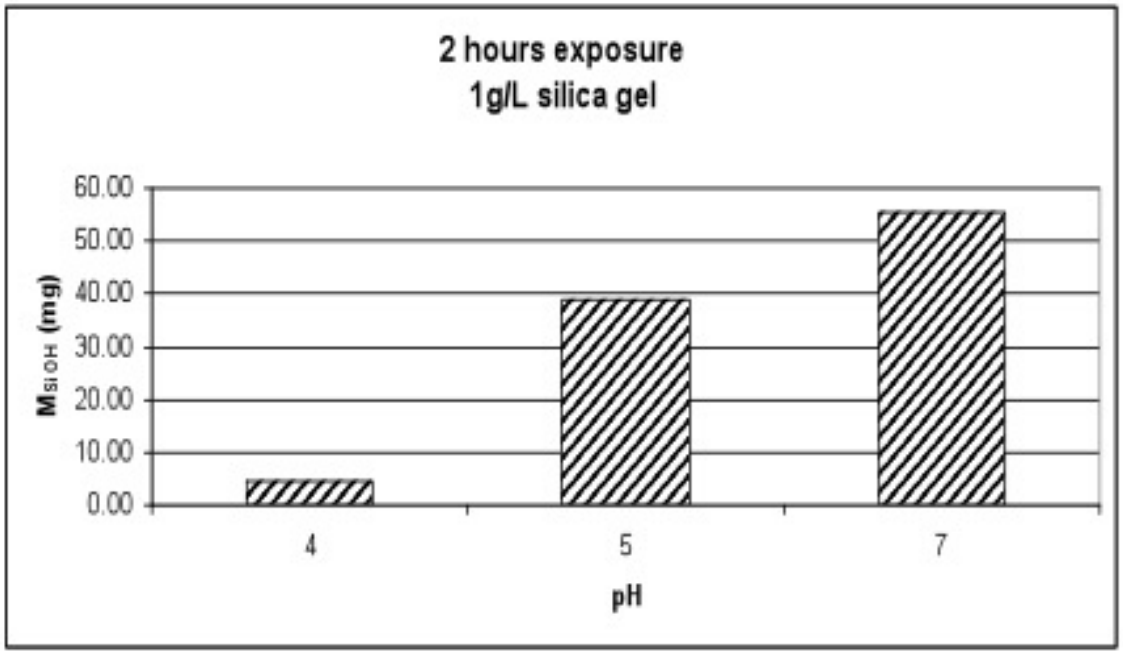

Figure 3.17 Effect of pH on initial adsorption rate of Davisil 643

Since silica gel is hydrophilic, it is prudent to verify the adsorption equilibrium timescale of hydrophobic particles. Figure 4.18 shows the effect of hydrophobicity on particle adsorption, it is evident that acetylated controlled pore glass (A-CPG) has a smaller partition coefficient than silica gel at pH 5 and a roughly equivalent value at pH 7.

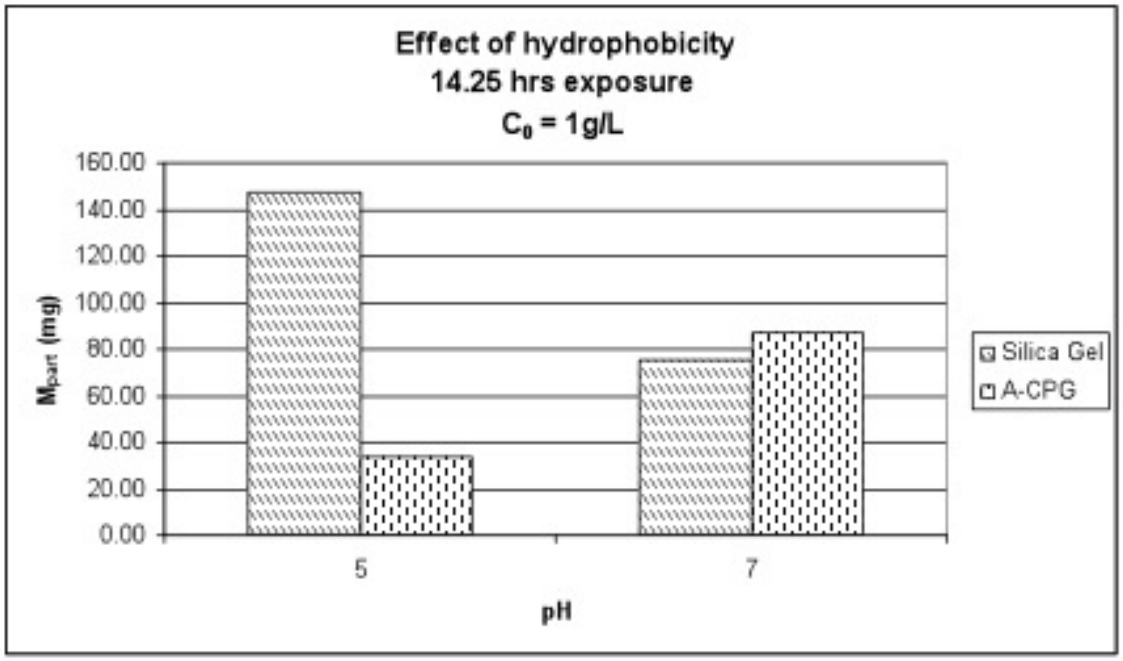

Figure 3.18 Effect of hydrophobicity on particle adsorption

The observations in Figure 4.16 and Figure 4.17 are in agreement with the findings of Bastidas et al., (2005) using reconstituted cellulose films and functionalized AFM tips. At low pH, dissociated protons in the media screen the cellulose from the silica gel and inhibit hydrogen bonding The pKa of bacterial cellulose is not well defined, but it is possible that the silica gel or BC hydroxyl groups are partially deprotonated at pH 4, which would also cause a significant decrease in hydrogen bonding. As pH increases, shielding effects are reduced and increased London forces enhance adsorption. The observations of Figure 4.19, however, do not agree with the AFM results. Bastidas et al. (2005) observe stronger interactions between cellulose and hydrophobic groups at pH 4, which reverses at pH 6 and is more disparate by pH8. A possible explanation for the different behaviors of different cellulose samples is that the morphology of BC is unique and unlikely to be reproduced by cellulose films precipitated onto glass slides. For example, the cellulose molecules align anti-parallel with respect to dipole direction in BC gels, have dispersed regions of crystallinity and amorphousness, and are hierarchically coiled into fibrils and fibers. Any of these characteristics has the potential to alter the exposure of the particle to the hydrophobic regions equatorially adjacent to the cellulose molecule.

An empirical tool for analyzing and comparing non-covalent interactions between particles and surfaces is the Langmuir isotherm. The Langmuir equation, (4.11), relates the mass of particles adsorbed on a surface, M*, to the concentration of particles in environment around the surface, C_p. The parameters that characterize the relationship are M_{sat}, the maximum mass of particles that can attach to the surface, and K_m, the half-saturation coefficient, an empirical fitting parameter.

$$M^* = M_{sat} \frac{C}{K_m + C} \tag{3.11}$$

Jeweler's rouge is frequently used in the initial surface studies because of its visibility. The adsorption results for jeweler's rouge at pH 7 are shown in Figure 4.19 along with the results of fitting the data to the Langmuir equation with two popular methods: Lineweaver-Burk linear regression, Equation (4.12), and the Langmuir linear regression, Equation (4.13).

$$\frac{1}{M^*} = \frac{K_m}{M_{sat}} \frac{1}{C} + \frac{1}{M_{sat}} \tag{3.12}$$

$$\frac{C}{M^*} = \frac{C}{M_{sat}} + \frac{K_m}{M_{sat}} \tag{3.13}$$

Both methods are not without their criticisms, however. The Lineweaver-Burk fit is criticized for enhancing the effect of measurement error by the use of the M^{*-1} term and being biased towards low concentration data. The Langmuir fit is considered less sensitive to measurement noise, but biased towards middle and high concentration data points. The values of the Langmuir isotherm adsorption coefficients for Jeweler's rough are listed in Table 4.1.

Table 3.1 Langmuir isotherm coefficients for jeweler's rouge

	M_{sat} (mg)	**K_m (mg/mL)**
Lineweaver-Burk (4.12)	357.5	2.99
Langmuir (4.13)	265.9	1.79

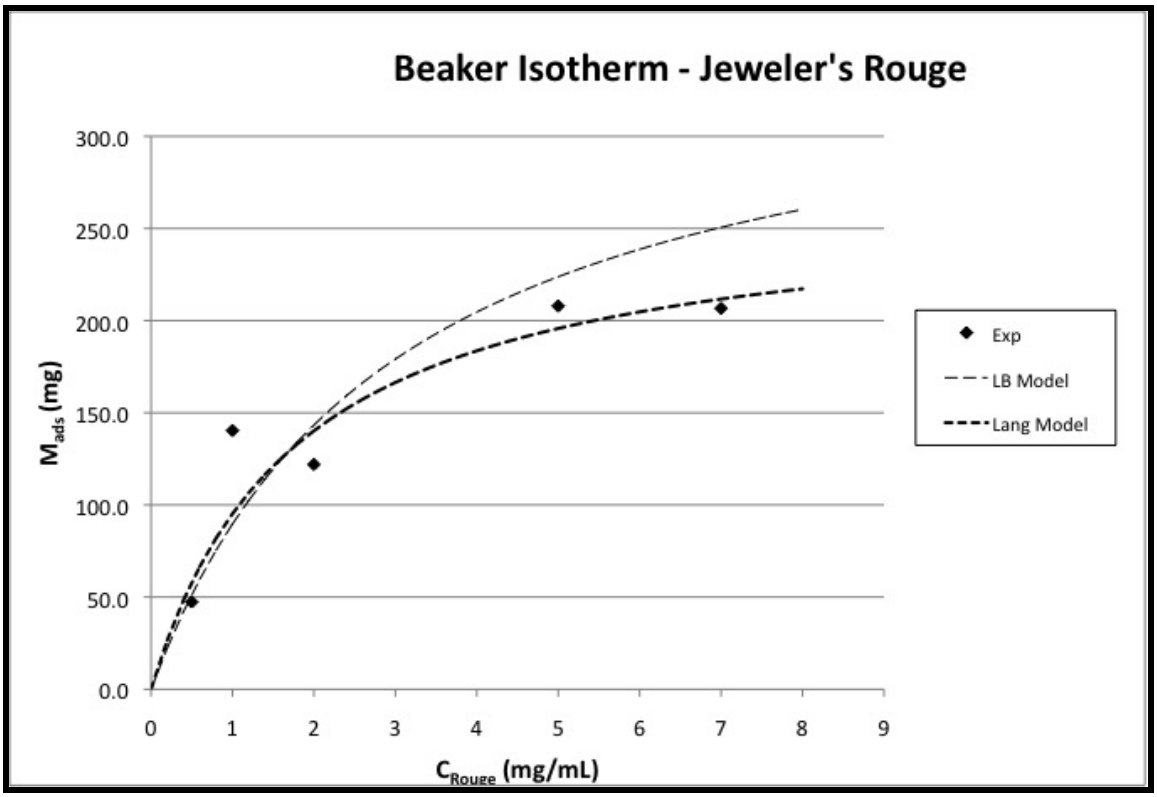

Figure 3.19 Adsorption data with Langmuir Isotherm fitting of jeweler's rouge at pH 7

3.3.3 Growth and Capture Phenomena

Paramount to the particle uptake process is the actual mechanism of incorporation. Serafica (1997) finds that 20μm is the particle size ceiling for integration into the BC matrix by diffusion. To confirm that this observation is not a residual effect of the mercerization step in his BC harvesting procedure, an experiment is designed to directly visualize the diffusive penetration of 15μm fluorescent microspheres. A fully formed BC gel, 10 days after inoculation, is harvested (BC remaining intact on disk; entire disk removed off shaft), boiled, and submerged in a stirred 3L solution of 1000 spheres/mL. After 6 days of particle exposure, cross sections of this gel are visualized in a fluorescent slide scanner. The penetration profiles shown in Figure 4.20 indicate that diffusion into the BC matrix is negligible.

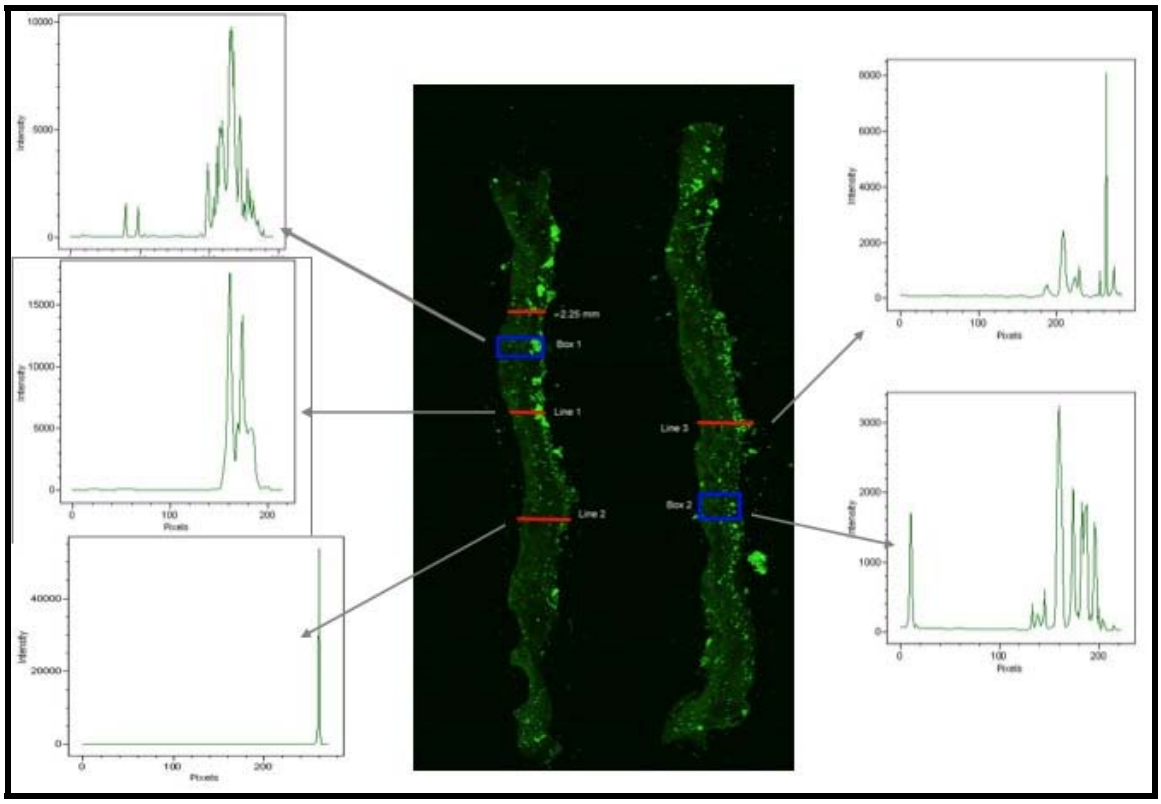

Figure 3.20 Penetration profiles of 15μm polystyrene fluorescent microspheres into non-growing RDB BC

The uptake mechanism proposed by this work assumes that particles are incorporated into the BC by being captured by the thickening gel. In other words, the *G. xylius* community in the BC continues to extrude new cellulose fibers around the particles and weaves them into the cellulose matrix. An experiment that tests this hypothesis adds particles to two otherwise identical reactor chambers with BC on the rotating disk, where one chamber has had the cellulose matrix sterilized immediately prior to particle addition (i.e., the BC growth is static) and the other has not (BC still growing). The growing and static BC gels rotate at 12RPM and are exposed to crystal violet lactone (CVL) surface modified silica gel. Figure 4.21 shows the mass distributions measured in the harvested BC products. The nearly flat profile of the static gel is due to the low affinity of CVL-Silica gel for the native BC surface. In agreement with the hypothesis, the growing gel shows appreciable uptake, which is solely due to mechanical entrapment of the particles as the BC thickens.

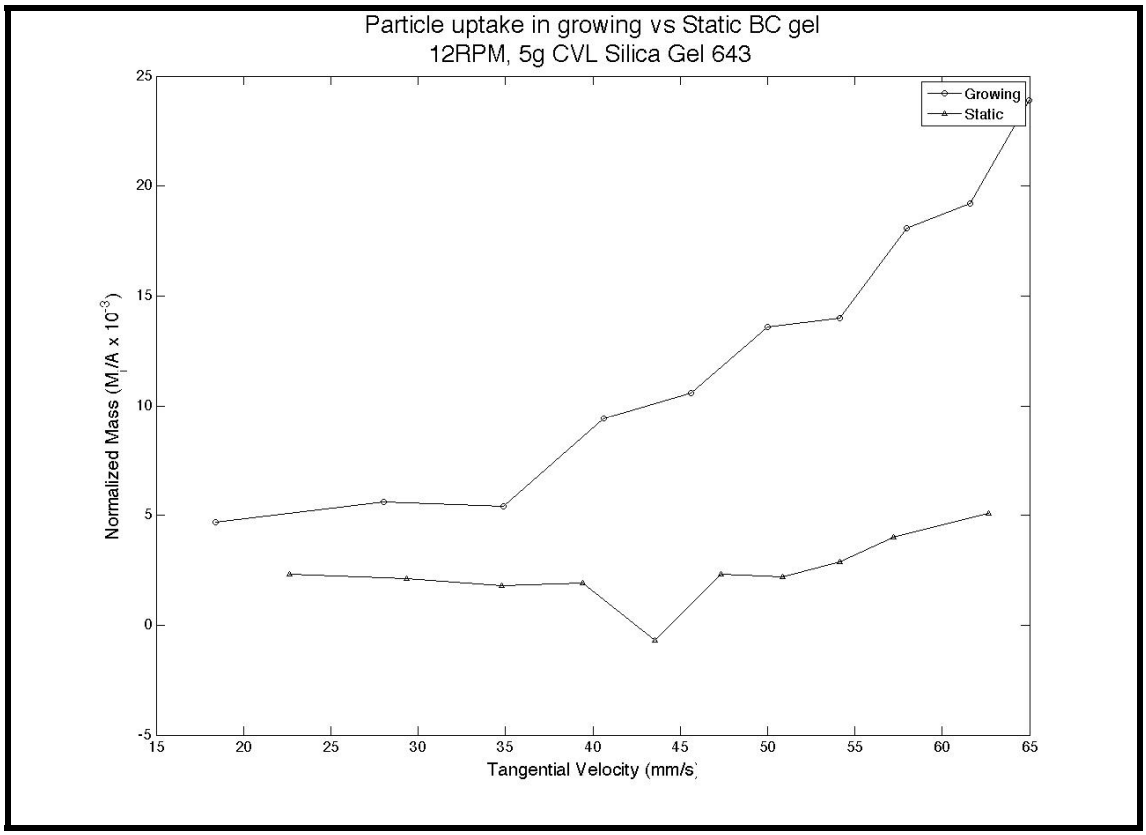

Figure 3.21 Comparison of mass distribution in BC for growing and non-growing gel at 12 RPM

It is reasonable to assume that at the instant one of the chambers in this experiment was sterilized, both BC gels would have similar mass distribution profiles and if particles were uniformly incorporated into the BC gel, the profile of the growing chamber would retain the shape while increasing in value. However, at the outer regions of disk, the rate of incorporation is much high than the central regions, as seen by the increased slope of the "Growing" profile in Figure 4.21. A postulated explanation for this is that the gel does not thicken uniformly and that it thickens more rapidly at the outer regions of the disk.

This reasoning can be tested by directly measuring the BC gel thickness along the disk radius at sequential time intervals. The results of a preliminary experiment are shown in Figure 4.22 and suggest the hypothesis is partially correct. The thickness profile at the early time-point, 119.5 hours, does indeed show that cellulose production at the disk edge has outpaced production towards the center. The unexpected observation is that the profile at the second time-point, 164.75 hours, has become nearly uniform due to an

increased rate of cellulose production in the disk's inner region. The bottom plot in Figure 4.22 shows the variation in BC gel thickening rate over the disk radius between these two time-points.

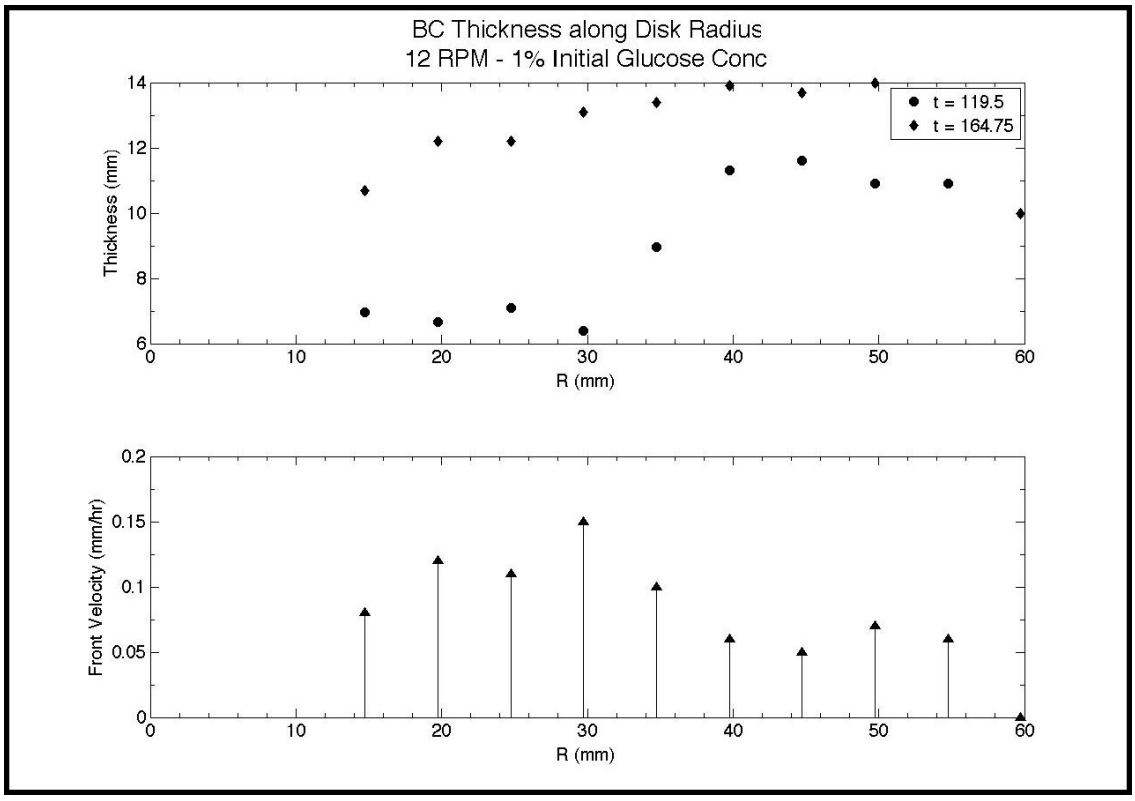

Figure 3.22 RDB thickness profile evolution at 12 RPM

Although Figure 4.22 is only a preliminary result, it suggests BC thickening is more dynamic than previously believed. Apparently, the gel does not thicken uniformly and the location of accelerated growth varies over time. This claim has important consequences to biocomposite production and will be subject to extensive experimental investigation.

3.4 Validation Studies

The typical shape of the radial distribution of mass in the harvested RDB product is confounding, as well. The discontinuity appears to be linked to radial position and invariant to rotational speed. Preliminary measurements of the bacterial cellulose (BC) thickness profile evolution indicate that it is also non-uniform at the exterior of the disk.

Further experiments will be carried out to determine if a causal connection exists between these two patterns. An experimental observation that will prove relevant here is the flow field on bulk liquid's horizontal surface. The streamlines are visualized with hydrophilic aerogel tracer particles, a schematic diagram of which is presented in Figure 4.23. At the outer tip of the trailing edge of the disk the particles aggregate and aeration is enhanced by from the boundary layer-fluid film instability collapse. These flow patterns are observed at all rotational speeds studied. A related observation is that these flow patterns form regardless of the aspect ratio of the rotating disk diameter to the chamber diameter. The consequence is that if superficial currents cause the outermost bacteria to thrive by enhanced nutrient transport or aeration or they simply increase the rate of incorporation by increasing the concentration driving force, it may not be possible to design against this in the RDB platform. To examine answer the question of uneven mass or thickness profiles being inherent to the RDB, experiments will be performed the pump around jets oriented in parallel straddling the disk. It is not intuitive if the jets should point with or against the direction of rotation, so both will be investigated.

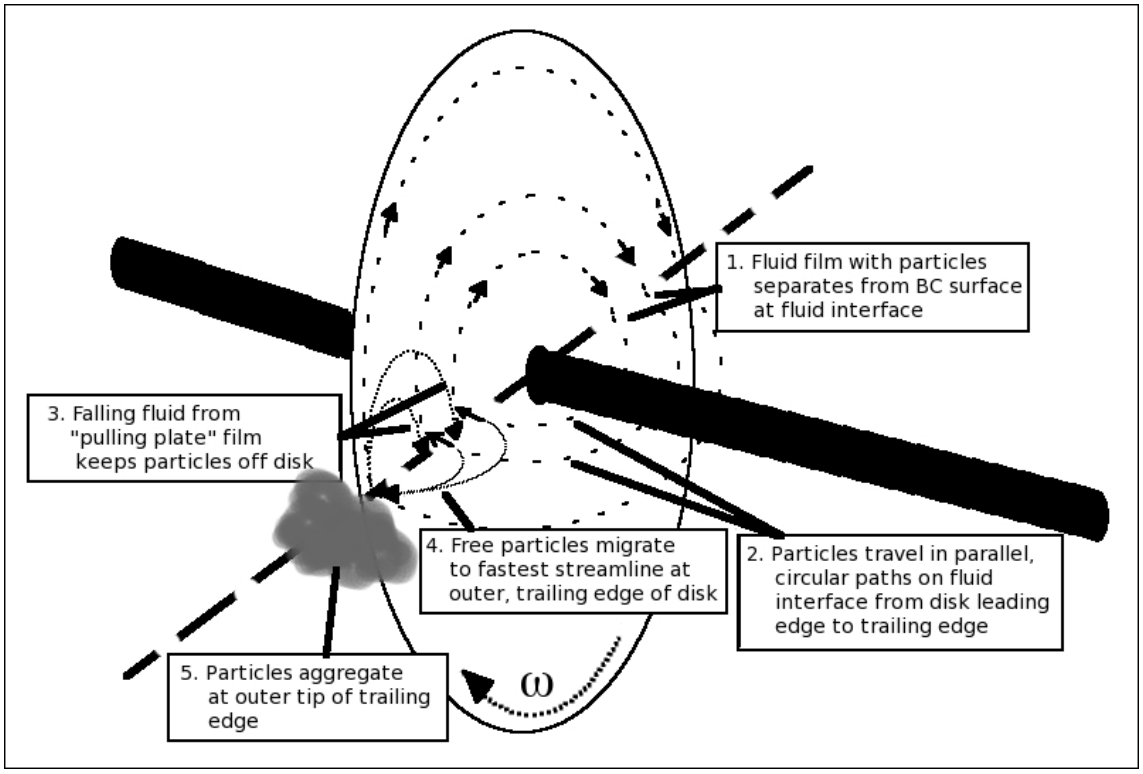

Figure 3.23 Schematic diagram of flow field on surface of bulk liquid and entrenched fluid film

3.5 Summarizing Remarks

The results herein present four areas where the understanding of suspended particle incorporation into bacterial cellulose (BC) growing in a rotating disk bioreactor (RDB) has moved beyond previous efforts. First the shortsighted assumptions and poor experimental designs of earlier researchers are laid out alongside the consequences to the creditability of their findings, but also with improved designs and protocols. Second, data is presented to verify, in the upgraded apparatus, that particle incorporation does occur. Third, a three-step incorporation mechanism is proposed. The chemical engineering principles in each step are discussed and experimental evidence of each step is presented. The three steps are 1. Particle transport across a boundary layer from the well-mixed bulk phase to the particle surface; 2. Particle adsorption to the BC surface by non-covalent interactions including hydrogen bonding and van der Waals forces; and 3. Particle encapsulation by gel thickening. Lastly, the unanticipated discontinuity in the radial distribution of mass profiles from early experimental trials is presented and

analyzed. The profiles show a steep increase in the particle mass contained in the outer edges of BC product. Tracer particle visualization studies are performed to understand this occurrence and it is concluded that boundary collapse as the disk withdraws from the liquid phase creates eddies at the outer disk edge, which draw in material and greatly increase particle uptake in that extreme outer region.

In the final part of this study, two methods of validating the main hypothesis motivating this work will be pursued. The first is comparing experimentally determined particle distribution profiles to profiles arising from hydrodynamics to determine on what particle uptake is dependent. An argument is made, however, as to why the entrained film thickness predicted by plate withdrawal theory is unlikely to arise in the RDB environment. Essentially, gravity driven flow down the disk face during rotation will alter the thickness profile. As an alternative, an empirical correlation from an RDB-related field will be used to predict the film thickness profile. It will need to be determined *posteriori* if the empirical profile can be used to extract a particle uptake relationship from experimental data.

The final proposal put forth is a course of uptake experiments with microscopic assessment to determine if particle uptake is a dependent on rotation rate, tangential velocity, or neither of the two. A dependence on tangential velocity will be shown if particle concentration at locations of similar tangential velocity is the same in experiments run at different rotation rates. Alternatively, a dependence of uptake on rotational speed will be shown if radial particle concentration distributions vary monotonically with rotational speed. If this type of relationship exists, the uptake rate is expected to be directly proportional to rotational speed because of the inverse relationship between rotational speed and diffusion boundary layer.

4. Proposed Work

The incorporation of suspended particles into the growing bacterial cellulose (BC) matrix produced by *Gluconacetobacter xylinus* in a Rotating Disk Bioreactor (RDB) has been observed. The most frequently used technique, thus far, for particle distribution determination is gravimetric analysis (ashing) of the product. A feature common to all the ashing results is the high concentration of mass at the sample's outer edge. Experimental observations of the surface currents in the RDB system inform a theory, put forth in §4.4, explaining the profile discontinuity. The theory is that boundary layer collapse upon disk withdrawal creates a chaotic flow environment at the outer disk edge and draws material towards it. This observation refutes any assumptions about the transition of a fluid element from submerged boundary layer to entrained fluid film being smooth along the disk face. Another important assumption to examine is the consistency of the entrained fluid film as the disk rotates from withdrawal to submergence. In the section, §5.1 Empirical Fluid Profile, an empirical entrained fluid film thickness correlation is presented from the literature. A plan to compare the empirical result to the analytical result from flat plate withdrawal theory is presented. The significance of this comparison will also be discussed in regards to particle incorporation in the RDB. In brief, the empirical film thickness correlation is derived by regression analysis of a very large number of measurements on a rotating disk apparatus. This correlation is studied because the regression includes an independent variable for rotational position, i.e., the changing orientation of gravitational to centripetal acceleration vectors in a fluid element moving with the disk. A more realistic evolution of the fluid film thickness profile over the duration of rotation through the air phase will better establish the distributions of particle concentration gradients on the exposed disk face and this, in turn, will enable a more accurate calculation of particle incorporation in the air phase. The overall hypothesis about the dependence of particle uptake on tangential velocity will be verified, in part, by matching experimental radial distributions of particles in the BC product with either the predicted air phase incorporation profile or the predicted submerged incorporation profile.

The second means of validating the overall hypothesis is observing particle incorporation rates at points of similar tangential velocity from trials run at different rotational

speeds, e.g. r = 2.4cm at 16RPM and 4.125cm at 9RPM (40mm/s). Gravimetric analysis, however, is ill suited to provide data of sufficient accuracy to compare uptake at these similar points with confidence. This is because the ashing method extracts radial information from the BC product by physically sectioning the disk into annuli and ashing each ring in a ceramic crucible. It is the requirement to use ceramic crucibles that calls into question the veracity of the data; namely that the mass of the empty crucible and the mass of the ashed crucible very similar and very large compared to the mass of particles contained in the sample (c. 25g vs 25mg). It is only the similar values of replicate measurements and common profile trends of many experimental results that give the method credence. Nevertheless, the gravimetric data lacks the accuracy and precision to address the hypothesis regarding particle uptake. Microscopy is a more meticulous analytical method for BC products and it will be used to analyze the final experiments. The proposed experiments and how they will confirm or refute the hypothesis is explained in the second section of this chapter, §0 The final step is to see if the profiles calculated from the empirical correlation characterize have a relationship to disk rotational speed or tangential velocity. To do this, "calibration" radial profiles will be calculated at 9, 12, and 16RPM with all other parameters identical and plotted against tangential velocity. If the profiles collapse onto a smooth curve, then this method is valid and similarity between empirical and experimental profiles at the same conditions indicates a relationship between incorporation and tangential velocity. If the "calibration" curves do not collapse onto a smooth curve then the hypothesis cannot be answered using this technique.

Model Validation Experiments.

4.1 Empirical Fluid Profile

The analytical method for confirming the overall hypothesis is comparing the measured radial particle distributions to both the submerged boundary layer thickness and the air phase entrained fluid film thickness. The relationship between thickness and uptake is not the same for each region. The hydrodynamic boundary layer thickness is directly proportional to the diffusion boundary layer thickness, which inhibits flux from the bulk to surface. The entrained fluid film thickness, on the other hand, is proportional to the

total quantity of material available to adsorb to the surface. The hydrodynamic boundary layer thickness does not vary in the radial direction, according to the Blasius solution (Coulson et al., 1999), but with rotational speed. The entrained fluid film thickness in the air phase predicted by infinite plate withdrawal theory, however, varies with pulling speed, which in the RDB is the tangential velocity and has radial dependence. Therefore, if the measured particle distribution profiles in harvested BC are flat, uptake varies with rotational speed and if the profiles exhibit monotonic, radial variation, particle uptake rate depends on tangential velocity.

This interpretation is shortsighted, however because the analytical infinite plate withdrawal solution is only valid at disk emergence. As the fluid moves on a real rotating disk, the entrained fluid film thickness profile will change as over the course of the rotation as gravity driven flow occurs on the surface.

An empirical correlation from the Rotating Biological Contactor (RBC) literature (Vijayraghvan and Gupta, 1982) will be used to estimate the steady-state thickness of the fluid film on the air-phase disk surface. The correlation is derived from regression analysis of 486 experimental measurements. The correlation is presented as Equation (5.1).

$$T = \frac{7.96(\eta)^{\quad}(\eta)^{\quad}(\Re)^{\quad}}{(Ca_s)^{\quad}(\chi)^{\quad}} \tag{4.1}$$

where T is the dimensionless film thickness, Ca is the Capillary number, η is a dimensionless surface tension, $\Re$ is the dimensionless disk submergence depth, Cas is the Capillary number at the disk edge, and χ is a dimensionless radial component of the acceleration of gravity. This correlation will be used to generate a matrix of fluid film thicknesses at with discrete radial positions as rows and discrete rotational positions as columns. Disk geometry requires that there either be more rotational nodes at the outer edges than at the inner to maintain constant node spacing or have the same number of nodes, but with greater spacing farther from the disk center. For this analysis, maintaining constant spacing with more nodes is preferred because the gravity driven flow will originate at the outer edge due to the initially thicker fluid film. Placeholder zeros can fill the matrix for small radius rows with fewer nodes. A sample node arrangement and corresponding thickness matrix are shown in Figure 5.1 for clarification.

$$M = \begin{bmatrix} h_{11} & h_{12} & h_{13} & h_{14} & h_{15} & 0 & 0 & 0 & 0 & 0 & 0 & 0 & 0 \\ h_{21} & h_{22} & h_{23} & h_{24} & h_{25} & h_{26} & h_{27} & 0 & 0 & 0 & 0 & 0 & 0 \\ h_{31} & h_{32} & h_{33} & h_{34} & h_{35} & h_{36} & h_{37} & h_{38} & h_{39} & 0 & 0 & 0 & 0 \\ h_{41} & h_{42} & h_{43} & h_{44} & h_{45} & h_{46} & h_{47} & h_{48} & h_{49} & h_{410} & h_{411} & h_{412} & h_{413} \end{bmatrix}$$

Figure 4.1 Sample RDB node diagram and corresponding matrix

The radial profile of interest is derived by numerically integrating the thickness profile in the rotational direction at each radial location. With MATLAB, trapezoidal integration of matrix **M** is performed with the *trapz* command as shown in Equation (5.2).

$$T = trapz(M') \quad \textbf{(4.2)}$$

The final step is to see if the profiles calculated from the empirical correlation characterize have a relationship to disk rotational speed or tangential velocity. To do this, "calibration" radial profiles will be calculated at 9, 12, and 16RPM with all other parameters identical and plotted against tangential velocity. If the profiles collapse onto a smooth curve, then this method is valid and similarity between empirical and experimental profiles at the same conditions indicates a relationship between incorporation and tangential velocity. If the "calibration" curves do not collapse onto a smooth curve then the hypothesis cannot be answered using this technique.

4.2 Model Validation Experiments

Mormino (2002) observes that the uptake of Sigmacell 20 (20µm) filamentous fibers suspended in the media into growing bacterial cellulose (BC) decreases with disk rotational speed, as shown in

Figure 5.2. It is not yet clear if the same relationship is observed with suspended particles. This will be ascertained by experiments with 35-70µm crystal violet lactone (CVL) -colored silica gel particles in rotating disk bioreactors (RDBs) operating at 9, 12, and 16RPM. Direct visualization of BC cross sections with light microscopy is the primary measurement technique. The motivating hypothesis of this work, that particle uptake is proportional to tangential velocity, will be verified if regions of similar tangential velocity, from experiments at different rotational speeds, contain similar particle concentrations in the BC product. If the microscopically observed particle concentrations are not the same at positions with the same tangential velocity, then it will be verified if there is at least a relationship between particle uptake and rotational speed.

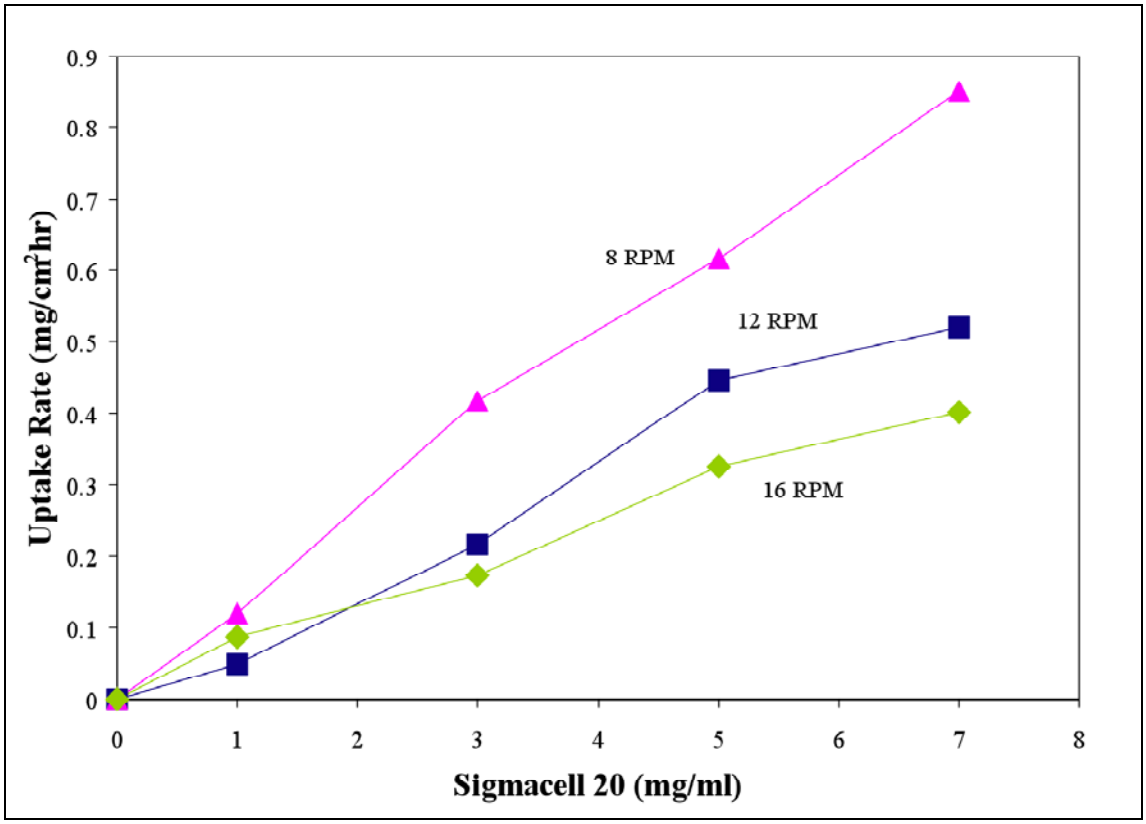

Figure 4.2 Uptake of fibers varies inversely with rotational speed (Mormino, 2002)

For this study, it is imperative that the particle studied be discernable from cellulose in the micrographs. In principle, the crystallinity of silica gel imbues it with this characteristic, but the effect is enhanced with a dye. CVL dyes the silica gel bright blue. The color is lost on contact with ethanol. There is an additional consequence of adsorbing CVL to the silica gel particle and that is to alter the surface chemistry. Nominally, silica gel has a negative surface charge, which shifts to neutral at low pH. CVL, on the other hand, is positively charged at low pH. In Figure 5.3, the ring opening at the center (quaternary ammonium denoted with ⊕) of the CVL molecule is the site of silica gel adhesion. The three NR_3 sites are where excess protons in the low pH environment adhere and give the molecule a positive charge. The exposed charges on the CVL-silica gel complex are expected to enhance uptake as cellulose is negatively or neutrally charged. There may also be permanent dipole-dipole London interactions as both the NR_3 sites and cellulose chains are polar.

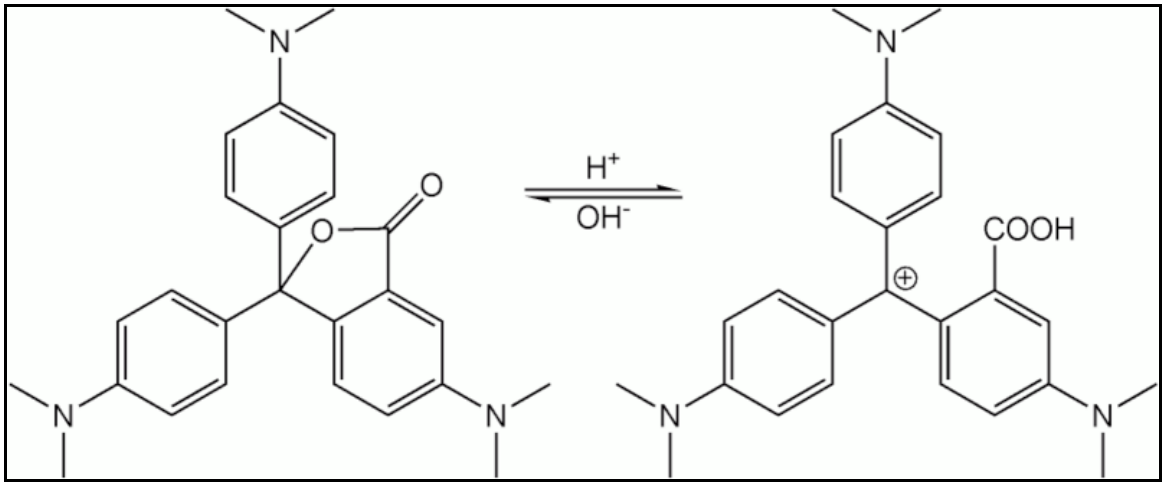

Figure 4.3 Structure of crystal violet lactone (Wikipedia)

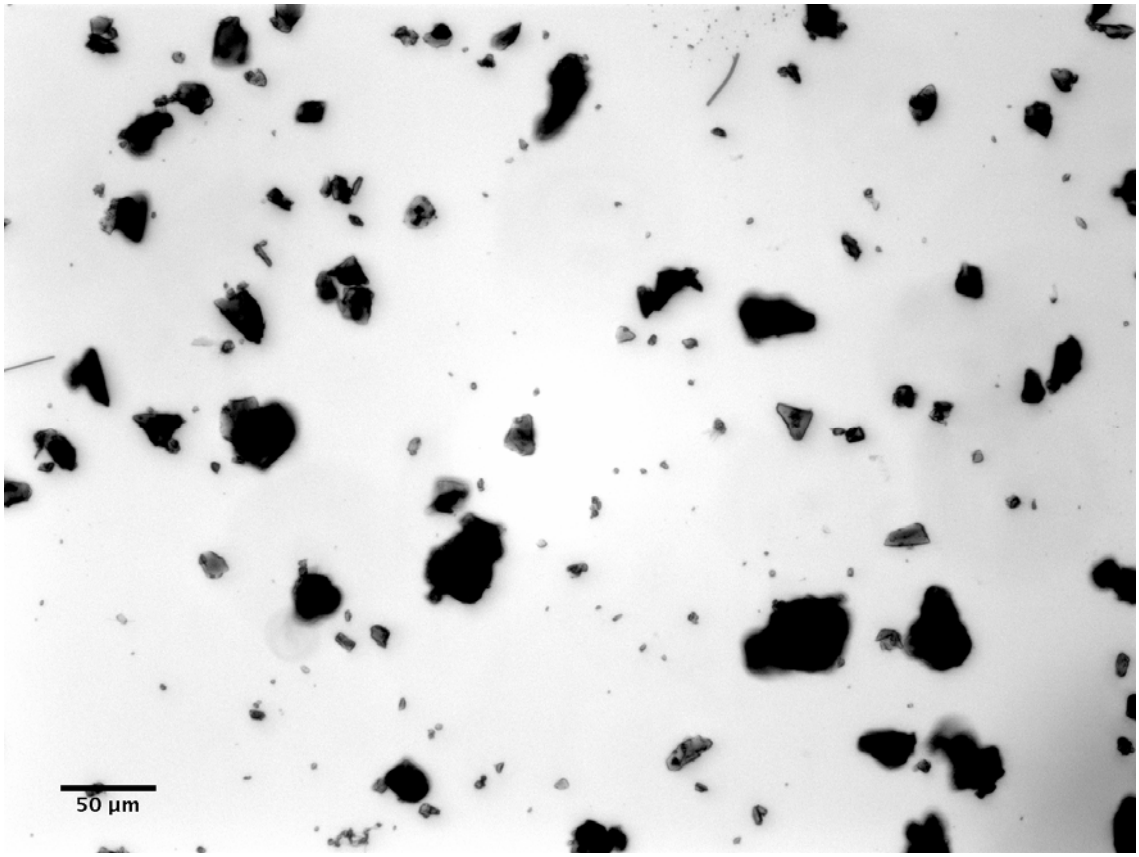

Figure 4.4 CVL-colored 60-70um silica gel (8% area coverage)

To verify the hypothesis, experiments need to be designed to observe the dependency of particle uptake on tangential velocity and to distinguish this from a dependence solely on rotational speed. The experiment that will confirm the former over the latter is to run trials at different rotational speeds, but with overlap of tangential velocity at respective points on the disk surface. Experiments will be performed in two identical, two-chamber recirculating RDBs at 9, 12, or 16 RPM at 30°C.

To increase cell number, 700mL (w/10g glucose) of media will be pre-inoculated in a flask 2-3days before the reactor trial is started. The reactor is prepared by a 45-minute exposure to 0.75% bleach solution followed by two 30-minute rinses with autoclaved DI water. The reactor is then inoculated from the pre-inoculum with an additional 10g of glucose in an autoclaved 100mL solution added.

The reactor is initially operated without recirculation to promote BC cohesion. A thin film of BC typically forms on the disk in 3-4 days. Manual pH adjustments, to a setpoint of 4.2, will be performed twice daily. Once daily, the thickness profile of the BC across

the disk radius will be measured. When a preliminary BC film is formed (~5mm) the particles will be added to the media and the recirculation will be activated. Prior to addition to the reactor, particles will be soaked in DI water and autoclaved to pre-swell and sterilize them. The suspended particle concentration will be measured by grab sampling 10mL on both sides of the disk and averaging. Specifically, the sample point will be half-way between the disk and the chamber wall approximately 5cm deep.

The cornerstone of the experimental work will be to expose one concentration of particles to one rotational speed for a fixed time. Mormino studies 4-6 hours, but this study will expose particles for 48hrs to ensure sufficient BC growth that is required for uptake as discussed in §4.3.3. If grab sampling indicates that the particle uptake is altering the suspended particle concentration, an adjustment will be made by adding more particles.

The experimental schedule is listed as Table 5.1.

Table 4.1 RDB Experimental Summary

Week	**RDB 1**	**RDB 2**	**Notes**
Week 1	12 RPM CVL 5g/L & 10g/L	12 RPM CVL 15g/L & 20g/L	
Week 2	9 RPM CVL 5g/L & 10g/L	16 RPM CVL 5g/L & 10g/L	
Week 3	9 RPM CVL 15g/L & 20g/L	16 RPM CVL 15g/L & 20g/L	
EVALUATE RESULTS			
Week 4	Repeat or Q	Repeat or Q	
Week 5	Repeat or Q	Repeat or Q	
Week 6	Repeat or Q	Advanced Exp	311 Ricketts clean-up

The first series of experiments compare four particle concentrations (5, 10, 15, and 20g/L) at three rotational speeds (9, 12, and 16RPM). At the end of this course of trials, the data will be evaluated to determine the clarity of a relationship between incorporation and tangential velocity. If all the data show a clear correlation, then a second particle set will be investigated in the remaining time. If no pattern is evident, then the

course will be run again for a second time. The second particle of interest is Q Sepharose FF.

Similarly to CVL-dyed silica gel, Q Sepharose FF, is positively charged at low pH and able to be differentiated from the BC background of a micrograph. Q Sepharose, however, is spherical (see Figure 5.5) while CVL-silica gel is crystalline. Testing the incorporation of these particles will give insight into the effect of roughness on particle uptake.

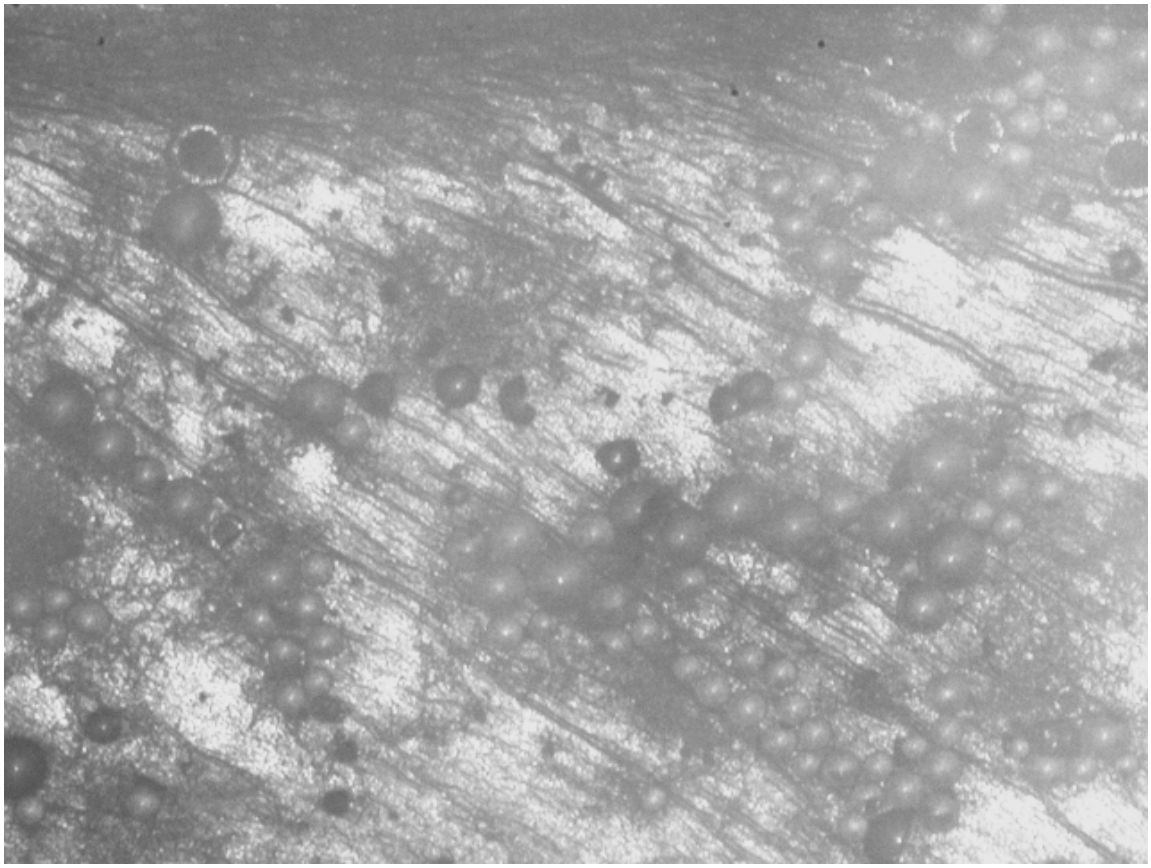

Figure 4.5 Q Sepharose FF on BC

Measurement of particles in the BC product will be done by examining gel cross-sections under a microscope, as shown in Figure 5.6. Three cross-sections will be harvested from each gel. Along the length of the sample, corresponding to disk radial position, particles will be counted every 5mm. To assist in positioning of the microscopic field, a millimeter scale is attached to each microscope slide with adhesive plastic film, as shown in Figure 5.7. Precaution is taken to avoid air bubbles becoming caught

between the plastic film and the glass slide, as seen in Figure 5.7, because they will impede particle counting.

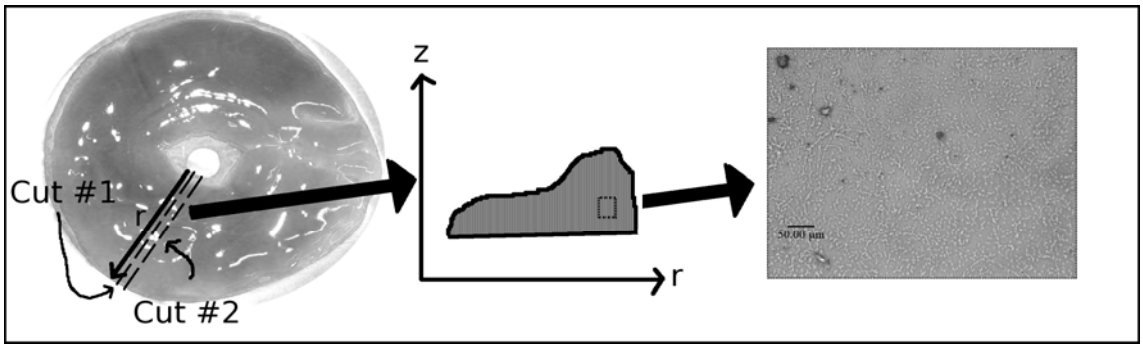

Figure 4.6 RDB BC Sample Preparation

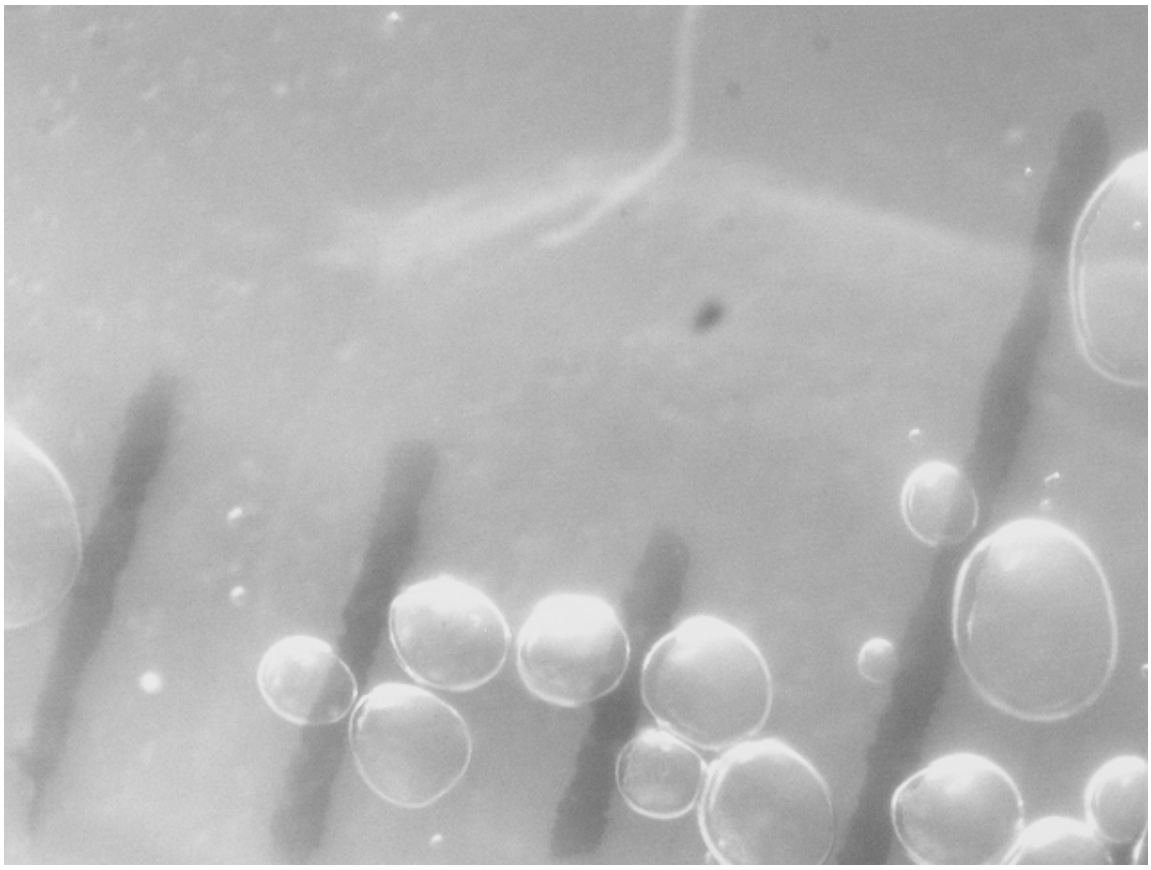

Figure 4.7 Scale marks on slide

It is important to select the microscope field appropriately in order to gain statistically meaningful data about particle distributions. A single image is too narrow for its contents to be representative of the gel at that location. The sampling area is made larger by taking a series of nine micrographs, around a center location, as shown in Figure 5.8.

The individual images are stitched together with software and processed with image analysis software. At least 500 particles should be in the combined field for statistical significance.

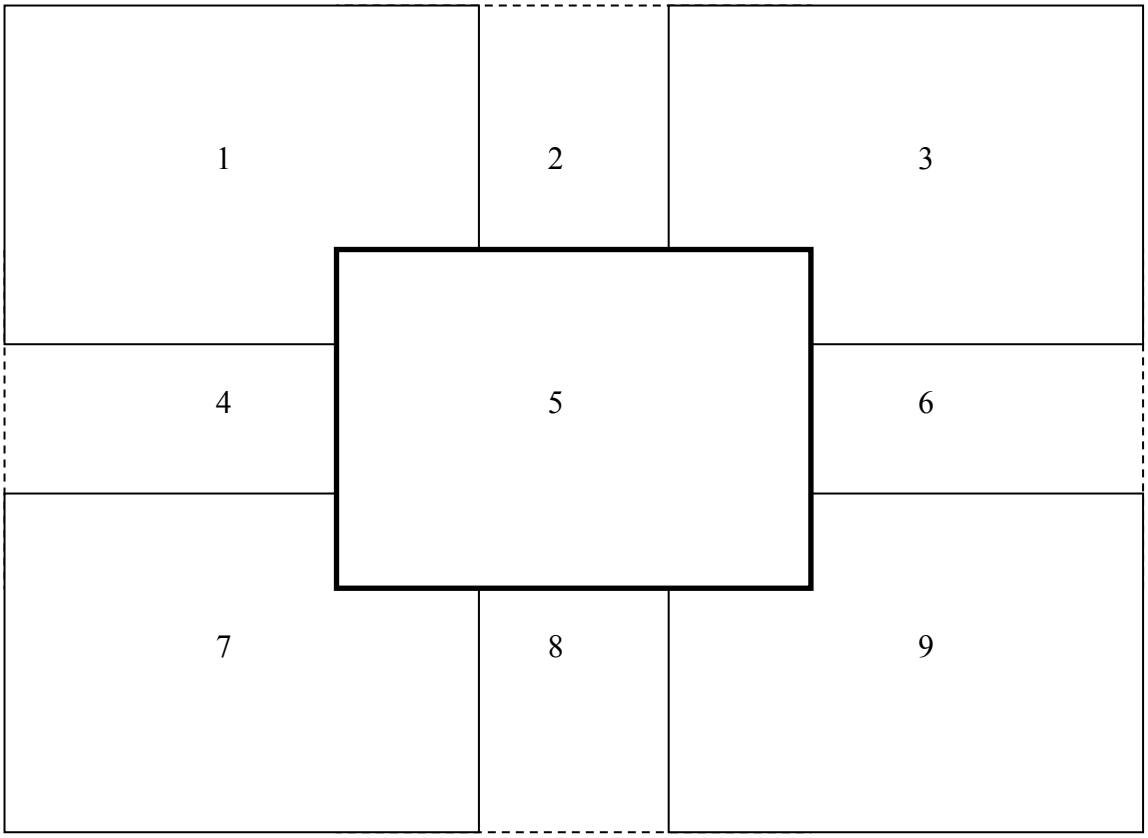

Figure 4.8 Schematic diagram of composite microscope field

The reflection microscope captures images with MATLAB (Mathworks) and the transmission ones with SPOT Advanced (Diagnostic Instruments). To avoid data loss photomicrographs are stored and manipulated in TIFF format. The sequences of images captured at each radial position are stitched together with Hugin (hugin.sourceforge.net, Date Last Accessed: 11/25/2008) panorama software. Image manipulation is performed using the GIMP (www.gimp.org, Date Last Accessed: 04/01/2009).

There are two approaches to particle image analysis: contrast differences and feature matching. In the former, photomicrograph is converted to grey scale and an intermediate grey threshold value is selected where the background is on one side of the threshold and the particles are on the other. The program ImageJ is used for contrast-difference particle analysis. Alternatively, feature matching scans an image to find patterns in the image

that match a reference object. Features of a pattern that can be matched are size, shape, and color. Software used for this method of particle analysis is MATLAB and LABVIEW (National Instruments).

The FARSIGHT toolkit (www.farsight-toolkit.org, Date Last Accessed: 07/07/2007) is an image-analysis platform that is based at Rensselaer. It has yet to be investigated as a solution to RDB BC image analysis, but may be useful once some familiarity is developed.

4.3 Expected Outcomes

These computations and investigations are proposed to answer the question: Does the rate of suspended particle incorporation into a growing bacterial cellulose (BC) gel in the rotating disk bioreactor (RDB) depend on the tangential velocity of the surface? Alternatively, does it depend upon disk rotation rate? Neither? A combination of both? Currently, data from gravimetric analysis shows that incorporation does not occur by one mechanism over the entire disk face. As discussed in §4.4, the exponential mass profile in the disk outer region is invariant to rotational speed and is intrinsic to the multiphase RDB setup. The mass profiles of the inner region will give uptake rate dependency information by comparing their shape to characteristic profiles arising from the reactor hydrodynamics. Specifically, flat radial BC mass profiles imply rotational speed dependence and fractional power law profiles imply tangential velocity dependence. Physically, this heuristic corresponds to incorporation occurring more profoundly at the submerged disk face or the face passing through the air-phase, respectively.

There are, however, two caveats to this profile matching strategy. The first is the role of particle charge. As put forth by Riley and Carbonell (1993A):

> When surface and particle charge are the same, deposition occurs during surface withdrawal. When surface and particle charge are different deposition occurs when the surface is submerged and depositions is much higher.

Within the experimental pH range of 3-5, the BC surface will only be weakly protonated and will be negatively charged. The expected observations are summarized in Table 5.2

Table 4.2 Expected outcomes for profile matching

Particle Charge	Deposition location	Radial mass profile
Positive	Submerged face	Uniform
Negative	Air-phase face	Fractional power law

The second caveat to the profile matching strategy is that entrained film thickness profile predicted from pulling plate theory is strictly applicable only at the immediate site of disk withdrawal. The movement of the fluid during rotation due to gravity and disk curvature may be significant. Section 5.1, Empirical Fluid Profile, explains how a more realistic profile will be determined for comparison against experimental data. It is expected that the profiles computed from the empirical correlation will be different the analytically predicted ones. It is also expected for this difference between empirical and analytical predictions will be affected by rotational speed. At 16RPM, it takes 1.875 seconds to travel from withdrawal to submergence. As the entrained fluid crosses the apex of its rotation, it spends 0.875 seconds with a horizontal component to the velocity vector 90% or greater than the vertical, meaning there is negligible force counteracting downward acceleration of gravity during this period. At 9RPM, this increases to 1.56 seconds. It is possible that realistic film profiles will not be usable for extracting uptake dependencies from experimental data. It is the analytical result's fractional power law dependence on tangential velocity that gives rise to the matching technique and it is impossible to comment *a priori* if the empirical result will contain such a feature.

On the other hand, visualization of experimental BC samples at points of similar tangential velocity from trials at different rotational speeds will provide data that is more straightforward to interpret. The sample sectioning and slide mounting procedure may slightly distort the edges of the sample, introducing uncertainty into the absolution radial location of the microscope field. It is expected, however, that by capturing several overlapping fields and forming a composite image in software, this uncertainty will dampen out. There are additional elements of the experimental design that will provide confidence in the data, e.g., taking photomicrographs from several cross sections of the same BC product, and requiring at least 500 particles in the composite image for statistical significance.

If the motivating hypothesis is not validated by microscopy and image analysis, another uptake relationship will be investigated. To demonstrate a dependence of particle uptake on rotational speed, particle concentrations at similar radial positions will be measured. As discussed in §4.3.1, hydrodynamic theory predicts the boundary layer on the submerged BC surface is radially uniform and monotonically decreases with rotational speed. If the particle concentration profiles measured by microscopy are flat and increase with rotational speed (boundary layer thickness and transport driving force are inversely proportional), the dependence of uptake on rotational speed will be confirmed.

In contrast with Mormino's (2002) fiber uptake results presented in Figure 5.2, it is expected that if there were an uptake rate dependency on rotational speed, higher rates of particle incorporation would occur with faster disk rotation. This is the expected trend because at higher speeds there is less contact time between the moving disk and the stationary bulk liquid, which means a thinner boundary layer develops. The consequence of a thinner hydrodynamic boundary layer is a thinner diffusion boundary layer, which means there will be a greater driving force for mass transfer to the disk. Two proposed rationales for the disagreement between particle expectations and fiber observations are: the higher rates of shear at higher speeds will affect the transport of light fibers more than heavy particles and the increased contact time between fibers and BC at slower speeds in between interfacial crossings allowing fibers to unfold and align along the surface, increasing non-covalent interactions. It is left as the suggested next project on BC composite production in the RDB to propose and validate a theory that unifies incorporation observations of particles and fibers.

5. Literature Cited

Bastidas, J., R. Venditti, J. Pawlak, R. Gilbert, S. Zauscher, and J. Kadla, "Chemical force microscopy of cellulosic fibers," *Carbohydrate Polymers*, 2005, **62**, 369-378.

Bintanja, H. H. J., J. Van der Erve, and C. Boelhouwer, "Oxygen transfer in a rotating disc treatment plant," *Water Research,* 1975, **9**, 1147-1153.

Borzani, W. and S. J de Souza, "Mechanism of the film thickness increasing during the bacterial production of cellulose on non-agitated liquid media," *Biotechnology Letters,* 1995, **17**, 1271–1272.

Brown, A. J., "On an acetic ferment which forms cellulose," *J. Chem. Soc., Trans.,* 1886, **49**, 432-439.

Brown, R. M., J. H. M. Willison, and C. L. Richardson, "Cellulose biosynthesis in *Acetobacter xylinum*: Visualization of the site of synthesis and direct measurement of the *in vivo* process," *Proc. Natl. Acad. Sci.,* 1976, **73**, 4565-4569.

Chao, Y. P., Y. Sugano, T. Kouda, F. Yoshinaga, and M. Shoda, "Production of bacterial cellulose by *Acetobacter xylinum* with an air-lift reactor," *Biotechnology Techniques*, 1997, **11**, 11, 829-832.

Choy, V., N. Patel. and J. Thibault, "Blood glucose monitor: an alternative off-line method to measure glucose concentration during fermentations with *Trichoderma reesi," Biotechnology Letters*, 2007, **29**, 1075-1080.

Coulson, J. M., J. F. Richardson, J. R. Backhurst, and J. H. Harker, Chemical Engineering. Sixth Edition, Vol. 1. Oxford: Butterworth-Heinemann, 1999, 573-599.

De Wulf, P., K. J. Joris, and E. J. Vandamme, "Improved cellulose formation by an *Acetobacter xylinum* mutant limited in (keto)gluconate synthesis," *J. Chem. Tech. Biotechnol.,* 1996, **67**, 376-380.

Deen, W. M. Analysis of Transport Phenomena. New York: Oxford University Press, 1998.

Di Palma, L., C. Merli, M. Paris, and E. Petrucci, "A steady-state model for the evaluation of disk rotational speed influence on RBC kinetic: model presentation," *Bioresource Technology*, 2003, **86**, 193-200.

Embuscado, M. E., J. S. Marks, and J. N. Bemiller, "Bacterial cellulose. 1. Factors affecting the production of cellulose by *Acetobacter xylinum," Food Hydrocoll.,* 1994, **8**, 407-418.

Forng, E. R., S. M. Anderson, and R. E. Cannon, "Synthetic media for *Acetobacter xylinum* that can be used for the isolation of auxotrophic mutants and study cell biosynthesis," *Applied and Environmental Microbiology*, 1989, **55**, 1317-1319.

Geyer, U., D. Klemm, and H.P. Schmauder, "Kinetics of the utilization of different C-sources and the cellulose formation by *Acetobacter xylinum*," *Acta Biotechnol.,*1994, **14**, 261-266.

Groenveld, P., "High capillary number withdrawal from viscous Newtonian liquids by flat plates," *Chemical Engineering Science*, 1970a, **25**, 33-40.

Groenveld, P., "Low capillary number withdrawal," *Chemical Engineering Science*, 1970b, **25**, 1259-1266.

Groenveld, P., "Laminar withdrawal with appreciable inertial forces," *Chemical Engineering Science*, 1970c **25**, 1267-1273.

Groenveld, P., and R. A. Dortmond, "The shape of the air interface during the formation of viscous liquid films by withdrawal," *Chemical Engineering Science*, 1970, **25**, 1571-1578.

Gromet, Z., M. Schramm, and S. Hestrin, "Synthesis of cellulose by *Acetobacter xylinum*: 4. Enzyme systems present in a crude extract of glucose-grown cells," *Biotechnology Journal,* 1957, **67**, 679-689.

Haigler, C. H., A. R. White, R. M. Brown, and K. M. Cooper, "Alteration of *in vivo* cellulose ribbon assembly by carboxymethylcellulose and other cellulose derivatives," *Journal of Cell Biology*, 1982, **94**, 64-69.

Hestrin, S. and M. Schramm, "Synthesis of cellulose by *Acetobacter xylinum*: 2. Preparation of freeze-dried cells capable of polymerizing glucose to cellulose," *Biotechnology Journal,* 1954, **54**, 345-352.

Holmes, D. "Bacterial cellulose," *Master's Thesis, University of Canterbury, Christchurch, New Zealand*, 2004.

Hornung, M., M. Ludwig, A. M. Gerrard, and H. P. Schmauder, "Optimizing the production of bacterial cellulose in surface culture: evaluation of substrate mass transfer influences on the bioreaction (Part 1)," *Eng. Life. Sci.*, 2006a, **6**, 537-545.

Hornung, M., M. Ludwig, A. M. Gerrard, and H. P. Schmauder, "Optimizing the production of bacterial cellulose in surface culture: evaluation of product movement influences on the bioreaction (Part 2)," *Eng. Life. Sci.*, 2006b, **6**, 546-551.

Hwang, J. W., Y. K. Yang, J. K. Hwang, Y. R. Pyun, and Y. S. Kim, "Effects of pH and dissolved oxygen on cellulose production by *Acetobacter xylinum* BRC5 in agitated culture," *Journal of Bioscience and Bioengineering*, 1999, **88**, 183-188.

Iguchi, M., S. Yamanaka, and A. Budhiono, "Review: bacterial cellulose – a masterpiece of nature's arts," *Journal of Materials Science*, 2000, **35**, 261-270.

Jeffreys, H. "The draining of a vertical plate," *Mathematical Proceedings of the Cambridge Philosophical Society*, 1930, **26**, 204.

Jonas, R. and L. F. Farah, "Production and application of microbial cellulose," *Polymer Degradation and Stability,* 1998, **59**, 101-106.

Kondo, T. "Hydrogen bonds in cellulose and cellulose derivatives" Polysaccharides: Structural Diversity and Functional Versatility. Second Edition,.Ed. S. Dumitru. New York: Marcel Dekker, 2005, 69-98.

Krystynowicz, A., W. Czaja, A. Wiktorowska-Jezierska, M. Goncalves-Miskiewicz, M. Turkiewicz, and S. Bielecki, "Factors affecting the yield and properties of bacterial cellulose," *Journal of Industrial Microbiology and Biotechnology*, 2002, **29**, 189-195.

Landau, L. and B. Levich, "Dragging of a liquid by a moving plate," *Acta Physiochim. URSS*, 1942, **17**, 42-54.

Masaoka, S., T. Ohe, and N. Sakota, "Production of cellulose from glucose by *Acetobacter xylinum*," *J. Ferment. Bioengng*, 1993, **75**, 18-22.

Mormino, R. P. "Evaluation and applications of a rotating disk reactor producing bacterial cellulose," *Ph. D. Thesis, Rensselaer Polytechnic Institute, Troy, N.Y.,* 2002.

Mormino R. P., and H. Bungay, "Composites of bacterial cellulose and paper made with a rotating disk bioreactor," *Appl. Microbiol. Biotechnol.*, 2003, **62**, 503-506.

Oikawa, T., T. Ohtori, and M. Ameyama, "Production of cellulose from D-Mannitol by *Acetobacter xylinum* KU-1," *Biosci. Biotech. Biochem*., 1995a, **59**, 331-332.

Oikawa, T., T. Morino, and M. Ameyama, "Production of cellulose from D-Arabitol by *Acetobacter xylinum* KU-1," *Biosci. Biotech. Biochem.,* 1995b, **59,** 1564-1565.

Patwarhan, A.W. "Rotating biological contactors: a review," *Ind. Eng. Chem. Res.,* 2003, **42**, 2035-2051.

Pushparaj, V. L., M. M. Shaijumon, A. Kumar, S. Murugesan, L. Ci, R. Vajtai, R. J. Linhardt, O. Nalamasu, and P. M. Ajayan, "Flexible energy storage devices based on nanocomposite paper," *Proc. Natl. Acad. Sci.,* 2007, **104**, 13547-13577.

Rislove, D. J. “Ethanol Sensitive Solid,” U. S. Patent 4791065, Dec. 13, 1988.

Riley, D. J. and R. G. Carbonell, “Mechanisms of particle deposition from ultrapure chemicals onto semiconductor wafers: Depostition from bulk liquid during wafer submersion,” *Journal of Colloid and Interface Science*, 1993a, **158**, 259-273.

Riley, D. J. and R. G. Carbonell, “Mechanisms of particle deposition from ultrapure chemicals onto semiconductor wafers: Depostition from a think film of drying rinse water,” *Journal of Colloid and Interface Science*, 1993b, **158**, 274-288.

Ross, P., Y. Aloni, H. Weinhouse, D. Michaeli, P. Weinberger-Ohana, R. Mayer, and M. Benziman, “Control of cellulose synthesis in *Acetobacter xylinum*. A unique guanyl oligonucleotide is the immediate activator of cellulose synthase,” *Carbohydrate Research,* 1986, **149**, 101-117.

Ross, P., H. Weinhouse, Y. Aloni, D. Michaeli, P. Weinberger-Ohana, R. Mayer, S. Braun, E. De Vroom, A. Van der Marel, J.H. Van Boom, and M. Benziman, “Regulation of cellulose synthesis in *Acetobacter xylinum* by cyclic diguanylic acid,” *Nature,* 1987, **325**, 279-281.

Ross, P., R. Mayer, and M. Benziman, “Cellulose biosynthesis and function in bacteria,” *Microbiological Reviews*, 1991, **55**, 35-58.

Samejima, M., J. Sugiyama, K. Igarashi, and K. E. L. Eriksson, “Enzymatic hydrolysis of bacterial cellulose,” *Carbohydrate Research*, 1997, **305**, 281-288.

Serafica, G. C “Production of bacterial cellulose using a rotating disk film bioreactor by *Acetobacter xylinum*,” *Ph.D. Thesis, Rensselaer Polytechnic Institute, Troy, N.Y.*, 1997.

Serafica, G. C., R. P. Mormino and H. Bungay, “Inclusion of solid particles in bacterial cellulose,” *Appl. Microbiol. Biotechnol.* 2002, **58**, 756–760.

Schmauder, H. P., L. Einfeldt, U. Geyer, and D. Klemm, “Biosynthesis of cellulose by *Acetobacter xylinum* using of glucose and modified carbon sources,” *Mededelingen van de Faculteit Landbouwwetenschappen Rijksuniversiteit Gent*, 1992, **57**, 1797-1799.

Schramm, M. and S. Hestrin, “Factors affecting production of cellulose at the air/liquid interface of a culture of *Acetobacter xylinum*,” *J. Gen. Microbiol.* 1954, **11**, 123–129.

Suga, K. and A. Boongorsrang, “A new model of mass transfer in a rotating disc contactor,” *Chemical Engineering Science*, 1984, **39**, 767-773.

Swissa, M., Y. Aloni, H. Weinhouse, and M. Benziman, "Intermediary steps in *Acetobacter xylinum* cellulose synthesis: studies with whole cells and cell-free preparations of the wild type and a celluloseless mutant," *Journal of Bacteriology*, 1980, **143**, 1142-1150.

Toyosaki, H., T. Naritomi, A. Seto, M. Matsuoka, T. Tsuchida, and F. Yoshinaga, "Screening of bacterial cellulose-producing *Acetobacter* strains suitable for agitated culture," *Biosci. Biotech. Biochem*., 1995,**59**, 1498-1502.

Turner Jr., V. L. "Process for determining amount and uniformity of distribution of colloidal silica," U. S. Patent 3032401, May 1, 1962.

Vandamme, E. J., S. De Baets, A. Vanbaelen, K. Joris, and P. De Wulf, "Improved production of bacterial cellulose and its application potential," *Polymer Degredation and Stability*, 1998, **59**, 93-99.

Verschuren, P. G., T. D. Cardona, M. J. R. Nout, K. D. de Gooijer, and C. van den Heuvel, "Location and limitation of cellulose production by *Acetobacter xylinum* established from oxygen profiles," *Journal of Bioscience and Bioengineering*, 2000, **89**, 414-419.

Vijayraghvan, K. and J. P. Gupta, "Thickness of the film formed on a vertically rotating disk partially immersed in a Newtonian liquid," *Ind. Eng. Chem. Fundam.*, 1982, **21**, 333-336.

Wantanabe, K., and S. Yamanaka, "Effects of oxygen tension in the gaseous phase on production and physical properties of bacterial cellulose formed under static culture conditions," *Biosci. Biotech. Biochem.,* 1995, **59**, 65-68.

White, D.A. and J.A. Tallmadge "Theory of drag out of liquids on flat plates," *Chemical Engineering Science,* 1965, **20**, 33-37.

Wilke, C. R. and P. Chang, "Correlation of diffusion coefficients in dilute solutions," *AIChE Journal*, 1955, **1**, 264.

Welty, J. R., C. E. Wicks, and R. E. Wilson, Fundamentals of Momentum, Heat, and Mass Transfer. Third Edition. New York: John Wiley & Sons, 1984.

Wolcott, C. C. "Colloidal silica films for cell culture," U. S. Patent 5814550, Sep. 29, 1998.

Yamane, T. and F. Yoshida, "Absorption in a rotating disk gas-liquid contactor," *J. Chem. Eng. Jpn.*, 1972, **5**, 55-59.

Yamanaka, S., K. Watanabe, N. Kitamura, M. Iguchi, S. Mitsuhashi, Y. Nishi, and M. Uryu, "The structure and mechanical properties of sheets prepared from bacterial cellulose," *Journal of Materials Science,* 1989, **24**, 3141-3145.

Zaar, K. "Visualization of pores (export sites) correlated with cellulose production in the envelope of the gram-negative bacterium *Acetobacter xylinum*," *Journal of Cell Biology*, 1979, **80**, 773-777.

Zuo, K., H. P. Cheng, S. C. Wu, and W. T. Wu, "A hybrid model combining hydrodynamic and biological effects for production of bacterial cellulose with a pilot scale airlift reactor," *Biochemical Engineering Journal*, 2006, **29**, 81-90.